POLITECNICO DI MILANO

Facoltà di Ingegneria Industriale

Laurea Magistrale in Ingegneria Spaziale

Wireless technology for space applications: effects of Antenna Diversity radio transceiver selection

Relatore: Prof. Michèle LAVAGNA
Co-relatore: Ing. Jean-François DUFOUR

Tesi di Laurea di:
Vincenzo TAUMATURGO Matr. 735141

Anno Accademico 2010-2011

Sed omnia praeclara tam difficilia, quam rara sunt
(Baruch Spinoza)

Abstract

The impact of the harness on a spacecraft mass budget can be around 5% of the total dry mass, moreover it leads to a further complexity in the design phase to think about an appropriate path for electric cables and data wired and to longer time spent for Assembly, Integration and Testing (AIT) activities. An alternative is offered by wireless technologies, developed for commercial usage in the latest 1990s and introduced in the space application technology development since few years only. Moreover always more Commercial-Off-The-Shelf components satisfy the aerospace applications strict requirements and they have been successfully used both in testing activities than in critical in-flight operations, however not a big amount of data is actually available about the behavior of these components under when exposed to radiation, even if this is one of the main requirements of a space application. In this thesis I evaluated the performances of a wireless IEEE 802.15.4 compliant radiotransceiver, designing a test sequence which aims to evaluate the possibility to use this component in an AIT activity, for instance as the communication block of a temperature sensor network. I tested the radiotransceiver in several scenarios representative for a space oriented application, like the Venus-Express mock-up. In particular the benefit of the Antenna Diversity mechanism is evaluated to assess its benefit on the link budget in multipath affected scenarios, as like as a metallic closed structure divided in cavities. Then I performed a Total Ionizing Dose test, evaluating the behavior of the device in terms of electrical and communication parameters. Then a practical example of a space oriented application of the tested device is provided, through the implementation of a wireless smart temperature sensor.

Keywords: wireless, Antenna Diversity, Commercial-off-the-shelf, smart sensor, IEEE 802.15.4.

Sommario

L'impatto dei cablaggi sul mass budget di un veicolo spaziale rappresenta circa il 5% della massa totale (carburante escluso). Inoltre porta a non poche complessità sia in fase di progetto, nel prevedere opportuni percorsi per i cavi che rispettino i requisiti di compatibilità elettromagnetica, sia in fase di assemblaggio, integrazione e test, a causa dei chilometri di cavi impiegati per sensori e apparati, da posare e verificare ad ogni utilizzo. Una valida alternativa è rappresentata dalla tecnologia wireless, nata nel mondo commerciale nella seconda metà degli anni '90 e da qualche anno utilizzata per lo sviluppo di tecnologie in campo aerospaziale. Inoltre i severi requisiti delle applicazioni spaziali vengono spesso soddisfatti oggigiorno da componenti commerciali, utilizzati sia per attività di test non critiche, sia per applicazioni in volo. In questa tesi ho valutato le prestazioni di un radiotrasmettitore che segue lo standard IEEE 802.15.4, progettando una serie di test per valutare la possibilità di impiegare questo componente nell'ambito di un'attività di integrazione e test, ad esempio come il terminale di un rete di sensori di temperatura. Ho testato il radiotrasmettitore in situazioni rappresentative di una applicazione orientata all'utilizzo in ambito aerospaziale, ad esempio all'interno della struttura principale del satellite Venus-Express. In particolare ho valutato il guadagno sul link budget garantito dal meccanismo di Antenna Diversity, per contrastare l'effetto del cosiddetto multipath fading, fortemente presente in ambienti caratterizzati da numerose riflessioni, come la struttura metallica del satellite, suddivisa in cavità. Inoltre ho effettuato un test di esposizione a radiazioni, valutando il comportamento del componente durante e dopo l'esposizione, in termini di quantità elettriche e di parametri di comunicazione. Infine presento un esempio pratico di applicazione spaziale per questo componente: un sensore intelligente di temperatura, wireless e alimentato da una piccola batteria.

Parole chiave: wireless, Antenna Diversity, componente commerciale, sensore intelligente, IEEE 802.15.4.

Acknowledgements

I would like to express my gratitude to those people which made me able to write this thesis with their moral support and their valuable contribution, also giving me the possibility to complete my studies doing a very instructive experience at the European Space Research and Technology Centre. I'm grateful to Professor Michèle and to my external supervisor, Jean-François Dufour, for their patience and availability, then I thank Giorgio Magistrati, Head of On-Board Computers & Data Handling section and all the TEC-EDD section members because they enabled me to work in the best possible conditions. Thanks to Maria, Farid, Gianluca, Max and Marco for the time they always found for me and I have to thank also Alberto, Javier, Michele, Alfonso and all the people who have been more than work mates for me. Then I can't forget who supported and encouraged me throughout my life and especially during these last five years: my Mother and my Sister, who stood by me even though I was annoying and obnoxious because I was under stress and my girlfriend who treated my kindly even if I had my head in the clouds. In the end I would like to thank my "brothers in arms" Fulvio, Davide, Marzio, Giò, Edo, Alex, Ste, Debby and Stefania who shared with me a lot of troubles and who helped me to ride over and to appreciate finally all the challenges handled with excitement and strength of will at the University.

Contents

List of Figures

List of Tables

Chapter 1

Introduction

The On Board Data Handling spacecraft subsystem is mainly made up of three components: the Central Processing Unit (CPU), the data memory (which can be volatile or non-volatile in dependence of its function) and the bus interface. The latter involves several problems due to the fact that it has to connect several devices or whole subsystems with very different features in terms of produced throughput, required data-rate and reliability of the data transfer. The past trend was the employment of reliable, military standard interface and the MIL-STD-1553 usage is a real evidence of this. It was developed in the early 1970s by a subcommittee of the Society of Automotive Engineers (SAE) to accomplish the task to integrate multiple avionics subsystems for a military aircraft application and it was successfully used in 1975 on board Air Force F-16 and US Army AH-64A Apache Helicopter [1]. It provides a 1 Mbps multiplex serial data bus able to manage, through a single connection, up to 32 terminals which can be connected each other through a twisted, shielded pair of wires [2]. In 1978 the MIL-STD-1553B replaced the earlier MIL-STD-1553A, the main difference between them was that the latest version specified several items which were user defined in the previous one, but the architecture remained mostly unchanged [3]. In despite of this, over the years it has been broadly used for the development of space applications, as the Space Transportation System program or the more recent International Space Station, for instance a new module as the Columbus, launched in 2008, has research laboratory accommodations interfaces based upon this standard. In 1988, the US Department of Defense (DoD) issued a military standard called MIL-STD-1773, a following version of the MIL-STD-1553 to promote optical fiber data buses usage in military

aircraft. This standard still only provided for 1 Mbps, even if, compared with the twisted copper pairs and coaxial cables, optical fibers have the advantages of large bandwidth, low loss, immunity to electromagnetic interference (EMI), less weight and small size, all features which make them suitable for space applications [4]. In fact it was used in 1997 for command and communication purpose on the Solid State Recorder box of the Hubble Space Telescope, after the successful test done on the Solar Anomalous and Magnetospheric Particle Explorer (SAMPEX), launched on a polar orbit in 1992. In 1995 the IEEE released a standard, the IEEE STD 1394 , based on a previous communication data transfer method developed by Apple's in the 1980s named FireWire [5]. It can act as a bridge or provide a serial bus and was used for space application on the Space Shuttle External Tank Thermal Protection System (ETTPS) digital camera, to take pictures of the external tank separation [6]. In 1983 the Robert Bosh GmbH company accomplished the development of a standard bus interface called Controller Area Network (CAN). The main purpose was the creation of a fast and reliable interface for automotive applications. It defines an upper limit data rate of 1 Mbps. Actually the CAN bus is broadly used in terrestrial applications, like cars or trains, whereas the experience in space on board applications is limited to few missions and small spacecrafts, as for instance the Surrey Satellite Technology Ltd (SSTL) satellites UoSAT-12, AlSAT-1, or SNAP-1, nevertheless several future European space missions have already opted for CAN Bus as the main On-Board Bus for their spacecrafts, subsystems or payloads [7]. The European Cooperation for Space Standardization (ECSS) in January 2003 published the guidelines of a new bus interface, namely SpaceWire, based on two existing standards, the IEEE 1355 and the Low-Voltage Differential Signaling (LVDS). SpaceWire provides a 2 Mbps (up to 200 Mbps), full-duplex serial bus with event triggered data transmission and has been adopted by several Agencies other than ESA, as like as JAXA and Roscosmos [8]. Moreover it is being used today on several scientific, Earth observation and commercial missions, as for instance GAIA, ExoMars, James Webb Space Telescope, BepiColombo and Lunar Reconnaissance Orbiter.

All the interfaces introduced above are quite common for space applications and have been used successfully until now. Besides this they share one feature more: they are wired. The impact of the harness on a spacecraft mass budget can be around 5% of the total dry mass, moreover it leads to a further complexity in the design phase to think about an appropriate path

for electric cables and data wired, taking into account the Electromagnetic Compatibility (EMC) requirements. An alternative is offered by wireless technologies. Even if a wireless communication is more affected by extern interferences and require a higher level of security and authentication methods than a wired one, it leads to an easier communication system implementation and design, allowing greater flexibility and lower integration time, other than mass saving. Taking into consideration that a wireless solution deletes harness concern but requires power sources for the communication nodes, an ESA Concurrent Design Facility (CDF) study shows that using a wireless implementation instead of a common wired one, the system mass would be reduced by around 2% in total. Moreover the complexity reduction could lead, especially during Assembly, Integration and Testing (AIT) phases, to shorter assembly and test processes time. Simulations have shown that substituting 70% of the replaceable data harness of a medium-class satellite (for example the Mars Express) with wireless technologies results in about 20% reduction of Flight Model integration time and relevant associated integration phase cost (for Mars Express, it represents 25 days saving out of 130 for a team of about 15 people) [9]. Today two basic technologies, which operate in different frequency bands, are actually used to develop a wireless communication system: infrared (IR) and radio frequency (RF). The IR wave length is around 900 nm and even if it provides very high data rates (in the order of Mbps or hundreds of Mbps using laser) and no electrical interference issues, it requires a direct line-of-sight (LOS) and it is no able to travel through walls or other obstacles, so it is not suitable for scenarios with nodes which don't see each other and it is less flexible in comparison to RF transmission. Moreover actually there is more experience in using RF, both in commercial and industrial field, than in space application domain. The standards which find an application within space technologies are the IEEE 802.11 (commonly named Wi-Fi), the IEEE 802.15.1 (or Bluetooth), the IEEE 802.16 for wide area networks (named also WiMAX) and the IEEE 802.15.4 standard for wireless sensor networks. In 1997 the IEEE developed the 802.11 standard for Wireless Local Area Network (WLAN) building. The standard gives specifications about the physical layer (PHY) and the medium access control (MAC) sublayer for moving and portable nodes within a local area network (par. 2.4.1). It is suitable for spacecraft internal local area network development, with data-rate in the order of 1 Mbps or more and range of 100 meters, using a transmission power with an

order of magnitude of one Watt. In 1994 Ericsson developed a low-power and low-cost radio interface to connect two devices without wires between them. The potentiality of this standard opened the possibility to connect more than two devices, so building an operational network. Five years later, in 1999, the first IEEE 802.15 working group released the first version of the IEEE 802.15.1, commonly named Bluetooth. It provides a data-rate of 1 Mbps covering distances in the order of $10 \div 30$ meters, with a transmission power lower than 1 mW. In 1999 an IEEE working group started working on the development of a Wireless Metropolitan Area Network protocol, with covered range in the order of kilometers. Two years later the first IEEE 802.16 standard was published. Actually it is well known as WiMAX and provides data-rates up to 100 Mbps, using a transmitting power of tens of Watts. The IEEE 802.15 fourth working group developed in 2003 the first version (superseded in 2006 by the latest version) of a standard named 802.15.4 with the aim to define the protocol and the interconnection of several devices in a Wireless Personal Area Network (WPAN), within a range of tens of meters, a maximum data-rate of 250 kbps (in the 2.4 GHz frequency band) and very low transmission power (less than 1 μW).

It is obvious that wireless technologies have been developed later in comparison to the wired ones (between the MIL-STD-1553 and the IEEE 802.15.4 there is a 30 years and more time interval), therefore the experience in development and design of wireless interface is not comparable to that acquired with wired ones, especially for space applications. However several wireless technologies implementations, even if relatively simple, have been already tested in flight: astronauts on the Shuttle and International Space Station have on board Wi-Fi for their palmtop computers, wireless temperature sensors have been placed within the Shuttle wings to acquire in-flight data and the ISS is equipped with an External Wireless Instrumentation System (EWIS) to provide long-term structural dynamics measurements of the solar array trusses while deployed on-orbit, using 10 wireless triaxial accelerometers to measure the structural response also during orbital reboosts or docking manoeuvres [10]. The Ariane V launcher contains 27 sensors candidates to be replaced by wireless ones, the European Next Generation Launcher is expected to utilize 220 sensors, which forty percent of could be replaced by a wireless version to monitor the conditions inside the launch fairing. Moreover the NASA Inflatable Lunar Habitat design is planning to use wireless sensors for remote shape monitoring. A further application is

actually in development to simplify the ISS inventory procedures using radio frequency identification (RFID) tags to place inside the cargo bags, making them easy to find with a simple RF scan, as already done for terrestrial application which uses a RF scan and which doesn't require a direct line-of-sight. Moreover wireless sensors already being routinely used in terrestrial hospitals are planned to be used to monitor the astronauts conditions, creating a sensor network for health monitoring purposes. About sensors, several experiments have been done aboard small satellites, especially nanosatellites, as Delfi-C^3 of the Delft University of Technology in the Netherlands, which has developed a fully autonomous wireless sun sensor (AWSS), integrating the sensing part, solar cells for power and a wireless data link using a patch antenna operating in the 915 MHz band.

There are several possible applications for wireless technology in aerospace area of interest, as not only it is a potential alternative to the common wired interface solution, making possible to build a wireless local area network for information communication and data exchange between multiple nodes, without the concern to place and verify hundreds of meters or even kilometers of wires and cable harnesses, but also it offers a powerful flexibility which could be used in multiple scenarios. Inside a spacecraft, within a range of around ten meters, a wireless network can be used for monitoring purposes, as crew members position and health control system, or using for instance a network of temperature or pressure sensors for environmental quantities control or strain gauges for spacecraft condition monitoring. These kind of network can require up to hundreds of nodes and are suitable for IEEE 802.11 and IEEE 802.15.1 usage in case of medium high data-rate, whereas for low data-rates, as the case of a not critical temperature sensor, the IEEE 802.15.4 standard is more appropriate. Moreover they can be an important resource to simplify the inventory management, especially in large space vehicle, as for instance the International Space Station. Another scenario well-suited for wireless technology application is that inside launchers. The great height of the launchers, normally between 30 and 50 meters, leads to very long cables for instruments and spacecraft health monitoring during operational, test and verification phases, other than for launcher monitoring, during the launch phase. Thermistors, thermocouples and accelerometers have to be operative, during the launch phase, only for few minutes, so the power required to feed a wireless sensor is compatible with the one supplied by a battery, therefore wireless technology usage is not so hazardous in this case. More-

over wireless is always a valuable alternative for lines redundancy creation. Outside of a spacecraft, within a range of tens of kilometers, Inter-vehicle activities can exist, as data exchange between two different spacecrafts using the IEEE 802.16 standard inside a formation flying or satellites constellation. Astronauts could be aided during their Extra-vehicular activities and their health conditions monitored for all the duration of the operation in the deep space or on a planetary surface by a sensors Local Area Network using the 802.11 standard if within 100 meters, or by a bigger network using the 802.16 standard if the distances are in the order of kilometers. About planetary operations, surface to orbiter or surface to surface (for instance lander to rover) links could be possible using a standard which offers high range and data rate, as the 802.16. Then robotic activities can plan the usage of sensor network for checking purpose or of transceivers for data exchange. In case of robotic application and not critical measurements with a low data-rate, also the 802.15.4 standard could be adopted. Moreover self-powered wireless sensors can increase the science data acquisition return, creating a network of science instruments placed in different locations on the planetary surface or released during the descent phase and connected to acquire and exchange data. It is possible to create meteorological and geological units transmitting, on a periodic basis, parameters such as atmospheric pressure, temperature, wind speed, humidity, light intensity, and soils constituents. Study of the seismological behavior of planetary would be easier due to the wide area coverage allowed placing a lot of sensors which act as network nodes [9].

An important additional wireless space application domain is that of assembly, integration and test activities. The development of a reliable wireless sensors network would make the AIT activities more efficient and less expensive in terms of money and time. Temperature, pressure, humidity, radiation, acceleration measurements can be done in multiple spots where a node of a wireless network is easily placed, with the only concern of the power feeding, which can be done through a button cell battery in case of a low transmission power required by the standard. The IEEE 802.15.4 is the most suitable for this application, as it requires very low power, increasing the autonomy of self-powered battery feeded nodes up to hundreds of hours, depending on the duty cycle and the specific application. This standard is affected, as well as all the others wireless standards, by several problems to take into account, due to the fact that the data transmission is done through an un-

bounded medium and no shield is possible against the interaction with the surrounding environment. This leads to strict security practices implemented to prevent from data leak and information theft. Moreover the surrounding environment represent a noise source for the wireless link, generating thermal noise and spurious energy detected by the receiver antenna. Besides decreasing the signal quality, the introduction of the noise into the channel has the effect to increase the number of wrong bits or wrong packets received. This leads to an increased Bit Error Rate (or Packet Error Rate if packets are considered instead of bits), which indicates a less reliable transmission. Moreover the surrounding environment is also an attenuation source for the traveling signal, other than being source of interference, generated by interaction with other signals in the same frequency band. In the specific case of the IEEE 802.15.4 operating in the 2.4 GHz frequency band, interaction with standards 802.15.1 and 802.11, which operate in the same frequency band and can have some channels overlapping, has to be taken into account, especially for an AIT activity, usually done in laboratories where the Wi-Fi signal and Bluetooth using devices are commonly used, whereas it is not a big concern for a potential in-flight usage. Other than noise, attenuation and interference, a further problem is fading, generated by interaction with obstacles between the transmitter and the receiver. In particular reflections, which create different paths followed by the signal, generate multipath fading. This is a not predictable, not deterministic effect which can cause distortion or even loss of the transmitted signal on the receiver side. Several techniques have been implemented to compensate the multipath fading effect, in particular using more than one receiver antenna it is possible to strongly increase the probability that the received signal is above the defined threshold, in terms of quality, or strength, or signal to noise ratio. This mechanism is named Antenna Diversity and can be implemented in several ways, so giving different results, depending on the specific application.

The usage of wireless technology for aerospace application development follows the opposite course in comparison with the so called spin-off, which happen when a space oriented technology finds a new application in the industrial or in the commercial world. Standards as Wi-Fi were born for commercial use, as like as the IEEE 802.15.4, which has been already used to build wireless sensors networks, monitoring temperatures or other quantities inside civil environments, as factories or offices, or to build safety networks, made of sensors and cameras, or to create an object position tracking system

in large spaces, as airport hangars. These technologies are already available, therefore the introduction of wireless technology into space area of interest doesn't require to develop it from scratch, but to test the already available systems to assess their employment for space application, doing a so called spin-in process. Since several years this process is leading commercial-off-the-shelf (COTS) components to be used for space application. In 1991 Meteor-3 was the first mission to use a commercial solid state recorder as data recording device for its Total Ozone Mapping Spectrometer (TOMS) payload and ten years later, in 2001, ESA mission Proba-1 launched in orbit commercial off the shelf components, as like as the next mission Proba-2, in 2009. Moreover several studies have been done to assess the opportunity to use COTS components for future mid-term missions, as GAIA or BepiColombo [11]. Anyway the employment of commercial components for technologies aimed to space, requires a preliminary and accurate evaluation of the performances, to be tested for the specific application and in the same scenario which in the component will have to be used. This includes test to evaluate if the requirements can be accomplished with the chosen component, in terms of precision, accuracy and sensitivity but also environmental tests which evaluate the component response to radiation exposure and its disposition to Single Event Effects (SEE). Actually not so many data have been acquired about the behavior of commercial components during and after the exposure to radiation, namely the effects due to Total Ionizing Dose (TID).

The purpose of this thesis is to assess the performance of an IEEE 802.15.4 compliant radio transceiver to identify its possible employment in a space oriented application. In particular I designed a test sequence to evaluate the performances, in terms of communication parameters, inside a representative space environment, as the mock-up of the Venus Express spacecraft is. I created several situations to simulate possible scenarios of an AIT activity, using the device I tested as a communication block of a wireless sensors network. I did an evaluation of the environment where I tested the device, verifying the interaction of the signal generated by the tested device with an interference signal due to the Wi-Fi network present inside the laboratory where I did the measures. I evaluated the different behavior of the device putting in comparison the results obtained by experimental tests done inside the laboratory with the results of the same tests repeated inside an anechoic chamber. Then I tested the device inside the structure of the Venus Express mock-up, which is divided in six cavities, highlighting the effect of reflections

and of multipath fading on the link budget. Then I compared the results I obtained with a previous study made by the European Space Agency and the EADS Astrium company to evaluate the possibility to use an IEEE 802.15.4 radio transceiver inside the Venus Express mock-up. I developed the software to program the micro-controller connected to the radio transceiver to make the operations needed to accomplish all the tests tasks and I developed a LabView interface to control the device by a Personal Computer and to execute automatic and time repeated operations to obtain the results I present. I designed also a test to evaluate the behavior of the device while exposed to radiation. The TID test has been made in the Co-60 facility of the European Space Research and Technology Centre (ESTEC) following the ESCC Basic Specification 22900 and I did all the experimental measurements to evaluate the performances and their changes not only in terms of communications parameters, as like as strength of the signal, quality of the exchanged packet and Packet Error Rate, but also in terms of physical parameters, as current consumption and operational voltage. This thesis has been developed during a working period of six months at ESTEC in Noordwijk, in the Netherlands.

In this Chapter an introduction to the problem has been provided, highlighting the area of interest of the work, its background and its purpose. In Chapter 2 a few theoretical concepts are introduced, to understand the terms widely recalled in the rest of the thesis and to be aware of which theoretical reference they come from. In Chapter 3 an introduction to the main features of the device I tested is provided, to better understand what can be a possible application of this component and what is the test purpose. In Chapter 4 the test sequence is explain. After an overview about the target of the activity and the way I proposed to achieve it, I go more into deep with the description of the operations I did and their motivation with the possible alternatives. The software I developed to accomplish all the targets is also introduced in this chapter. I describe the full tests sequence in terms of performed operations, whereas results are reported in Chapter 5. In Chapter 6 I show an application example using the radio transceiver I tested, introducing an example design of a wireless temperature smart sensor. Finally in Chapter 7 I report the main conclusions obtained from this work and the possible future development about this device and in general about wireless technology for space application.

Chapter 2

Basic networks and communication theory

The device under test is an IEEE 802.15.4 compliant radio transceiver. It is necessary to introduce some main features of this standard to understand the concepts shown in this thesis and the terms extensively used from this point forward. First an introduction to radio frequency propagation and network theory is provided, paying attention to one of the main issues of the wireless narrow-band communication, which is the multipath fading, and to the tested solution, the Antenna Diversity mechanism. Moreover the Multi-mode cavity theory is recalled, as it is used during the test phase in the mock-up. A brief introduction to Open Systems Interconnection (OSI) model is provided, then the IEEE 802.15.4 standard is shown, paying particular attention to those concepts tightly related to the special features of the device under test.

2.1 RF Propagation

One of the factors to take into account when designing a wireless link is the propagation in multiple means which leads to several losses due to absorption, spreading, and reflection. In a free space environment, that is an environment with no scattering objects or material losses outside of the antennas, the Friis transmission equation provides a good relationship between the transmitted and the received power.

$$P_{RX} = \frac{P_{TX} G_{TX} G_{RX} \lambda^2}{(4\pi d)^2} \qquad [W] \tag{2.1}$$

which in P_{RX} and P_{TX} are respectively the received and the transmitted power, G_{TX} and G_{RX} are the transmission and reception antenna gain, λ is the wave length and d is the distance between the emitter and the receiver.

The term $\left(\frac{4\pi\lambda}{d}\right)^2$ is named free space Path Loss (PL) and is often evaluated in dB:

$$PL = 10n\log_{10}(d) + 10n\log_{10}\left(\frac{4\pi f}{c}\right) \qquad [dB] \tag{2.2}$$

which in n is the PL exponent. In particular for the used standard IEEE 802.15.4, it is recommended a two segment function with a PL exponent of 2.0 for $d \leq 8m$ and equal to 3.3 for $d > 8m$. Referring to [12], the path loss model used in this thesis is:

$$PL(d) = \begin{cases} 40.2 + 20\log_{10}(d) & \text{if } d \leq 8m \\ 58.5 + 33\log_{10}(\frac{d}{8}) & \text{if } d > 8m \end{cases} \tag{2.3}$$

Even if the free space model is not strictly valid in an environment with a medium between the transmitter and the receiver, it offers a good model if there is no multipath or other effects inducted by reflections [13]. If reflections are present, other models have to be used to take into account the effect they induce, which is most of the time a signal attenuation, for instance the two ray ground model takes into account the ground reflection, using a PL exponent equal to 4, whereas further models exist to assess multipath effects.

2.1.1 Multipath fading

When the RF signal encounters objects that reflect it, multiple wavefronts are created, resulting in multiple wavefronts which reach the receiver. Multipath propagation occurs when RF signals take different paths from a source to a destination. As a result, part of the signal encounters delay and travels a longer path to the destination. At the receiver side this delay is equal to a phase shifting and, in the worst case, if two wave arrive out of phase, then the signals may cancel each other. Moreover, if the two signals are of comparable amplitudes, the cancellation may be complete (total loss of signal). For a path length difference Δl, the phase change $\Delta\phi$ between two waves at the frequency f is shown in eq. 2.4.

$$\Delta\phi = \frac{2\pi\Delta l}{\lambda} = 2\pi\Delta t \cdot c \cdot \frac{f}{c} = 2\pi\Delta t \cdot f \qquad [rad] \tag{2.4}$$

Also the coherence bandwidth B_c, that is a statistical measure of the range of frequencies over which the channel has approximately equal gain and linear phase, is related to the time delay Δt as reported in the eq. 2.5.

$$B_c = \frac{1}{2\pi\Delta t} \qquad [Hz] \tag{2.5}$$

In general the effect of the multipath can be defined as the result of the combination of the original signal plus the duplicate wave fronts that come from reflection of the waves on obstacles between the transmitter and the receiver. This result can lead to data corruption, loss of signal, amplitude signal increase or decrease [14].

Data Corruption It occurs when multipath effect is so severe that the receiver is unable to detect in the correct way the transmitted information.

Signal Nulling It occurs when the reflected waves arrive exactly in antiphase with the main signal and cancel the main signal completely.

Increased Signal Amplitude It can occur when the reflected waves arrive in phase with the main signal and add on to the main signal, thereby increasing the signal strength.

Decreased Signal Amplitude It may happen when the reflected waves arrive out of phase to some extent with the main signal thereby reducing the signal amplitude.

Several models have been developed to take into account the effect of multipath fading, as the Rayleigh and the Rician fading models. The former assumes that the phase is uniformly distributed between $[0;\ 2\pi]$ radians and the phases of each path are independent. It is commonly used to describe the statistical small-scale rapid time-varying nature of the envelope of the received signal existing when there isn't a strong received component (not line-of-sight situations), whereas the latter is more suitable in scenarios with a dominant stationary signal component (line-of-sight) [15].

The effect of multipath fading becomes very important in a closed metallic environment, where the RF wave is subjected to many reflections due to the enclosure space walls which encounters traveling from the transmitter to the receiver [16]. This environment is very important for space applications of wireless technologies, because the general structure design of a spacecraft is

made up of one or more conductive boundary cavities, nevertheless inside a cavity, free-space and surface propagation models are not applicable. The electric field propagation inside a cavity is dependent on its dimensions, relative to the signal wavelength, and on the features of its material, which can be more or less reflective and lossy. For Ultra High Frequencies (UHF) the cavity size is often much bigger than the wavelength, so that the multi-mode (or over-sized) cavity model can be applied. Inside an over-sized cavity, the field structure can be quite complex, particularly if the quality factor Q, defined in eq. 2.6 as the ratio of the resonance frequency f_0 to the width of the resonance curve Δf is high [17], [18].

$$Q = \frac{f_0}{\Delta f} \tag{2.6}$$

However the multi-mode cavity theory simplifies the evaluation of the electric field inside a cavity, making the assumption that inside an over-sized cavity the electric field is almost homogeneous. This has a strong impact for the test sequence design, as explained in par. 2.1.2.

2.1.2 Multi-mode cavity theory

Numerical analysis made by ESA and EADS Astrium, which follow the theory developed by T.H. Lehman [16], demonstrate that inside a conductive enclosure with a large characteristic length in comparison to the signal wavelength, the radiated power is uniformly absorbed by the walls, then re-radiated in all directions, producing an homogeneous and isotropic electric field [19]. This leads to independence of the RF power level detected by a receiver antenna in respect of its orientation and location inside a cavity. The immediate result for a space oriented application is the possibility to place a wireless sensor provided with a radio transceiver, inside a cavity without take care about its antenna polarization, orientation or specific location, as it doesn't affect the link budget. A multi-mode cavity has a different behavior in respect to the free space or a resonant cavity, therefore a loss model is required to do a link budget assessment. Assuming as a multi-mode consequence that the RF signal power is uniformly attenuated by the presence of the enclosure, it is possible to identify an only fixed loss parameter for each cavity. This is called cavity insertion loss, X_c, it is related to the Quality factor (defined in eq. 2.6) and is equal to the ratio of the power detected by a receiver placed inside the enclosure (P_{RX}) to the power injected into the

cavity (P_{inj}), as shown in eq. 2.7.

$$X_c = \frac{P_{RX}}{P_{inj}} \tag{2.7}$$

The total insertion loss is dependent on the total surface of the cavity and its apertures, if present, other than on the electrical characteristics of the material, hence it is made up of two components, X_r and X_σ. These are respectively the radiative component and the conductive component, the former takes into account of the loss due to apertures, whereas the latter includes the loss in the material:

$$\frac{1}{X_c} = \frac{1}{X_r} + \frac{1}{X_\sigma} \tag{2.8}$$

$$\frac{1}{X_r} = \frac{4}{3}\frac{8\pi}{\lambda^2}\sum_{i=1}^{N} S_i^{(a)} \tag{2.9}$$

$$\frac{1}{X_\sigma} = \frac{4}{3}\frac{8\pi^2}{\lambda^3}\sum_{i=1}^{N}\left(S_i - S_i^{(a)}\right)\delta_i \tag{2.10}$$

In the equations above λ is the wavelength, N is the surface materials number, S the internal surface for the $i-th$ material, $S_i^{(a)}$ is aperture surface for the $i-th$ material and δ_i is the skin depth of the $i-th$ material, defined as:

$$\delta_i = \frac{1}{\sqrt{\pi f \sigma_i \mu_i}} \tag{2.11}$$

which in f is the signal frequency, σ_i the electric conductivity in $\frac{S}{m}$ and μ_i the magnetic permeability in $\frac{H}{m}$ of the $i-th$ material.

After the evaluation of the insertion loss for each cavity, it possible to do a link budget analysis considering every electric field generated in a cavity as a source in the adjacent cavities, due to leakage through apertures. It is possible to evaluate the electric field detected in a cavity by identifying all the possible paths between this and the cavity where the emitter is placed, introducing the correspondent insertion loss factor to find the total insertion loss between the transmitter and the receiver. I used this method to perform a received power analysis during the test phase, as explained in par. 4.5.1.

The validity of this method is demonstrated to be lower bounded in terms of frequency, in dependence on the tested space minimum dimension d_{min}. The minimum frequency f_{min} is evaluated as:

$$f_{min} = 5\frac{c}{d_{min}} \tag{2.12}$$

which in c is the light celerity in vacuum. As the minimum dimension of the mock-up where I did the test is 1.4 m, f_{min} is around 1 GHz. The 2.4 GHz used frequency is well above this limit.

2.1.3 Antenna diversity

One of the common way to restrain the multipath fading effect is the usage of multiple antennas at the receiver or at the transmitter side. In this way it is possible to combine two different signal corresponding to the emitted wave and select the best one to achieve a good and reliable communication. This technique is named as Antenna Diversity (AD) and the way the signal is acquired, processed and selected is determined by the used antenna diversity mechanism. The main antenna diversity techniques are space, frequency, polarization, field component, angle and time diversity [20].

Space diversity Multiple receiver antennas are placed at different locations, so that each antenna receives the transmitted signal through different paths. The received signals of the different antennas are therefore mutually decorrelated. The amount of decorrelation depends on the antenna separation. In most cases, a separation of approximately half a wavelength is enough [21].

Frequency diversity As the fading effects of the radio channel are not the same for different carrier frequencies, transmitting the information using different carrier frequencies may result in uncorrelated signals. The frequency separation, for which sufficient decorrelation is obtained, is related to the coherence bandwidth (eq. 2.5).

Polarization diversity This implementation takes advantage of the fact that the electromagnetic field polarization has different orientations at different positions in space. Using more than one receiver antennas differently oriented the received signals are uncorrelated and it is more likely that one of these match the signal polarization, resulting in a higher received signal level. A common implementation uses two diversity antennas which have a certain angle with respect to the horizontal, e.g. 45°and -45°, because this offer better performances than that a horizontal-vertical (0°and 90°) implementation.

Field component diversity This implementation takes advantage of the fact that at a certain location in a multi-path environment with many

reflections the electric field strength can be completely different from the magnetic field strength, so uncorrelated signals are obtained using antennas that predominantly couple to only one of the field components.

Angle diversity A good angle diversity implementation is established either if a directional antenna that can change its directivity pattern is used or if more than one directional antenna is used. By using a directional antenna one of the reflected waves resulting by multipath can be selected and the other ones can be suppressed, deleting the interference between two or more reflected waves.

Time diversity This technique uses a multiple transmission of the message in time at the same frequency across the radio channel. In this way the probability of good reception is increased, but the available bandwidth in terms of bytes per second is decreased.

2.2 Node Topologies

A wireless network can be made up of a quite big number of devices connected. For instance the IEEE 802.15.4 standard allows to manage up to 65535 nodes. These are characterized by a different role inside the network, tightly related to the node type. The main types of a IEEE 802.15.4 wireless node are three: Coordinator, Router, End Device [22].

Coordinator The Coordinator is the central node in a Star network, whereas is the top (root) node in a Cluster-Tree or in a Mesh network. Its task is to control the routing and has a main role when the network is initialized. In fact it selects the frequency channel to be used by the network and allows other devices to join to build the network, through the association sequence. Moreover it can send commands to manage the network (for instance to disassociate a node) and beacons to synchronize the data exchange between the devices and can provide security management and other network services. A IEEE 802.15.4 wireless network requires one, and only one, coordinator.

Router It acts as a bridge between the nodes connected to it and the network main Coordinator. A Router device is present in Cluster-Tree and in Mesh networks, whereas in a Star network its tasks are achieved

by the Coordinator. The existence of routers allows to logically break the network in simple subsets, enabling an easier routing management.

End Device They send and receive messages, following the routing path defined by the network topology. They cannot relay messages or allow other devices to join them. In a Star network, they are defined as perimeter nodes, whereas in Tree and Mesh topologies networks, they are named leaf nodes. Anyway they are always at the extremities of a network. In a IEEE 802.15.4 network they are often battery-powered and, when not in transmission or reception mode, they can sleep in order to save power.

2.3 Network Topologies

The usage of a wireless transceiver provided device is tightly linked to the topology of the network which of it is part and to the role the device has inside the network. Several network topologies have been developed, to accomplish a wide range of different applications and requirements. Moreover two advantages of the wireless technology are the high freedom of placing and adding the network components, allowed by the lack of harness and the capability to manage the evolution of the network shape over the time, which can be caused by several factors, as the lack of power that leads a device to turn off, or a temporary obstacle which disturb and block the link to a network node. In fig. 2.1 several network topologies are shown, which in the green circles are the simple nodes, the yellow ones are the routers, and the red ones are the network coordinators. Three mean network topologies are supported by the standard used by the tested device: star, mesh (peer-to-peer) and cluster-tree.

Star In a star network a central device acts as coordinator for the full network. It has control functionalities and handles the building of the network (allowing nodes association and disassociation) and the information routing. All the nodes can communicate only with the central device, whereas the central node can communicate with all the network device. This is the network type implemented for the test phase described in par. 4.5.1.

Mesh (Peer-to-Peer) In a mesh network the transport of data can be done with multiple link or multiple hops in succession, therefore this type is

referred to as multi-hop network. The existence of multiple links creates a redundancy which makes the network more reliable in comparison to a star type one, but it requires a more complex management and routing algorithm implementation.

Cluster-Tree Several devices groups make sub-network, namely clusters, including their coordinator, which acts as a router inside the full network. There routers are then connected to the main network coordinator. The result is a less complex routing management in comparison to the mesh type.

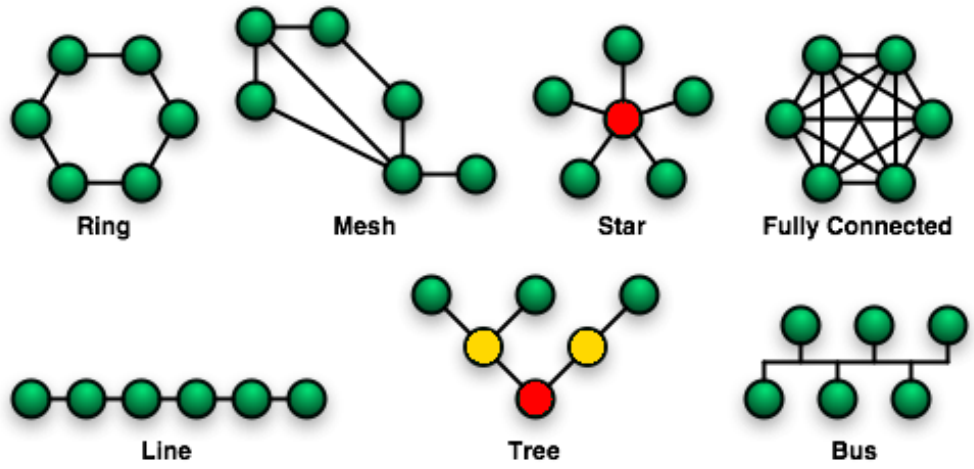

Figure 2.1: Network topologies

Even if for most of the cases the main network types explained above, combined with a good routing and management algorithm implementation, are able to accomplish the required tasks, in case no-one of these is suitable to the application to develop, it is always possible to build an Ad-hoc network. For instance only an Ad-hoc network provide the capability to achieve distributed (decentralized) operation, supporting dynamic topologies where roaming wireless nodes enter and leave the network in a random fashion [23].

2.4 Communication System Models

In the early 1980s the need to have a reference standard to understand and build a working communication system leaded the International Organiza-

tion for Standardization (ISO) to develop the Open Systems Interconnection (OSI) model. Even if other models have been proposed (as the 5 layers TCP/IP), the OSI example is still nowadays a reference point to understand and develop a network communication system. A brief introduction to this model is necessary to fully understand the IEEE 802.15.4 standard, used by the tested device.

2.4.1 OSI Model

The Open Systems Interconnection (OSI) reference model is an abstract model of how a communication system works [24]. It divides the full system in seven parts, called layers, each of them has its own functionalities, providing a service to the upper layer and receiving a service from the layer below. The OSI model orders the layers from lowest level to highest [25]. The total block of the seven layers forms the OSI stack, made by two main groups: the upper layers and the lower layers, as shown in fig. 2.2. Each layer within an end device inside a network communicates at the same layer within a different end device.

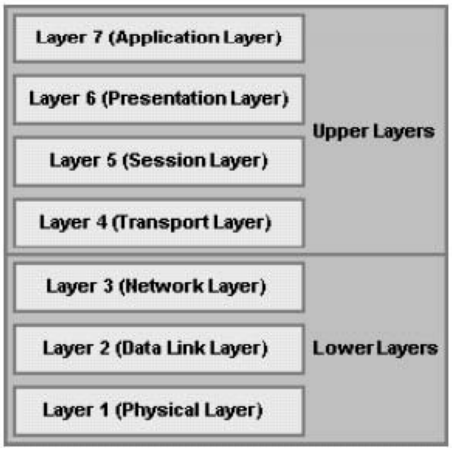

Figure 2.2: OSI model

The first three layers are media layers and have low level functionalities, for instance the PHY (Physical Layer) is related to the physical characteristics of the communication link, typically electrical signals. Cables, peripherals, pins are all part of the Physical Layer, which in a network receives data from another device and pass them to the next layer, the Data Link layer. This

is responsible to regulate the communication through two network members, checking errors inside the data frame, doing the encoding operations and managing the frame synchronization. These functionalities are split between two sub-layers: the Medium Access Control (MAC) and the Logical Control Link (LLC). The access of a device to the transmission medium is dealt to the MAC layer, which manage data transmission and reception through addressing operations , whereas error checking, flow control and frame synchronization are dealt to the LLC layer. The routing between different networks is managed by the Network Layer (Layer 3), which also defines logical addressing and packets fragmentation, to make these compatible with the maximum transmission packet size allowed by the medium. Examples of this layer are the common Internet Protocol (IP) and Internetwork Packet Exchange (IPX).

The upper four layers are called also host layers and have high level functionalities. The Transport Layer (Layer 4) manages the flow control and the error recovery, handling potential retransmissions in case of wrong communication and acknowledgements in case of successful one. A very common example of this layer is the complementary of the Internet Protocol, namely the Transmission Control Protocol (TCP). The Session Layer (Layer 5) is responsible to start, coordinate, manage and terminate the communication sessions. It includes also the management of multi-directional communications, namely simplex, half-duplex (as the walkie-talkies) or full-duplex (as the phone or the RS-232 triple wired); examples of this layer are the Data Link Control (DLC) and the Zone Information Protocol (ZIP). The sixth layer is the Presentation Layer, which makes the data understandable and usable by the Application Layer. It makes the data independent on the representation and syntax, mapping the data to Application Layer objects and managing the compression and the encryption of them. JPEG, ASCII, MPEG are all examples of the Presentation Layer. Above all there is the Application Layer, which provides data to (and receives data from) the Presentation Layer. It identifies the QoS (Quality of Service), handles the security of the access to the network and provides the features to use all the network services (e.g. data transfer). It is the interface between the network and the application, as are TelNet, the Hypertext Transfer Protocol (HTTP) and the File Transfer Protocol (FTP).

The entities managed by the layers, named above as *data*, are really defined as Protocol Data Units (PDU) and are *bits* at Physical Layer level, *frames*

at Data Link Layer level, *packets* for the Network Layer and *segments* for the Transport Layer. They are defined as *data* for the last three (Session, Presentation, Application) layers. During the transmission phase, every entity managed by a layer is passed to the layer below putting a header and, in some cases, a footer (trailer) to the real data to pass (the payload). In this way the payload of the Layer 7 is passed to the Layer 6 adding a header, so making a Protocol Data Unit and becoming a payload for the Layer 6, which adds its header to pass its PDU to the next Layer, and so on, until the Physical Layer translates the full Protocol Data Unit to a bit stream to send. This process is also called encapsulation. The reception phase follows the opposite route, removing the header (and the trailer if present) corresponding to that stage from the received data, before passing it to the layer above.
A practical example to understand how the OSI model represents a communication system is the connection to a Web site: at the Application level (Layer 7) the user types the address to reach using a browser. The target is identified by an IP address, which could be directly written inside the browser. If a format conversion is necessary this is performed by the Presentation Layer, then the Session Layer opens a call to contact the server that matches the address to reach. The Transport Layer, which in this case is the TCP, creates a segment which is sent to the target IP address. If the IP address is outside the Local Area Network (LAN), the message has to be directed to the router and the communication with this is managed by the Network Layer, which encapsulates the correct packet and send it to the Ethernet card driver. This can be considered as the Data Link Layer, which builds a frame putting the target address information inside the header. At this point the Physical Layer, made by the twisted cable which connects to the Local Area Network, completes the transmission. The opposite path, from the Layer 1 to the Layer 7, is made by a packet which is received by the user from the target address.

2.5 IEEE 802.15.4

The IEEE formed the 802 committee in February 1980 with the aim of standardizing LAN protocols. This resulted in the IEEE 802 series of committees that sit to develop worldwide standards for communications. Within the OSI model, the Data Link layer was split into two, the Media Access Control

(MAC) sub-layer and the 802.2 Logical Link Control (LLC) sub-layer.

The development of a space wireless application has to take into account several factors, which lead to choose the right standard to follow. First of all, the application could require a well specific network topology (referred to par. 2.3) and this has to be compatible with the chosen standard, for instance the IEEE 802.15.4 supports Star, Mesh and Cluster-Tree network topology. Moreover the transmission power is another important feature as it is linked to the power consumption, in turn linked to the power supply lifetime, then it affects the distance range between communicating devices. In the end the amount of data to exchange, which affect the needed Data Rate, has to be compliant with the maximum value guaranteed by the standard. The IEEE 802 develops Local Area Network (LAN) and Metropolitan Area Network (MAN) standards, mainly for the lowest 2 layers of the ISO Reference Model for Open Systems Interconnection [26]. In tab. 2.1 are shown some WPAN and WLAN standard features, all these are considered suitable for space application and putting in comparison the data rates values and the power consumption indications between the standards, the IEEE 802.15.4 seems to be the best choice for low power, low data-rate, and low duty cycles applications, allowing the development of battery supplied devices working for long time, like a smart sensor.

Table 2.1: WLAN/WPAN details

IEEE standard	**Data-rate [Mbps]**	**Frequency band**	**Range [m]**	**Network Topology**	**Power**	**Max Nodes**
802.11	1,2,11	2.4 GHz	150	P2M[1]	High	32
802.11a	6,9,12,18,24,54	5.8 GHz	150	P2M	High	32
802.11b	1,2,5,11	2.4 GHz	150	P2M	High	32
802.11g	54	2.4 GHz	150	P2M	High	32
802.15	0.02, 0.25	868, 915 MHz	10			
	11, 55	2.4 GHz				
802.15.1	1	2.4 GHz	10	Ad hoc	Medium	8
802.15.3	55	2.4 GHz	10	Ad hoc	Medium	
802.15.4	0.04	900 MHz	10 to	Star,	Very low	255
	0.25	2.4 GHz	100	mesh		65535

[1] P2M: point-to-multipoint

2.5.1 Supported devices

The IEEE 802.15.4 standard supports two types of device: Full Function Device (FFD) and Reduced Function Device (RFD). Full Function Devices have three possible operative modes: WPAN coordinator, simple coordinator and node, whereas a Reduced Function Device can operate only as node, because a FFD can communicate with both FFD than RFD, whereas a RFD can communicate only with a FFD.

2.5.2 Supported networks

Three network types are supported by the IEEE 802.15.4 standard: Star type, Mesh (named also as Peer-to-Peer) type and Cluster-Tree type.

The Star type is made up of one FFD which operates as the network coordinator and several RFDs that act as nodes. This is the network type implemented during the test phase.

The Mesh network includes several devices able to communicate each other without passing through the coordinator, which is only also in this case. As every node is a FFD, this kind of network is well suited for scenarios that require self-configuring or Ad-hoc networks.

The Cluster-Tree network is made up of several nodes subsets that make smaller networks. These have their own simple coordinator which act as a router between the subset and the other part of the network. The subsets are defined as clusters and are coordinated by cluster-heads which are in turn coordinated by one FFD that acts as the network coordinator.

2.5.3 Layers Features

As said at the beginning of the par. 2.5, this standard refers to the first two layers of the OSI model. The Physical Layer is split into two components with different tasks: the PHY data service deals with the Physical Protocol Data Unit reception and transmission, whereas the Physical Layer Management Entity (PLME) provides management and control features. The main tasks of the Physical Layer are:

- channel choice, between 27 available channels (depending on the selected frequency band)
- Energy Detection (ED): power scan and detection on the used channel

- radio transceiver management: switch on/off the radio and packets transmission/reception
- Clear Channel Assessment (CCA): scan of the channel and detection of idle/busy state
- Link Quality Indicator (LQI): indication of the quality of the link.

Two possible frequency bands are implemented in the standard, with different bit rates and modulation techniques, all the characteristics are reported in tab. 2.2 [12].

Table 2.2: IEEE 802.15.4 Frequency bands features

PHY	Frequency	Spreading parameters		Data parameters		
(MHz)	band (MHz)	Chip rate (kchip/s)	Modulation	Bit rate (kb/s)	Symbol rate (ksymbol/s)	Symbols
868/915	868–868.6	300	BPSK	20	20	Binary
(optional)	902–928	600	BPSK	40	40	Binary
868/915	868–868.6	400	ASK	250	12.5	20-bit PSSS
(optional)	902–928	1600	ASK	250	50	5-bit PSSS
868/915	868–868.6	400	O-QPSK	100	25	16-ary Orthogonal
(optional)	902–928	1000	O-QPSK	250	62.5	16-ary Orthogonal
2450	2400–2483.5	2000	O-QPSK	250	62.5	16-ary Orthogonal

Both of the frequency bands use a Direct Sequence Spread Spectrum (DSSS) modulation technique. It means that every symbol (of 4 bit length) is multiplied by a Pseudo-Noise sequence, of different length depending on the used frequency band, before been modulated. Inside the 2.4 GHz frequency band (2400 ÷ 2483.5 MHz) the data rate is 250 kbps and there are 16 channels (11 ÷ 26) with a 3 MHz bandwidth and a 2 MHz span. Therefore the span between the channel central frequencies (f_c) is 5 MHz and these can be easily calculated as:

$$f_c = 2405 + 5(k - 11) \qquad [MHz] \tag{2.13}$$

with the channel number k = 11 ÷ 26. The standard defines that the tolerance of the central frequency and of the data rate is ± 40 ppm. Inside the second band the data rate is 20 kbps for the 868.3 MHz channel and 40 kbps for the 10 available channels between 902 and 928 MHz. A lower bit rate leads to less susceptibility to noise and interferences, even if it provides

a lower available throughput. Moreover a higher transmission frequency is more affected by path loss, so that the communication coverage range is lower. The advantage of a higher frequency is the smaller time required to send data, due to a higher bit rate. The minimum transceiver sensitivity suggested by the standard is $-85\ dBm$ for the 2.4 GHz band, whereas is $-92\ dBm$ for the 868.3 $\div$ 928 MHz band

The selection of the channel is performed after an Energy Detection scan. Inside a range of around 40 dB, an estimation of the power of the received signal inside the bandwidth of a chosen channel is mapped in a 8 bit unsigned number (0 to 255), where the lowest value (0x00) indicates a detected power less than 10 dB over the sensitivity of the receiver. The standard specifies that inside the 40 dB range the reading operation has to be linear with a tolerance of ± 6 dB.

The LQI estimation is an important feature of the standard. It is a characterization of the link quality, done for every packet received. This estimation can be done using the information of the Received Signal Strength Indicator (RSSI), which indicates the strength of the signal, or doing an estimation of the Signal to Noise Ratio (SNR), or combining both of the ways. Also the LQI value is mapped into a 8 bit unsigned number (0 to 255)

The CCA is a measurement of the power level present inside the chosen channel. As the IEEE 802.15.4 medium access is of shared type, namely Carrier Sense Multiple Access (CSMA), every device listens to the medium and uses it only if it is idle, otherwise it waits for a defined amount of time defined in the standard. This way to access the medium leads to compatibility problems with other standards which use the same frequency, as Wi-Fi or Bluetooth [27]. The evaluation of the channel availability can be performed in three ways:

CCA Mode 1: if the energy detected is above the defined threshold (typically around -78 dBm) the channel is considered busy, even if the modulation is different compared to the one used by the standard.

CCA Mode 2: if it is detected a carrier with the same modulation of the standard, the channel is assessed to be busy. It is done no measurement of the strength of the signal.

CCA Mode 3: the channel is assessed to be busy only if the modulation detected is the same of the standard and the power of the signal is above a threshold.

As previously said in par. 2.4.1 every data is passed from a layer to the upper layer putting a header. In this way the full data frame which is passed is called Protocol Data Unit, whereas the effective payload is named Protocol Service Data Unit (PSDU). The Physical Layer Protocol Data Unit (PPDU) is the packet that, after modulation, is transmitted. The transmission starts from the Least Significant Bit (LSB) and the maximum length of a PSDU is 127 octets (or bytes). In fig. 2.3 are shown the other components of the PPDU.

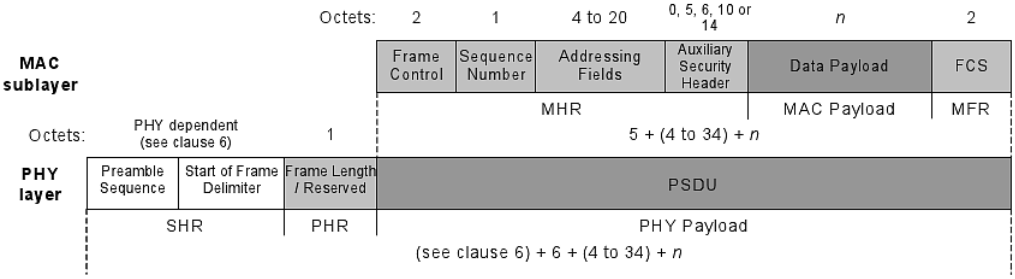

Figure 2.3: PPDU and Data MPDU format

These are the synchronization header (SHR), which allows the symbol synchronization, containing the Preamble Sequence and the start-of-frame delimiter (SFD) fields, and the PHY header (PHR), containing the length of the PHY payload in octets. The PPDU payload makes the MAC Layer Protocol Data Unit (MPDU). The second layer implemented in the standard is really an OSI Layer 2 sublayer: the Medium Access Control Layer. It is split in two different entities with their own tasks: the MAC Data Service Unit (MDSU) manages the MPDU reception and transmission, whereas the MAC sublayer Management Entity (MLME) has a control functionality. The main tasks of the MAC layer are:

- beacon, acknowledgement and data frame management and control
- channel access control
- Guaranteed Time Slot (GTS) management
- device association/disassociation inside the network
- security and encryption features.

Four packet types are supported by this layer:

- beacon, used by the coordinator to verify the functionality of the link and eventually of the associated device
- data, used to transfer data
- acknowledgement, used to confirm a right reception
- command, used by the coordinator to configure and control the nodes

As the data frame transmission can require an acknowledgement answer, it is implemented an error correction functionality which leads to retransmit the packet if no answer is received.

The access to the medium is not deterministic, unlike Time Division Multiple Access or Frequency Division Multiple Access, but the channel is shared. When several devices want to use the same channel at the same time a contention exists and it can leads also to collisions. This medium access way is useful when the medium usage is not the same for all the devices, so that it is not efficient to give them equal resources, like time slots or a frequency. If the algorithm which manages the medium access works properly, it gives more resources to the device which require them, without waste of time or used frequency. The implemented algorithm is the Carrier Sense Multiple Access with Collision Avoidance (CSMA-CA), which avoids collisions sensing the medium and using it only when it is detected to be idle. The algorithm is the following [12]:

1. initialize the number of times (NB) and the backoff exponent (BE) to zero
2. delay for a random number of complete backoff periods in the range 0 to 2^{BE}–1
3. send a request to PHY to perform a CCA
4. if the channel is idle, transmit, otherwise shall increment both NB and BE by one, ensuring that BE shall be less than *macMaxBE*
5. if the value of NB is less than or equal to *macMaxCSMABackoffs*, the CSMA-CA algorithm shall return to step (2). If the value of NB is

greater than *macMaxCSMABackoffs*[1], the CSMA-CA algorithm shall terminate with a channel access failure status.

The ordinary way to apply it is without beacon (unbeaconed mode) without using superframe, neither time slots. In the standard it is also implemented a slotted version with the usage of periodic beacons which give time slots, but no details are given in this thesis about this because the tested device was used with the unslotted version of the CSMA-CCA algorithm.
The four MAC frame types have the same main structure, shown in fig. 2.4

<table>
<tr><td>Octets: 2</td><td>1</td><td>0/2</td><td>0/2/8</td><td>0/2</td><td>0/2/8</td><td>0/5/6/10/ 14</td><td>variable</td><td>2</td></tr>
<tr><td rowspan="2">Frame Control</td><td rowspan="2">Sequence Number</td><td>Destination PAN Identifier</td><td>Destination Address</td><td>Source PAN Identifier</td><td>Source Address</td><td rowspan="2">Auxiliary Security Header</td><td rowspan="2">Frame Payload</td><td rowspan="2">FCS</td></tr>
<tr><td colspan="4">Addressing fields</td></tr>
<tr><td colspan="7">MHR</td><td>MAC Payload</td><td>MFR</td></tr>
</table>

Figure 2.4: MPDU general format

The Frame Control field is 2 octets in length and contains information defining the frame type, addressing fields, and other control flags. The Frame Control subfields are:

Frame Type is 3 bits in length and defines the frame type between the four available (Beacon, Data, Acknowledgment, Command)

Security Enabled is 1 bit in length, if set to one it indicates that the frame is protected by the MAC sublayer

Frame Pending is 1 bit in length and its value is one if the device sending the frame has more data for the recipient

Acknowledgment Request is 1 bit in length and specifies whether an acknowledgment is required from the recipient device on receipt of a frame (data or MAC command)

PAN ID Compression is 1 bit in length and specifies whether the MAC frame is to be sent containing only one of the PAN identifier fields when both source and destination addresses are present

[1] *macMaxBE* and *macMaxCSMABackoffs* are thresholds defined by the standard.

Destination Addressing Mode is 2 bits in length and indicates if the Destination Address field contains a 16 bits field (Short Address) or 64 bits (Extended Address)

Frame Version is 2 bits in length and specifies the version number corresponding to the frame (IEEE Std 802.15.4-2003 compatible or not)

Source Addressing Mode is 2 bits in length and indicates if the Source Address field contains a 16 bits field (Short Address) or 64 bits (Extended Address)

The Sequence Number field is 1 octet in length and specifies the sequence identifier for the frame. For a data, acknowledgment, or MAC command frame, it is used to match an acknowledgment frame to the data or MAC command frame.

The Destination PAN Identifier field, when present, is 2 octets in length and specifies the unique PAN identifier of the intended recipient of the frame. A value of 0xffff in this field represents the broadcast PAN identifier, which is accepted as a valid PAN identifier by all devices currently listening to the channel. It is included in the MAC frame only if the Destination Addressing Mode subfield of the Frame Control field is nonzero.

The Destination Address field, when present, is either 2 octets or 8 octets in length, according to the value specified in the Destination Addressing Mode subfield of the Frame Control field and specifies the address of the intended recipient of the frame. A 16-bit value of 0xffff in this field represents the broadcast short address, which is accepted as a valid 16-bit short address by all devices currently listening to the channel. It is included in the MAC frame only if the Destination Addressing Mode subfield of the Frame Control field is not null.

The Source PAN Identifier field, when present, is 2 octets in length and specifies the unique PAN identifier of the originator of the frame. It is included in the MAC frame only if the Source Addressing Mode and PAN ID Compression subfields of the Frame Control field are not null and equal to zero, respectively. The PAN identifier of a node is initially determined during association to a coordinator on a PAN.

The Source Address field, when present, is either 2 octets or 8 octets in length, according to the value specified in the Source Addressing Mode subfield of the Frame Control field and specifies the address of the originator

of the frame. This field is included in the MAC frame only if the Source Addressing Mode subfield of the Frame Control field is not null.

The Auxiliary Security Header field has a variable length and specifies information required for security processing. This field is present only if the Security Enabled subfield is set to one.

The Frame Payload field has a variable length and contains information specific to individual frame types. Further details are in [12, par. 7.2.2].

The Frame Control Sequence (FCS) field is 2 octets in length and contains a 16-bit ITU-T Cyclic Redundancy Check (CRC).

Chapter 3

GP500C device

The purpose of the activity is the evaluation of an IEEE 802.15.4 compliant radio transceiver, provided by GreenPeak. The GP500C radio transceiver offers several interesting features, suitable for the development of an Intra-Spacecraft Wireless application, as the low power consumption (between 18 mA and 25 mA in communication mode, 30 nA in Event Sleep Mode) and the preamble-based Antenna Diversity mechanism, which promises an overall gain up to 9 dB on the link budget. Moreover the GP500C has an integrated real time MAC, which allows using a less powerful associated μC and a simpler software. In fact the integrated MAC manages the transmission and reception of the packets and the CSMA mechanism to access to the medium. In fig. 3.1 the traditional design and the GP500C design are put in comparison, underlining the integrated MAC feature. Then, the Packet-in-Packet resynchronization feature, which allows receiving, between two packets in collision, the one with a stronger RSSI, can be useful in hidden node situation, as a WPAN inside a spacecraft [28]. A radio transceiver device is obtained combining a GP500C chip with a 16 MHz crystal (and eventually with an optional 32 kHz crystal), some supply decoupling capacitors and the transmitter (receiver) antenna. The tested device is equipped with two printed circuit antenna, exactly two Planar Inverted-F Antennas (PIFA) placed at 90°each other and has an interface to the micro-controller implemented using a Serial Peripheral Interface (SPI) bus. The PCB containing the GP500C chip, the crystal, the SPI module and the necessary resistors and capacitors is named as *GP500C SPI module*. Further details about these components are given in Chapter 6.

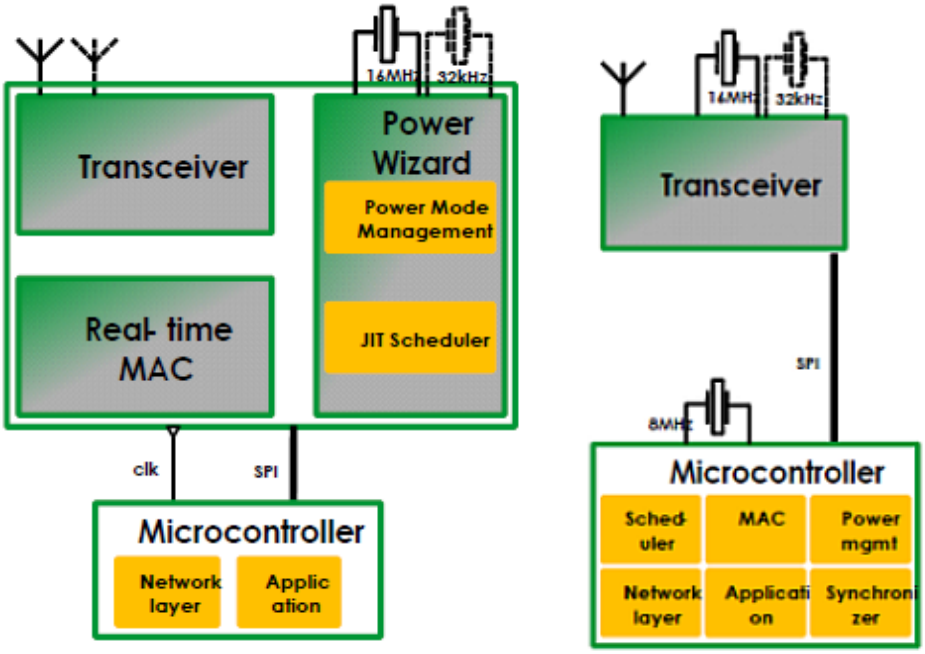

(a) GP500C design (b) Traditional design

Figure 3.1: GP500C vs traditional system block scheme

A picture of the *GP SPI module* device I tested, with in evidence the GP500C chip and the two PIFAs, is in fig.3.2.

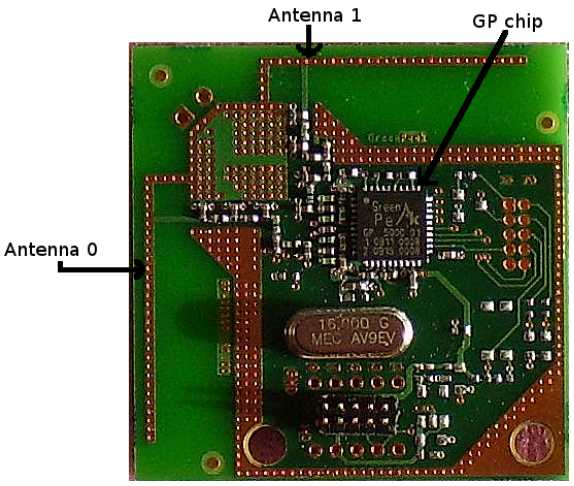

Figure 3.2: GP500C SPI module device

3.1 Power consumption

The GP500C low power consumption make it suitable for battery supplied applications, as a smart sensor feeded by a lithium button cell battery. An useful feature of the device is the battery lifetime monitor, which tracks the Voltage trend providing a warning in case of exhaustion. Moreover the chip has a Power Supply Management (PSM) functional block, which aims to do power management operation. This is specially useful when the device is used in combination with a micro-controller, as it offers three different power modes: master, slave and shared mode.

- **Master power supply mode**: the GP500C is the Master, whereas the μC acts as Slave. The GP500C manages the μC operation mode controlling when it is active and when it has to go to sleep, then waking it through an interrupt pin. Moreover the GP500C can supply the Clock and the Reset signals to the μC. As the μC is disabled when the GP500C is not active, the Master device has to be active when the Slave device is active. A wake up pin allows to make the GP500C active when an external event occurs while it is in sleep mode.

- **Slave power supply mode**: the μC is the Master, whereas the GP500C acts as Slave. The μC manages the GP500C operation mode, making it active or making it entering in one of the three supported sleep modes. This means that the μC has to be active when the GP500C goes from active to sleep mode and vice-versa. Clock and Reset signals are separated between the Master and the Slave device.

- **Shared power supply mode**: both the GP500C than the μC share the Power Supply Management, so that one can be in sleep mode while the other one is active. This mode allows to optimize the power consumption, as the GP500C integrated MAC can perform autonomously several operation (as packet transmission or reception) without need that the μC would be active. In this way each component has to be active only when it has to execute tasks.

The GP500C supports three different sleep modes which are useful to save power when no tasks have to be executed. During a sleep mode the device is in standby, maintaining the scheduling feature and the external interface pins functionalities. Thanks to the scheduling feature it is possible to program

the device to execute an event (e.g. a packet transmission) at a defined time, or multiple events (e.g. multiple transmission) with a defined time interval between them. This allows to define the power duty cycle of the device, setting it to perform operations at the desired time and to go to sleep for the rest of the time. The device is commonly supplied between 3.0 and 3.3 V, a summary of the current consumption for the main operative modes are shown in tab. 3.1 (referred to [28]).

Table 3.1: Power modes summary

Mode	Use	Current
Off mode	All Off	0 nA
Event sleep mode	Wake up on external trigger with data and state retention in between triggers	30 nA
32 kHz sleep mode	Scheduled wake-up, high accuracy	250 nA
16 MHz sleep mode	High duty-cycle scheduled wake-up, high accuracy	550 μA
Active idle mode	Radio OFF, SPI communication, security processing	2 mA
Active receive	Packet reception	25.5 mA
Active transmit	Packet transmission at 0 dBm	24.7 mA

For the test phase, the μC is used as a Master device, whereas the GP500C is used as a Slave. Event sleep mode, active idle, transmit and receive mode are used for the test sequence.

3.2 Event Scheduling

The Event Scheduling feature is possible because of an integrated timing engine which provides a time base with a maximum of 30 minutes and a resolution of $2\mu s$. The time base is generated using a 32 kHz or a 16 MHz clock, depending on the power saving mode chosen. If the 32 kHz clock is used, an interpolation is performed using the 16 MHz clock to reach the $2\mu s$ resolution. The time base is kept by the device also when it is in sleep mode and allows to schedule periodically events like packet transmission or radio enabling/disabling, to listen to the medium at the desired time, moreover it is possible to schedule interrupts to the μC to send it to sleep mode or to wake up it, allowing a further power saving. There are three main ways to schedule an event: using absolute time, relative time, or responding to an external event.

- **Absolute Event**: this mode allows to execute events at the desired time. It uses the reference time generated by the Event Scheduler, giving the possibility to schedule up to 16 events. If the device is active, it executes the event (e.g. sends a a packet) when the set time comes, otherwise if it is in sleep mode, it wakes up and executes the event at the defined time, then going back to sleep if programmed.

- **Relative Event**: this mode allows to perform an action a specified time after it is scheduled. If a relative event is scheduled, the GP500C device doesn't go to sleep. It is possible to schedule an immediate event, setting the relative time to zero.

- **External Event**: if this mode is used, an action is performed when the GP500C wake up pin is triggered. If it is active, it executes the event immediately, otherwise if it is in sleep mode, it wakes up and executes the event.

3.3 Hardware integrated MAC layer

The integrated MAC layer leads to no need to implement a MAC software to manage the operations performed by the MAC layer (par. 2.5.3). This leads to a simpler and smaller software, which means that a smaller micro-controller memory is required. Moreover, the GP500C can perform these operations autonomously, without need that the micro-controller is active, leading to power saving. For instance the GP500C can send and receive packets independently and can wake up the micro-controller only if they satisfy the addressing filtering criteria [12]. Then the integrated MAC perform an acknowledgement management, for instance when a packet is received and it has an acknowledgement request in the frame control field, the devices automatically answers transmitting an acknowledgement frame. In transmission mode, if a packet is transmitted including an acknowledgement request, it automatically enables the receiver to wait for the answer frame and check it. In case no answer is received in the proper time interval, a retransmission is automatically performed, repeating this operation until the maximum retransmission times number is reached (if this is the case, the packet transmission doesn't succeed). If no acknowledgement is used, when transmitting the MAC confirm to the micro-controller that the packet transmission succeeded, whereas when receiving it is processed to check if the address fields

match those of the receiver device.

Moreover the integrated MAC perform all the medium access operations. Each packet can be set to be transmitted using one of the three supported medium access modes: CCA, CSMA-CA or without check. If the former is selected, a clear channel assessment is performed before sending the packet. Alternatively it is possible to select a full CSMA-CA algorithm operation, which is IEEE 802.15.4 compliant and allows to avoid collisions. The latter choice allows to send the packet immediately, without listening the medium before the transmission. This is a risk, but it is useful especially for synchronization operations, for instance using beacons, which have to be sent at defined time interval, without the random wait time introduced by the CSMA-CA algorithm.

3.4 Antenna Diversity

A polarization antenna diversity mechanism is implemented on the GP SPI module using two antennas to receive data through two different means. Then the GP500C chip preamble based antenna diversity mechanism analyze the two signals and selects the one with the best SNR, taking it from the correspondent antenna. In this way this mechanism automatically switch between the two available antennas, selecting the one with the best SNR. In case of interference or noise sources, it selects the one with the best SNR, mitigating for instance the effect of multipath fading and leading to a valuable gain on the link budget. Otherwise if the SNR is good enough, the antenna to be used is arbitrarily selected.

3.5 Packet-in-Packet resynchronisation

The Packet-in-Packet resynchronisation feature allows to limit the received packet losses due to collisions. In case one coordinator device is configured in a network with multiple nodes sending information (this can be the typical case of a WSN), it can happen that when the coordinator is receiving a packet from one node, it is interrupted by the reception of a stronger packet coming from another node. In this case the GP500C receiver resynchronizes to the latter and continues to receive and process this packet, avoiding that both of the packets would have been lost. The resynchronization is always performed on the packet with the bigger strength of the signal.

Chapter 4

Test sequence

In this chapter I explain the sequence of tests I did, highlighting the reasons which justify each task, followed by the explanation of the way I implemented each phase and by the elements which affected the choices I did to accomplish all the tasks. Moreover it is introduced what I expected to find doing these tests, to put in comparison the expectations with the effective results, exposed in the next chapter.

4.1 Test sequence tasks and purposes

The purpose of the test sequence I designed is mainly the characterization of the GP500C radio device to assess its employment for a space oriented application, in particular for an AIT activity. An evaluation of the performances, in terms of transmission power, quality and reliability needs to be performed in several scenarios. It is necessary to evaluate the effect of the device interaction with the environment where test operations are performed to fully understand the performances achievable with the tested radio transceiver and to evaluate the effects of the antenna diversity technique in different scenarios. Then an evaluation of the device behavior during and after radiation exposure is required, in particular a Total Ionizing Dose test has to be performed and characterization of physical quantities and communication parameters is required.

To accomplish the tasks introduced above I designed a sequence of test I did inside the Avionics Laboratory, which is a representative environment of an AIT activity possible location, and inside a more specific application environment, as is the V-EX mock-up. Then the evaluation of the device

behavior while irradiated and after radiation exposure is accomplished with a specific operations sequence I designed, following the ESCC Basic Specification 22900 for TID test, performed in ESTEC Co-60 facility. Details about the work environments where I performed all the operations are in Appendix A. The test plan includes 5 different tasks to achieve, as shown below.

I. Functional test: this task verifies the capability and the reliability to communicate with the device, to configure it, to send and receive commands and data. It includes the development of the software necessary to perform all the required operations and the creation of an user friendly interface to make easier the execution of automated and time scheduled operations and data acquisition. All the devices planned to be used for the next tasks have to be submitted to this test.

II. Physical parameters test: this task aims to measure electrical quantities of interest, as current consumption or supply voltage. These quantities have to be measured in several operative modes during normal device working sessions, so giving reference values to be compared with the same quantities measured during the radiation test sequence.

III. Communication parameters test: the purpose of this activity is the measurement of communication parameters of interest and performances, as received signal power and quality. It includes an evaluation of the interaction with the test environment, in particular the effect of interference and multipath fading is evaluated putting in comparison the results obtained inside the Avionics Laboratory with the results of the same test performed in a reference and ideal environment, namely the anechoic chamber.

IV. V-Ex test: this is made building a GP500C devices WPAN in the Venus Express mock-up and evaluating link budget and communication performances between nodes. This aims also to evaluate the Antenna Diversity benefit in different scenarios, simulating several AIT activity situations.

V. Radiation response test: this test aims to investigate device response to radiation exposure, through electrical and communication parameters variation monitoring. A Total Ionizing Dose test has to be following a standardized sequence but adding the operations performed in previously made tasks II and III.

4.2 Functional Test

4.2.1 Description

This test was performed individually on each used device or couple of devices. The purpose of this test was to validate all the devices planned to be used for the next tasks, for instance up to 12 devices were needed to be operative at the same time in a WPAN for task III and IV of test plan. This aimed also to test the functionality of the developed software, which includes a C code and a LabView script, and the reliability of the interface created with the GP device. Two possibilities have been taken in consideration: a step by step development and an all in one previous development.

The former plans to develop the needed software step by step, using it to perform the operations not in sequence, but individually and testing not all the devices, but only those ones required by the task to be performed one by one. This way would allow a faster development and operation performing, even if it is less robust in terms of error correction and feedback and is less flexible. This happens because several operations and code functions are needed for more than one task of the test, for instance the association sequence is executed both if only two devices are used (one as coordinator and the other one as a end node) than if more than ten nodes are used, joined to a WPAN coordinator. Therefore in case that an error in the developed code would be found during the execution of a specific operation which comes after a task is performed, it would be necessary to repeat the test on the full sequence of tasks before it. Again in reference to the association example, in a step by step scenario it would be possible that the code implementing the joining sequence, used only with two devices, is working. At that point all the operations of the test sequence which plan to use only two devices can be performed. Then if the same base code (as the association sequence is the same) is used to build a network made up of more than one end node and an error in the joining sequence is found, it is possible that also the code used with only two nodes is wrong and it is only apparently working in that specific case. Then it would be necessary to repeat also the test or measurements performed using the code developed before.

The latter possibility leads to bigger software development time, creating not an ad-hoc code for every operation to be performed, but a general code which can be used in several scenarios. The advantage is that the functionality test to assess the reliability of the code and of the interface with the

GP device has to be performed only one time, as there is only one code. I followed this second way to develop the needed software and the interfaces with the devices.

4.2.2 Setup

All the devices have been used in combination with a Microchip Picdemz board, equipped with a PIC18LF4620 μC. In this way it has been possible to use the example software developed by GP and to build on it the code to perform all the operations required by the tests. All the devices have been powered by the power supply of the boards. The development of the software has been made using one GP device connected by the RS-232 port of the picdemz board to a PC. The communication with the device was possible using HyperTerminal or LabView. I tested each device individually or inside a WPAN, to validate the code in several scenarios, the same then repeated to perform the other tasks of the test sequence.

4.2.3 Test

The test consists in using a device, controlled by the LabView interface through the serial port, sending commands and verifying that the device reacts properly and that the wanted behavior is achieved. At the same way two or more devices have to be used to build a network and make them communicate. I did the first phase of the test in an office environment, connecting up to three devices to a PC through RS-232 serial interfaces. Then I repeated the test inside the laboratory where the next tasks would have been performed, to verify the absolute compatibility between the developed software and the available hardware.

4.2.4 Software Development

I built the C code starting from the 3 example codes provided by GreenPeak. The operations allowed by the example code are reported below.

- **Hardware Abstraction Layer (HAL) code**: this code is based on HAL functions and allows to use one device as a coordinator and another one as a node, it starts the association sequence managing the primitives calls and assigning to the joining node a short address

defined in the code. The association sequence is shown in fig. 4.1, further details about it are in [12, par. 7.1]. Once the two devices are joined, they start exchanging data packets at defined time interval until the devices are switched off. The data transmission primitive calling sequence is shown in fig.4.2, further details are in [12, par. 7.1]. It is implemented also the Energy Detection Scan and the CSMA-CA algorithm, but no interaction with the device is planned and only two devices can be used, as a third node would have been assigned the same 16-bit address of the second joined node.

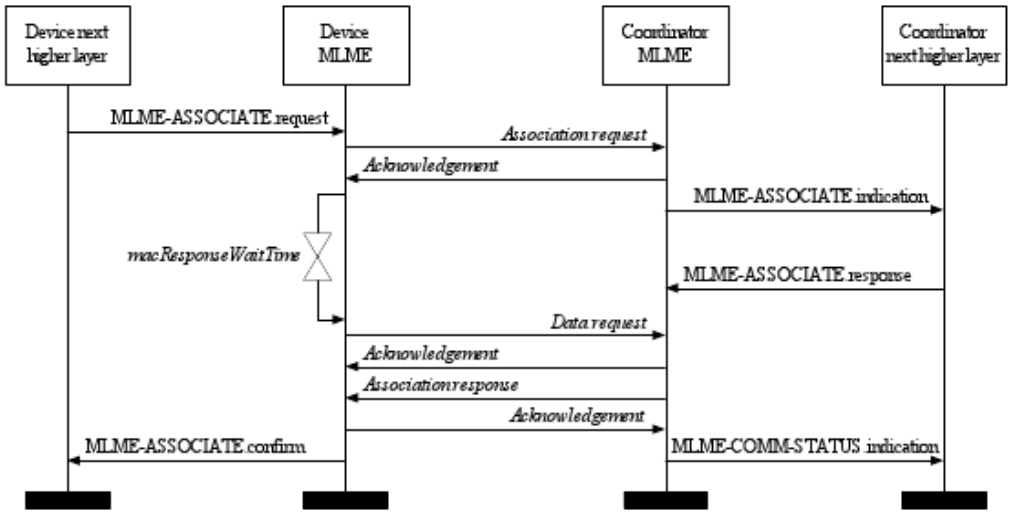

Figure 4.1: 802.15.4 devices joining sequence

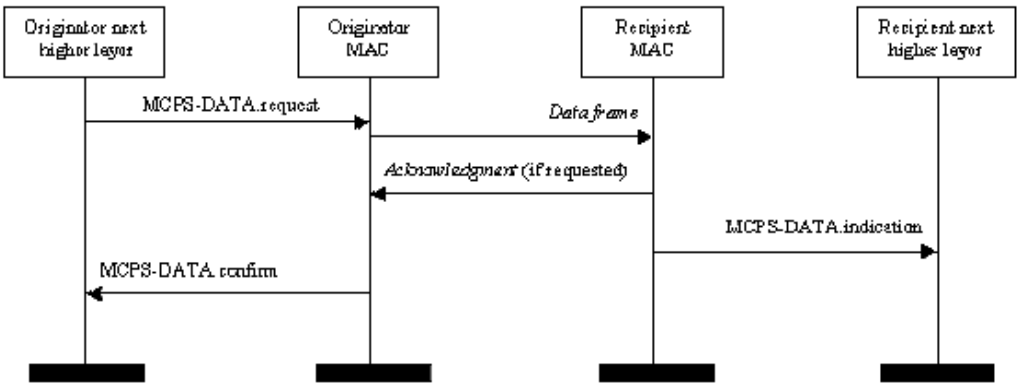

Figure 4.2: 802.15.4 devices data exchange sequence

Table 4.1: Setting parameters included in GreenPeak provided software

Setting Parameter	**Symbol**	**Possible values**
Transmission Power	P_{TX}	-12 ÷ 3
Antenna Diversity enabler	AD	0,1
Antenna to use	AN	0,1
Receiver enabler	RX	0,1
PiP enabler	PI	0,1
Channel to use	CH	11 ÷ 26
Sleep mode	SL	0 ÷ 2
Maximum backoff exponent	maxBE	1 ÷ 5
Minimum backoff exponent	minBE	0 ÷ 5
Maximum number of CSMA backoffs	MC	0 ÷ 5
Maximum number of transmission retries	MR	0 ÷ 5
CSMA-CA mode	CSMA	0 ÷ 2

- **Medium Access Control (MAC) Layer code**: this code implements the same operations of the HAL code, but using the MAC primitives, so taking advantage of the hardware integrated MAC of the device. A little interaction is allowed to the user because the association is allowed by the coordinator only when one of the two available button on the picdemz board is pushed, whereas the other button can be used to send data packets with a pre-defined payload to turn on or off the led on the boards of the node or of the coordinator.

- **Command Handler code**: this code implements an interaction with the device, that the user can exploit through a serial RS-232 connected to the board. It is implemented a state machine which reacts to commands and events. Input and output can be easily displayed using HyperTerminal. No association sequence is implemented in this code, neither other network functionalities (e.g. send commands or build a packet frame from user specified parameters, as data type, addresses, payload and so on). Instead, a full set of parameters is configurable with this code, shown in tab.4.1 with their range (referred to [12]) and symbol used in this document. Moreover full HAL for the used picdemz board and PIC18LF4620 μC is provided.

Details about example codes and available default commands are in [29], [30]. The main task I did has been the inclusion of the MAC-based application, with its network functionalities, inside the example command handler application which allows interacting with the device through a serial interface. Moreover I created from scratch new commands and functionalities to perform the operations planned by the test. Below are shown the new functionalities I developed, with their purpose and the way I did them. They are indicated in reference to the command associated inside the LabView interface, as like as the symbols in tab. 4.1.

SPAN: this command allows to set the 16-bit PAN Id. It reads the 4 digits on the serial interface (HyperTerminal or LabView) after the string SPAN and translates them in a 16-bit Unsigned number, using the predefined `Hal_SetPANID` function to set is as the Personal Area Network Identifier. I implemented this command to have the possibility to choose the PAN Id on the coordinator side and to see if the association sequence is correctly working. If this was the case, a node with a different predefined PAN Id in respect to the coordinator, after the joining sequence had the same PAN Id of the coordinator.

SSA: using this command I was able to change the 16-bit Short Address of the device. I used this command to debug the association sequence, as for the SPAN command, then in practice I assigned to every device a short address correspondent to the last 16 bits of the 64-bit long MAC address, which is unique. In this way I didn't have to manually assign a short address to every of the 20 devices I used.

PM: this command aims to set the Promiscuous Mode state parameter of the device, *macPromiscuousMode* [12, par. 7.5.6]. If it is on, the device accepts all the packets with a correct frame check sequence without any other filter level, otherwise it applies all the three filtering levels implemented in the standard. The *macPromiscuousMode* parameter is set by the predefined `Hal_SetPromiscuousMode` function.

RR: this command allows to read the value of one of the registers of the device. I used this command to check if the correct values are token by the register, as for instance the RSSI and LQI indexes. The 4 digits after the command are read as the 16-bit register identifier to read through the predefined `Hal_ReadReg` function.

WR: this command aims to allow the user to set directly parameters without passing through HAL or MAC functions. For instance the antenna to use can be set using a defined command or setting the corresponding register to the wanted value. I implemented this command for debugging purpose. It converts the first 4 digits after the command into the register address to change and the last digit into the 8 bit Unsigned value to assign to to the register through the `Hal_WriteReg` predefined function.

FFD: this command starts the association sequence as coordinator device. The joining sequence is shown in fig.4.1 and was available in the MAC based example software provided by GreenPeak. I included this sequence inside the command handler code, making the coordinator available to associate after the Energy Detection scan to identify the best channel frequency to set the network, and optionally assigning an user defined short address to the joining end device. The coordinator acts as a Full Function Device which enters in a state machine implemented using the time scheduling: after the initial scan to set the network channel, it continuously goes in Idle state waiting for joining devices and commands given through the serial interface.

RFD: I implemented this command to start the association sequence as a Reduced Function Device, typically an end node. Using the two buttons on the picdemz board I implemented the possibility to choose the data exchange mode between two alternatives: direct and indirect. In direct mode, the device sends data immediately, whereas in indirect mode the data to send is added to a transmission queue and sent to the recipient when a `Data_Request` is received. Using this mode the end node periodically asks the coordinator if there are available data, whereas in direct mode they are immediately sent by the device. I implemented both the possibilities starting from the predefined indirect mode, then I used especially the direct mode during the test phase. The end node executes a state machine created using the time scheduling, implementing the periodically data request if in indirect mode, or going in Idle state if in direct mode. In the latter case, the device waits for data from the coordinator or commands through the serial interface.

EXIT: I implemented this command to exit from *end node* or *coordinator* mode. This is useful to restart the joining sequence for any reason or to

use the devices in different way than inside a network, after it is joined. I created this command adding two states to the state machine inside the coordinator and the node mode codes, which unschedules all the planned operations, using the predefined `UnscheduleEvent` function.

RESET: I created this command to reset the device by software. Otherwise reset is possible using the button on the boards but this solution is unpractical in a scenario where the devices are not hand available, as during the test phase. After unscheduling all the operations through the `UnscheduleEvent` predefined function, the device is reset by the predefined `ResetSystem` function call.

ASSP: I created this command to allow or deny association. I used it to deny the association after all the nodes I wanted to use were joined. In this way unexpected joining were not allowed. I was able to create this command using the MAC based predefined function `MESetRequest` which allows to set several network parameters. The setting parameter in this case is `joinPermit`, an Unsigned 8 bits number obtained by the digit written after the command.

VERB: I set the logging level to obtain different information, depending on the requirements of the test to perform. I used this to have the maximum amount of useful information in a minimal string output. In fact I didn't need the same information for all the test, as will be more clear after the remote control functionality explanation in this paragraph. I used the predefined `printHT` function, which sends data to the RS-232 port.

TD: I created this command from scratch to send a packet using the MAC frame builder of the GP chip. The predefined way to send a packet is in fact using the HAL based function, forcing the user to define the full MAC MPDU (par. 2.5.3 or [12]). Instead using this command it is possible to define only some parameters (destination short address and PAN ID, data type, number of packets to send and time interval between them, data payload) and let the MAC predefined block to build the frame to send, scheduling a `DataRequest` function call. I used this command in some tests scenarios, for instance when I had to send packets periodically and to more than one device.

TDL: I implemented this command to set the transmitting/receiving mode, depending on the test to do (Communication, Radiation, Mock-up). For instance the radiation test payload is made up of 3 bytes repeated 3 times to create a 9 octets MSDU updated every time a packet is sent. This cycle is started setting a flag and scheduling a `DataRequest` function call with this command.

Remote control: I created this feature from scratch. Sending a packet with a specific payload header (the first 2 payload bytes), the following bytes are interpreted as the parameters to set. In this way it is possible to remotely set a device (typically an end node), without using the RS-232 interface. Moreover an answer packet is received, including a payload with all the parameters set, the RSSI and the LQI indexes. I used this to obtain the communication parameters of the two sides transmission: from coordinator to node and from node to coordinator. Moreover I was able to set the devices "wirelessy", allowing an easy employment and setting of up to 13 devices at the same time with only one connected by a serial cable. The setting parameters sequence making the 9 bytes payload, is formatted in the way shown here below.

Byte	1	2	3	4	5	6	7	8	9
Parameter	P_{TX}	RX	AD	AN	maxBE	minBE	MC	MR	CSMA

An example of the received packet and its output on the LabView interface screen is given in fig. 5.1.

Moreover the logging through the RS-232 port has been done test-oriented. In general the received packet logging is made up of the frame type (referred to par. 2.5.3), the received packet length, the Source Short Address, the payload, the LQI and the RSSI indexes. The received payload visualization is different for the test tasks to perform, as different information are needed, for instance when using the remote control packet, also the RSSI and the LQI of the packet sent from the device which receives an answer are shown. I achieved this modifying the predefined MAC based `Data_Indication` function. Finally I created other functions to achieve the tests, e.g. to evaluate the PER during the radiation test, two functions create a 9 bytes payload, updating 3 indexes every time a packet is sent by the transmitter or received by the receiver, so that the next packet payload to receive is always known.

I programmed the micro-controller using the Microchip provided MPLAB IDE and ICD 2 programmer, compatible with the used PIC18LF4620.

Because of the complexity and the high level of automation required in most of the cases to perform the test tasks, a LabView interface is needed, in fact it is impossible to accomplish all the objectives using HyperTerminal or a simple SPI connection to the device to send commands and receive answers. I created a HyperTerminal interface in LabView, together with the commands to build an IEEE 802.15.4 compliant MAC frame and to perform operations sequences. The higher part of the front panel of the LabView developed software to do the test inside the mock-up is shown in 4.4, the corresponding block diagram in fig. 4.3.

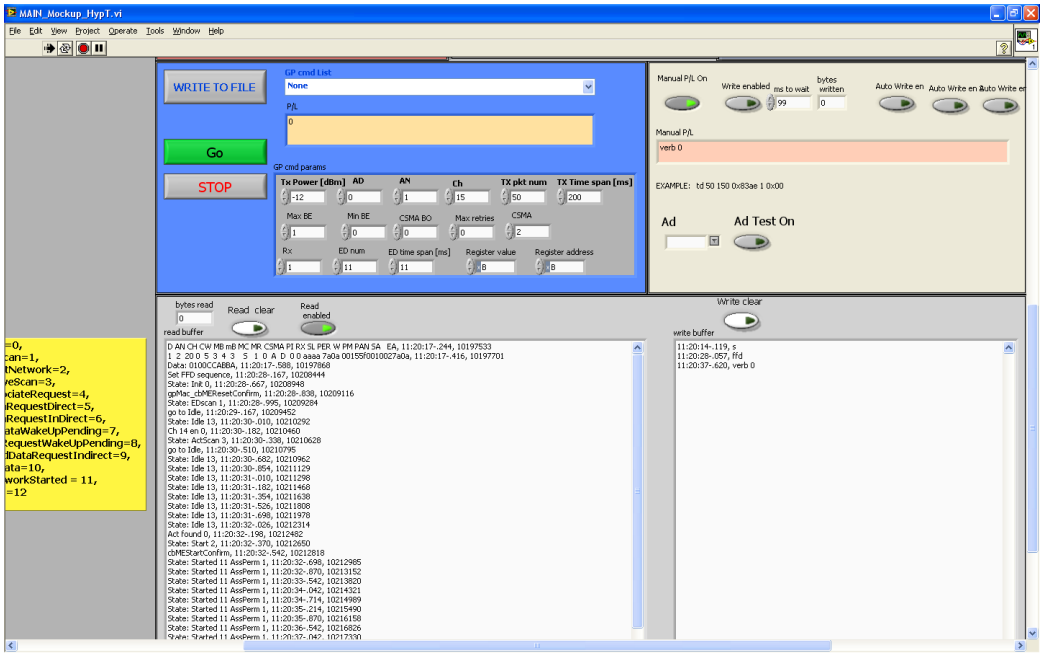

Figure 4.3: Front panel of a developed LabView software

I developed several interfaces like that one in fig. 4.3, simply disabling the useless part for the specific test to perform. The main structure is made up of the main blocks explained below.

Serial interface block: this block uses the Virtual Instrument Software Architecture (VISA) serial function of LabView and gives an output like the HyperTerminal screen, which is simply a string updated at every written command or received output on the RS-232 port. The

user can define the full serial parameters set, as the termination char, the timeout, the baud rate, the serial port (e.g COM1, COM2 and so on). It fully manages the reading/writing operations, putting on the screen the time and a tick count when requested.

Frame control block: this is the block that builds the 2 bytes frame control field of the MPDU. The user defines all the Frame Control fields, as the frame type, the PAN Id compression or the addressing modes, then the block builds the 2 octets field after some compatibility checks (referred to [12, par. 7.2.1]).

MHR block: I created this block to build the MAC MPDU header from user defined parameters, as PAN Id or Source and Destination Address. It allows to create compressed frame if the PAN Id compression field is one and adds the Auxiliary security header only if the Security Enabled field is not null, as indicated in [12, par. 7.2].

Control Payload builder: I created a block fully aimed to build the remote control payload from the user defined setting parameters. It receives all the setting parameters as inputs and builds the remote control payload adding the apposite header to be identified as a control packet by the receiver. This is especially useful for time scheduled operations or inside flat sequences with packets sent periodically, making possible to define the setting parameters only one time, before that the sequence starts.

MSDU builder: I developed a block which aims to manage the payload of the MPDU. In case it is a data frame, the payload can be manually specified or can be a 7 octets MLS randomly generated by the MLS generator. In case it is a command or a beacon frame, this block builds the payload compliant to [12, par. 7.2.2].

GP command block: this block implements all the commands defined inside the C code which controls the μC connected to the GP500C device, both the GP predefined commands than the new commands I created. With an user friendly drop-down menu in the front panel it is possible to select the command to send to the device and this block creates the equivalent string to output on the serial port.

MLS generator: this blocks uses the LabView Binary MLS generator which generates a maximum length sequence of ones and zeros using a modulo-2 primitive polynomial of the order specified by the user. It is aimed to create a MLS payload for a PER test.

Data output block: I created a block to manage the data exporting. When an input is given (pushing a button on the LabView front panel) or every given time intervals, this blocks creates comma separated files containing the input command buffer (the instructions typed by the user) and the output buffer (containing the GP500C answer), checking that the maximum file length is Excel compatible: if the rows number exceeds the maximum rows number allowed by Excel (65535 for the used 2003 version) it creates another file deleting the buffer already exported in another file. I used this block for every test I did and it was especially important during the Radiation test, because the devices continuously created output information for 168 hours, automatically managed and exported by this block.

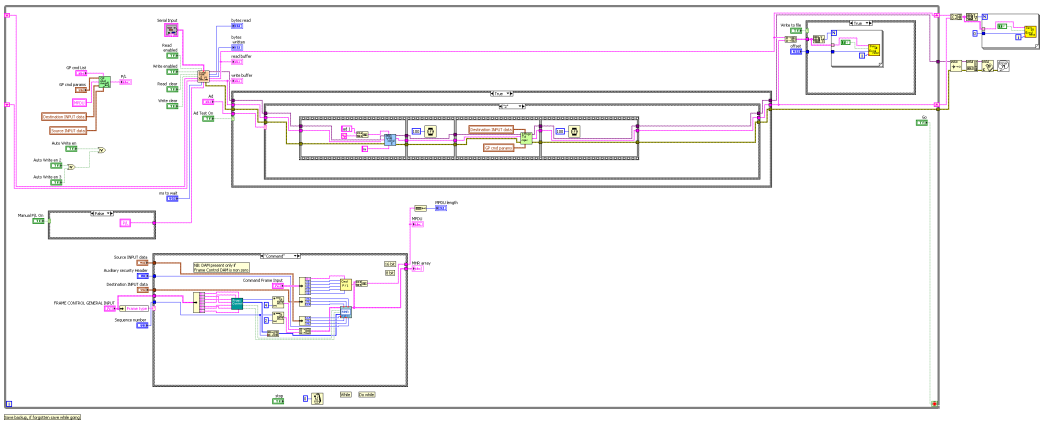

Figure 4.4: Block diagram of a developed LabView software

Then I built also some further ad-hoc blocks for specific operations to perform, always based on the main blocks explained above, because, as said at the beginning of this paragraph, I built a general software, more flexible than possible, to perform all the test tasks. An example of an ad-hoc block is the flat sequence structure in fig. 4.4 which sends to the GP device the commands needed to enable the user defined antenna, to write on the screen the actual setting, to send a remote control packet to the node identified by the user set Short Address and to write the received packet on the screen.

4.3 Physical parameters Test

4.3.1 Description

This test aims to measure electric quantities of interest. These are supply Voltage and current, because of the very low current consumption during specific operative modes. A summary of the operative modes currents is in tab. 3.1. The purpose of this test is not to verify the power consumption declared by the datasheet, but to perform some measurements to obtain the nominal values of these quantities during normal operative conditions of the device. These values are elements of comparison for currents and voltages measured during and after the exposure to radiation, to understand the behavior of the device under test and to give a correct interpretation to the result obtained by radiation test. All the current measurement have been done using the GP500C radio transceiver SPI module in combination with the Microchip picdemz board, provided with a PIC18LF4620 μC. I didn't perform direct measurements on the GP500C device only, because it was planned to be used in combination with the micro-controller during the radiation test, so voltages and currents monitored during that test are referred to the full device meant as a a group made of the radio transceiver, the picdemz board and the micro-controller. Moreover there was no way to measure directly the current consumption of the device in communication mode, because continuous device reset happened during the association sequence when I tried to use the radio transceiver with an independent supply in respect to the picdemz board. This was caused by trigger synchronization problem between reset and feed pins, when these were not directly connected to the micro-controller through the board connection. Anyway I evaluated the current consumption of the board, including the micro-controller, putting the GP device in event sleep mode. In this mode the current consumption of the radio transceiver was equal to 30 nA, well below the resolution of the measuring instrument, so that it didn't appear in the measured value. I did the measurements with the same instruments I planned to use for the radiation test measuring phase, namely the power supply of the Co-60 facility laboratory and the multimeter and the oscilloscope of the Avionics Laboratory.

4.3.2 Setup

The device has been connected through the serial interface to a LabView provided PC. In this way I was able to change the status of the device to perform several measurements in different operative modes. The device has been powered through the picdemz board too, therefore all the current measurements are referred to the block made of the device, the micro-controller and the board, as explained in the description paragraph. For the measurements done in Idle state and sleep mode, I used a device alone. Instead to obtain the values of current and voltages during communication, I used three devices together, making a WPAN with a coordinator and two end nodes. I used a total of three devices to repeat the measurement on different devices and to do the same measurement I did during the radiation test measuring phase.

4.3.3 Test

I evaluated the same quantities of interest I planned to measure during test task V: supply voltage and current of the GP500C device on the picdemz boards, for different operative modes, the voltage on the V_{ddDIG} pin, which is the device digital core input, of the GP chip and the output of the 16 MHz oscillator of the GP SPI module device (details about GP500C pins are in [28]). I measured supply voltage and current of the GP500C device using an Agilent E Series power supply with a voltage resolution of 0.01 V and a current resolution of 1 mA. I set the supply voltage to the nominal 5 V of the picdemz board, measuring the current consumption on the digital screen of the power supply. I did the measurement for Idle state, communication mode (receiving/transmitting), Event sleep mode and 16 MHz Sleep Mode. I repeated the measurements three times, unplugging the device every time and on each of the three tested device. I performed this task inside the Co-60 facility laboratory. Then I measured the voltage on the V_{ddDIG} using the multimeter mode of the Fluke 190 Serie which has a resolution of 1 mV. I repeated the measure three times on each of three devices under test. Moreover I measured the 16 MHz output of the oscillator with a sampling rate of 20 ns, suitable to display the expected frequency. These two last measurements have been done inside the Avionics Laboratory.

4.4 Communication parameters test

4.4.1 Description

This test aims to evaluate the behavior of the device in an environment representative of an AIT activity as the Avionics Laboratory. The main purposes of this task are the evaluation of the Antenna Diversity mechanism in this scenario and of the interaction of the GP device with the environment. I measured the performances of the transceiver in communication mode inside the Avionics Laboratory, putting in comparison the obtained results with those ones obtained by the same test done in an ideal environment as an anechoic chamber. In this way I evaluated the interaction of the device with the working environment, where there are reflections, multipath fading and interference sources. I identified the relevant parameters to evaluate the goodness of the communication in RSSI and SNR, as the former gives an indication of the strength of the received signal, to be related to the strength of the emitted signal and to the working scenario (e.g. existence of obstacles or no direct LOS between communicating nodes), whereas the latter gives information about the quality of the link, as it indicates how much greater is the expected received signal compared to the unexpected noise present on the channel. These two indexes have to be considered and measured together, as through them it is possible to evaluate the impact of the Antenna Diversity as a gain on the link budget. It is known that the Antenna Diversity mechanism of the GP device chooses the antenna to use after a SNR estimation, leading to use that one with a bigger SNR. Unfortunately the SNR estimation is not accessible directly in device registers, but GreenPeak provided formulas and curves to relate SNR to RSSI and LQI indexes. LQI is dependent on estimations of RSSI and SNR. The estimation of the RSSI, called `proto_RSSI`, is in turn linearly dependent on the true RSSI value, whereas the estimation of SNR, called `proto_LQI`, is not linearly dependent, but monotone, in respect to the real SNR value. Using provided data I was able to extrapolate the analytical relationship between LQI, RSSI and SNR. The analytical relationships between the measured indexes, namely `proto_RSSI` and `proto_LQI`, and their effective values, as like as the graph of `proto_LQI` $= f(SNR)$ obtained by experimental results, which are provided by GreenPeak, are not shown here, whereas the result of the extrapolation operation I did with these data, to obtain the $LQI = f(SNR, RSSI)$ relationship in respect to SNR, is shown as a three dimensional graph in fig. 4.5

and $SNR = f(LQI)$ curves for some RSSI values are shown in fig. 4.6.

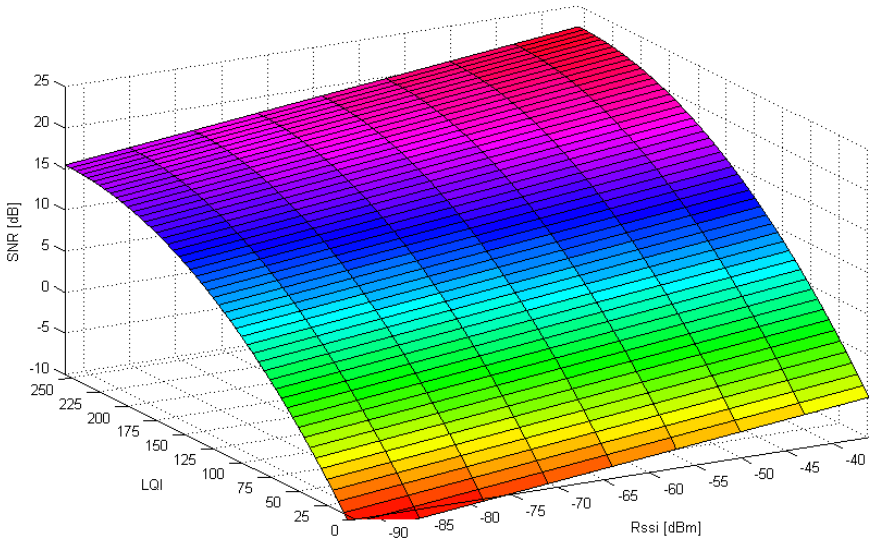

Figure 4.5: SNR(LQI,RSSI) 3D curve

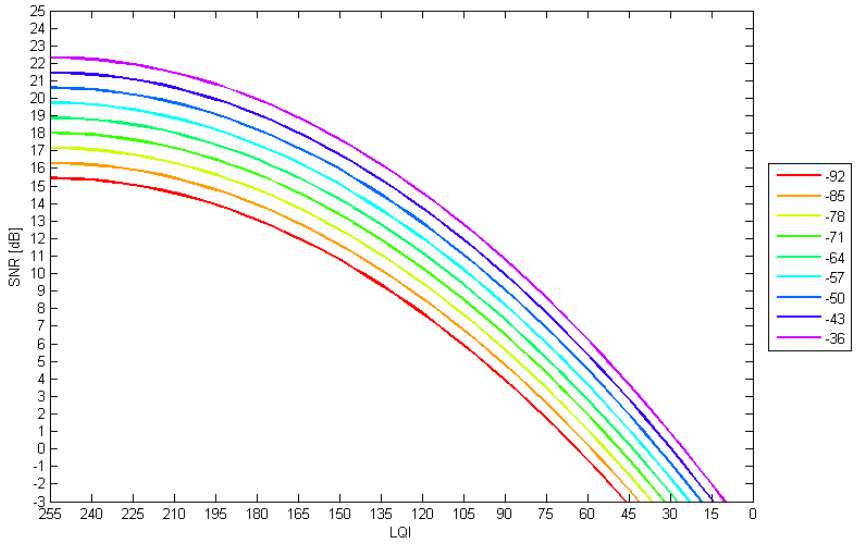

Figure 4.6: SNR(LQI,RSSI) curves

The analytical relationship I obtained between effective SNR and measured LQI and RSSI indexes is:

$$SNR = a \cdot LQI^2 + b \cdot LQI + c + d \cdot RSSI \tag{4.1}$$

with

$$\begin{aligned} a &= -4.2216 \cdot 10^{-4} \\ b &= 0.2153 \\ c &= -0.6887 \\ d &= 0.1227 \end{aligned}$$

and resulted in a R^2 index equal to 0.9868 in the $[-1, 15]$ SNR range and a Root Mean Square of Errors (RMSE) equal to 0.9335, so I considered it a good interpolation of the provided curve. I used the obtained graph and relationship together with the analytical formulas provided by GreenPeak to estimate the SNR from the values of the measured indexes. Anyway I used SNR values not in absolute, but in relative terms, as will be clear in par. 5.4, so any numerical error is limited. This explains why I measured RSSI and LQI, considering them as indexes of merit. Inside the Avionics Lab I did a sequence of measurements to find the $RSSI = f(d)$ relationship, where d is the distance between two communicating nodes. This test has been done using both of the two antennas available on the GP device, with Antenna Diversity enabled and not, moreover it has been repeated using both horizontal that vertical orientation of the antennas. Then I compared the result to the path loss model provided by the standard, introduced in par. 2.1, which doesn't take into account reflections and other interaction with the environment, as the multipath fading effect. I did these tasks creating a direct LOS between the two communicating devices. Then I tested two devices with their antennas vertically oriented at a fixed distance and with no LOS between them, putting a metallic plate between them. I had two goals doing this operation: the first one was to evaluate in a qualitative way the effect of a non direct LOS between two communicating devices in terms of received power, as this is the same scenario that I plan to have inside the Venus Express Mockup. The second target was to evaluate the effect of the Antenna Diversity mechanism with lower received power, as that expected putting an interfering medium between two communicating devices.

Inside the Anechoic chamber I repeated the same operations done inside the Avionics Laboratory to find the $RSSI = f(d)$ trend and to see the results on the received RSSI without reflections and without the interference of the IEEE 802.11 signal.

Finally I did a further operation to estimate the presence and the strength of the interfering IEEE 802.11 signal inside the Avionics Laboratory, doing an Energy Detection scan with the GP device on all the 16 available channels.

4.4.2 Setup

Inside the Avionics Lab I used two devices, fixed in the same position, shifted by 10 cm (because of the boards), and with the same orientation, as nodes. I used a device on a mobile support as coordinator and I obtained the $RSSI = f(d)$ curve by changing the distance between the transmitter coordinator and the receiving nodes. Then I changed the receiver antenna of one device, switching between antenna 0 and antenna 1, whereas the other device had the antenna diversity mechanism enabled. In this way I obtained the $RSSI = f(d)$ curves using antenna 0, antenna 1 and antenna diversity. I used all the devices in combination with a picdemz board provided with a PIC18LF4620 μC and I powered them through the board. All the devices have been controlled through the serial interface, sending commands and acquiring data from the RS-232 port using the LabView software and they have been placed on a desk at a distance of around 1 meter from the floor. Inside the anechoic chamber I used a fixed coordinator and only one mobile node. I had to use only one device connected to the PC because I had no more than one available RS-232 port, so I used the remote control functionality to set the only receiver node using its antenna 0, 1 or antenna diversity mechanism. I used only the fixed device, namely the coordinator, connected through the serial interface to a PC LabView provided. Moving the node I was able to obtain the $Rssi = f(d)$ curves using one of the two available antennas or antenna diversity. As inside the Avionics Laboratory, I used the devices in combination with the picdemz board, used also to power the GP500C transceiver. To test the effect of an obstacle which prevents a direct LOS between communicating devices, I fixed a device to a wall of the Avionics Laboratory and the other one on a desk, so that they were at the same height from the floor and at a fixed distance of 2 meters. Then I put a metallic plate between them during communication. To evaluate the in-

terference created by Wi-Fi or other sources on the same frequency channels of the IEEE 802.15.4 compliant transceiver, I did an Energy Detection on all the channels, using an only device put on a desk near the mock-up, to evaluate any interferences that could affect the task IV of the test sequence.

4.4.3 Test

Moving the mobile device (the coordinator in the Avionics Lab, the node inside the anechoic chamber) with a 0.5 m span in a range between 0.5 to 7.5 m, I obtained the $RSSI = f(d)$ curve. Every point of the curve has been obtained averaging the value on 50 packets sent by the coordinator every 100 ms to the node(s) at a default transmission power of 0 dBm. Inside the laboratory I chose the antenna to use sending commands through the RS-232 interface to both the transmitter than to the receiver, as they were connected to the PC with the LabView software, to test all the possible combination between transmitter and receiver antennas.In case of vertical orientation, the two PIFAs are situated at 90°each other, so it was possible that they gave different results, whereas when horizontally oriented (parallel to the floor) they gave almost the same result. Instead inside the anechoic chamber I selected the receiving antenna sending a remote control packet with the antenna field set to the proper value (0, 1, or 2 for antenna diversity mechanism) and then sending 50 packets to do the measurement, whereas the antenna selection on the transmitter side has been done simply sending a command through the serial interface, as the transmitter device was connected to a PC. Moreover inside the anechoic chamber I did a further test, putting the devices at a distance of 2 m, and changing the transmission power on the transmitter node. In this way I obtained a $P_{RX} = f(P_{TX})$ curve, where P_{TX} is the transmission power and P_{RX} is the received power with direct LOS between devices in a ideal environment. I repeated the same test, with two fixed devices with vertically oriented antennas inside the Avionics Laboratory, but putting a metallic plate in between to block a direct LOS between them. In both cases the two communicating devices exchanged 50 packets every 100 ms for every value of P_{TX}, changed from -12 to 3 dBm, all the available range. I did all the operations using direct communication mode. Finally, the Energy Detection Scan has been done using a device, put vertically on a desk near the mock-up and changing the channel from 11 to 26, all the available range. I did a scan every 1 ms for 25 seconds.

4.5 V-Ex test

4.5.1 Description

The purpose of this test is the evaluation of the behavior of the GP500C in a specific environment, representative of an AIT activity scenario. In fact, other than being used inside the Avionics Laboratory, as done also for the task III, for this test I built a WPAN inside the Venus-Express mock-up. The first phase is the evaluation of the multi-mode cavity theory validity, reported in [16], [31]. The second one is the determination of the $P_{RX} = f(P_{TX})$ function inside the mock-up, putting the obtained result in comparison to that one reported in [32], to verify that the overall signal power is above the sensitivity of the IEEE 802.15.4 compliant device. The third one is the evaluation of the real gain obtained using the Antenna Diversity mechanism in an environment characterized by several enclosures which introduce multipath fading into the communication link.

The first step of this test aims to measure if the electric field inside the six cavities of the V-Ex mock-up can be considered isotropic and homogeneous in each enclosure. In case the multi-mode theory reported in par. 2.1.2 is valid, it is possible to not take care about the specific location and the orientation of the devices to test inside the mock-up, as the measured value wouldn't be affected by these factors, making simpler the test fulfillment and the results analysis. I accomplished this task using 26 measuring points, which positions are indicated in fig. 4.8. I placed the nodes with different orientation, both horizontal than vertical, and in different cavities location, both on the floor than on the boxes connected to the walls, following the positions previously used in [32] to have a valid results comparison.

The second stage of the test aims to compare numerical results previously obtained by EADS Astrium with experimental data to find a further confirmation of the multi-mode cavity theory, in particular about the insertion losses evaluation. I used two devices per cavity as nodes in a WPAN, for a total of 12 nodes and one coordinator and I changed the transmission power between the full available range: $-12 \div 3\ dBm$ acquiring the received strength of the signal index. Then I compared this value with the theoretical one calculated in the way explained below.

- The generated electric field E_{TX} is dependent on the transmission power P_{TX}, the wavelength λ and the insertion loss X_{TX} of the emitter

cavity:

$$E_{TX} = \frac{4\pi}{\lambda}\sqrt{60 P_{TX} X_{TX}} \tag{4.2}$$

- Crossing apertures of the walls from cavity i to cavity j, electric field in cavity j to electric field in cavity i ratio, E_{ij}, is dependent on the crossing aperture surface S_{ij}, the insertion loss of the receiving cavity X_j and the wavelength λ:

$$E_{ij} = \frac{2}{\lambda}\sqrt{\pi X_j S_{ij}} \tag{4.3}$$

- The evaluation of the received electric field $E_{RX}^{(k)}$ after $L^{(k)}$ crossing and for all the possible P paths from emitting cavity to receiving cavity is obtained from all the E_{ij} :

$$E_{RX}^{(k)} = E_{TX} \prod_{l=1}^{L^{(k)}} E_{ij} \tag{4.4}$$

with $k = 1...P$

- The total received electric field E_{RX} is then evaluated as:

$$E_{RX} = \sqrt{\sum_{k=1}^{P} {E_{RX}^{(k)}}^2} \tag{4.5}$$

- Finally the total received power P_{RX} is evaluated from E_{RX}:

$$P_{TX} = \frac{1}{60}\left(E_{RX}\frac{\lambda}{4\pi}\right)^2 \tag{4.6}$$

The last part of this test is the evaluation of the Antenna Diversity mechanism gain. I put in comparison the indexes of merit measured using one of two available antennas with those ones obtained using antenna diversity. From data acquired with the first phase of this test, using a big number of measuring locations, I obtained an overall indication of the gain due to Antenna Diversity on strength and on quality of the signal, instead from data obtained with the second phase I obtained an indication of the Antenna Diversity gain in terms of SNR in dependence on received power. I used the RSSI index as indicator of Power level, whereas the LQI has a more

significant meaning, as it takes into account of either strength than quality of the signal. I measured these indexes directly, whereas the SNR has been obtained as explained in 4.4.1.

I performed the evaluation of the Antenna Diversity mechanism benefit defining two indexes of merit, a Gain and a Penalty, defined as:

$$Gain = A_D - \min(A_0, A_1) \quad (4.7)$$

$$Penalty = \max(A_0, A_1) - A_D \quad (4.8)$$

where A_D, A_0, A_1 refer to the evaluation parameter (RSSI, LQI) obtained using respectively antenna diversity, antenna 0 and antenna 1 of the GP500C radio transceiver. It is clear from fig. 4.7 that a negative Penalty is equal to a Gain, because the green curve (the A_D one) is above the others.

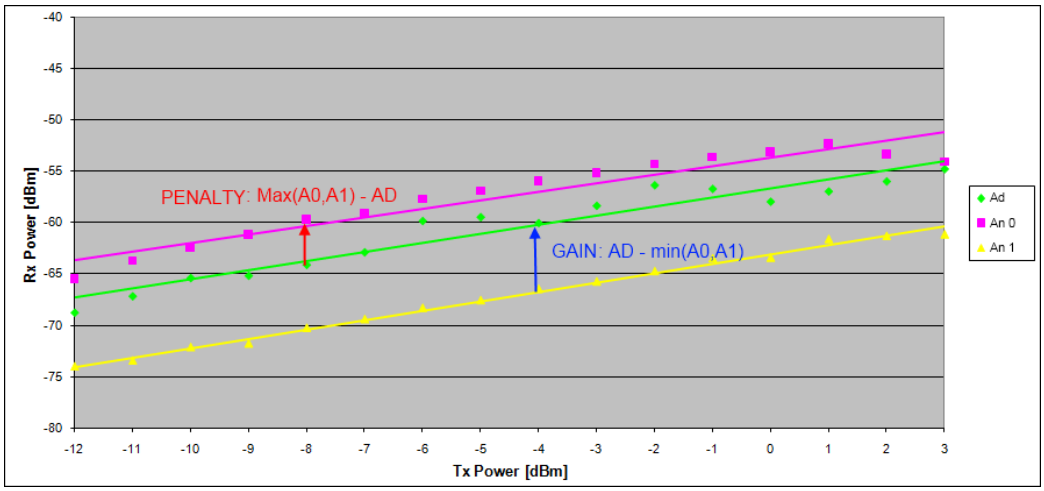

Figure 4.7: Gain and penalty definition

A negative Gain means that the Antenna Diversity causes a loss in comparison to the usage of the other two antennas, whereas the case with G > 0 and P > 0 has to be evaluated, because it is good only when G > P. Because of the resolution of the RSSI measurement, which is 3 dB, I discarded all the set of values with a difference between G and P equal or less than 3, because in this case it is impossible to have confidence with the obtained result.

An alternative way to evaluate Antenna Diversity performance could be using SNR, but its evaluation requires to solve eq. 4.1 with the RSSI and LQI measured values. This introduces numerical errors, because of the extrapolation from provided graphs and analytical formulas done to obtain the

eq. 4.1, leading to less accurate results in comparison to those ones obtained from direct measurements of RSSI and LQI. Moreover the LQI index includes also the contribution coming from SNR, so I wouldn't lose any information in my assessment just considering the two measured values. Anyway I did an evaluation of overall SNR Penalty and Gain, even if I considered these ones less accurate than the directly measured indexes values.

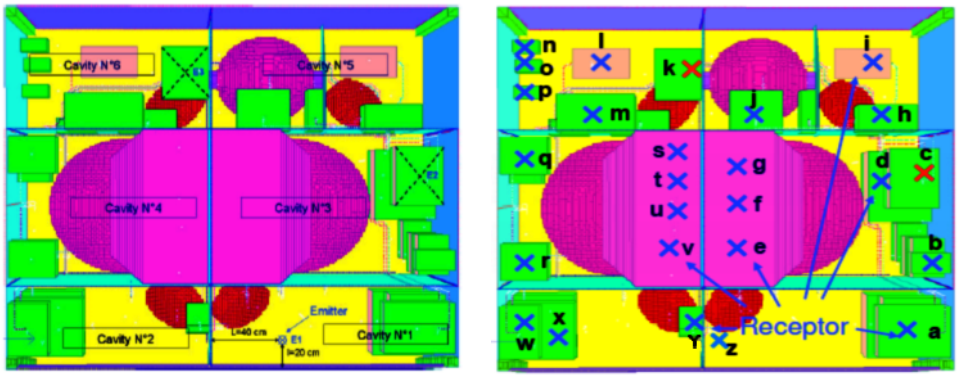

(a) Mock-up numbered cavities (b) Measuring points inside the mock-up

Figure 4.8: Cavities and devices position inside them

4.5.2 Setup

The measuring points were end node of a WPAN with a coordinator placed in cavity 1, connected by a serial cable to a PC with the LabView software, whereas the nodes have been used with the remote control functionality. All the devices have been used in combination with the picdemz board, microcontroller provided, used also to power the radio transceiver through feed lines. The maximum number of network members was 13 (1 coordinator and 12 nodes) due to devices availability, therefore I performed the measurements in all the 26 stations of the first phase moving the 12 devices under test. A top view of the mock-up is shown in fig. 4.8 [31], together with the position of the devices (indicated by crosses) inside it. A total number of 26 stations has been used for the first phase. I placed the coordinator horizontally, at a distance from the floor slightly bigger than 3 cm because for distances bigger than $\frac{\lambda}{4}$ there is no electric field variation inducted by conductive walls. Also the nodes have been spaced from the walls and I placed them horizontally (parallel to the floor) and vertically (parallel to walls) in equal number inside

an enclosure, both on cavity floor than on the boxes fixed on the walls. I tested a total of four conditions: open walls, with the main walls of the mock-up opened and closed walls, an example picture of these configurations is fig. A.2, moreover I put the coordinator both in cavity 1 than in the same cavity of the receiver. For the second phase, to test the variation of RSSI in respect to Transmission Power, I used only 12 nodes, two per cavity, building a WPAN with the coordinator in cavity 1, testing both the open than the closed walls configuration.

4.5.3 Test

I performed all the measurements sending 40 packets, with a time interval of 100 ms between them, from the coordinator to the nodes individually and using direct transmission mode. Using the remote control functionality, the coordinator receives, for every packet sent, an answer packet, containing the RSSI and the LQI of the packet received by the node. Switching between the Antenna 0, 1 and Antenna Diversity mechanism, both on the coordinator that on the node, I tested all the 9 possible antenna combinations using the coordinator either as a transmitter than as a receiver, as like as the nodes, for a total of 18 sets of measurements, each made up of 40 packets, for every node. The test has been repeated with the walls of the spacecraft closed and opened. The only device connected by RS-232 to a PC with the LabView interface was the coordinator, whereas the other devices were connected only to the power feed, through the supply of the picdemz board.

In this way, using 26 measuring stations, indicated in fig, 4.8, I tested the homogeneity of the Electric field and the Antenna Diversity gain. Then, using 2 devices per cavity,I evaluated the variation of the RSSI in respect to the Transmission Power by setting P_{TX} on the coordinator by the serial cable, and on the node by sending a remote control packet. In this case I didn't switch the antenna on the coordinator, but only on the node, but I repeated also this test both in open than in closed walls configuration.

4.6 Radiation Test

4.6.1 Description

Exposure of devices and circuits to radiation in space causes the semiconducting and insulating materials to be ionized, which leads to transient and permanent changes in device electrical properties, classified by their source as Single Event Effects (SEE) in case of interaction with a single energetic particle, and Total Ionizing Dose (TID) in case of effects inducted by collected radiation dose. The main purpose of this test is the acquisition of data about electrical parameters and communication indexes, to be related to the total radiation level absorbed by the device, with the aim to assess a potential device employment for space based application, in particular in flight operations. Results of these test can be compared to those one obtained from a similar component. I designed a test plan to evaluate TID effects, performing procedures compliant with ESCC Basic Specification 22900 [33]. The standard defines room conditions, mode and duration of device exposure to radiation, as well as the radiation level to reach. I identified the main parameters to be measured and built the software to perform the communication data acquisition and the setup to perform the electrical measurements. The electrical quantities of interest are the same of the test sequence task II, namely supply voltages and current consumption. These quantities are referred to the block made up of the GP radio transceiver and the Microchip picdemz board suppled with the PIC18LF4620 micro-controller. This is the only way I found to use the device to perform all the operations required by the test plan, moreover there was no way to perform current consumption direct measurement of the GP device only, as reported in par. 4.3.1. The communication parameters of interest are the same of the task III of the test sequence, namely LQI and RSSI, with the addition of PER. I considered the last one as a valuable parameter to be related to absorbed radiation level, in consideration of the big number of packets exchanged for all the duration of the test. The main goal of PER measurement is to assess a potential increase in errors due to exposure to radiation which could degrade radio transceiver components and if possible to obtain a quantitative estimation. The only available data about the GP500C radio transceiver is a PER equal to 10^{-5} for a standard 22 bytes length packet at a received power equal to -82 dBm. Further evaluation can be done starting from the BER formula indicated in [27] and obtaining Symbol Error Rate estimation using statistical

evaluation proposed in [34], but as the purpose was not the achievement of the $PER = f(SNR)$ "waterfall" curve, but the evaluation of possible PER increase due to radiation exposure, a simpler approach has been chosen. The number of error packets found to the total number of exchanged packets gives the PER value. This PER value, equal to the number of wrong packets E to the total number of exchanged packets N, is evaluated together with a confidence level CL, in turn function of the total number of exchanged packets and of found errors. I evaluated the confidence level doing reasonable assumptions, assuming that the number of error events follows a binomial distribution (I considered two transmission states: success and failure) and using the Poisson theorem to obtain a conservative estimate of the binomial distribution function, as shown in [35] and [36]. The relationship between N, E, PER and CL is resumed in eq. 4.9.

$$N = \frac{1}{PER}\left[-\ln\left(1-CL\right) + \ln\left(\sum_{k=0}^{E}\frac{\left(N\cdot PER\right)^{k}}{k!}\right)\right] \tag{4.9}$$

For a given PER equal to 10^{-5} the total number of found wrong packets in function of the total number of exchanged packets and its correspondent confidence level is obtained from eq. 4.9 which results in fig. 4.9.

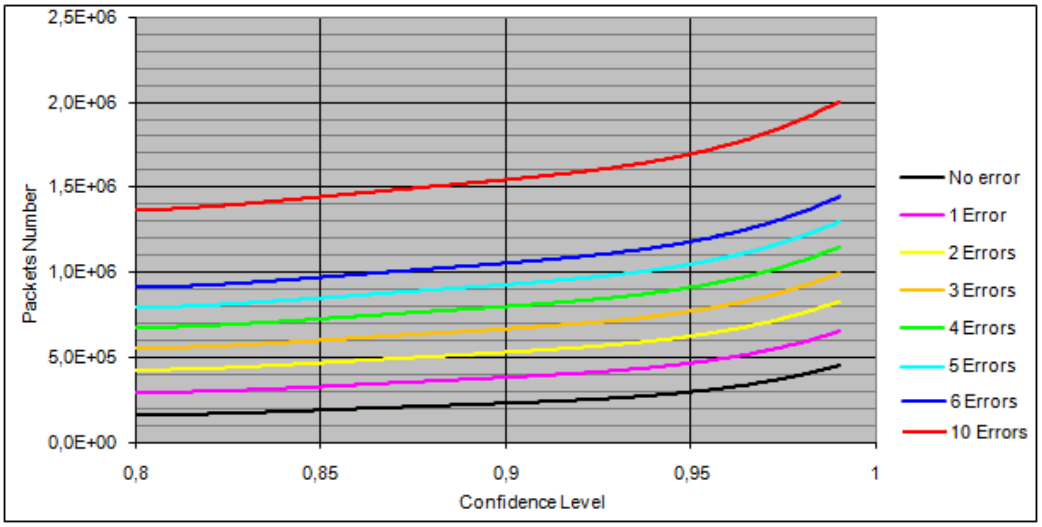

Figure 4.9: PER confidence level curves

4.6.2 Setup

Three nodes were used as nodes, continuously communicating with a coordinator. The three nodes were placed on a rigid support so that the GP500C was exposed to radiation. Also the oscillator and the other components of the PCB were exposed to radiation, whereas the picdemz boards with the μC were shielded by lead bricks. Also the boards were taped to a wood support, to make them steady for all the duration of the test. The coordinator was entirely shielded by the lead bricks, both the picdemz board than the GP device, because the nodes were the DUT, whereas the coordinator had the serial link to a PC with the LabView software outside the radiation chamber to monitor the communication with the three nodes, so it acquired all the useful data of the test and it had not to be influenced by radiation effect. All the devices were used in combination with a picdemz board supplied with a PIC18LF4620 μC and were powered through it with a common 5.0 V feed. The boards with the μC have not been exposed to radiation, as they were shielded by lead bricks. In fig. 4.10 it is shown the setup inside the Co-60 facility. The three GP500C devices were taped to a wood support and placed at the same distance from the radiation source, the little shift did not affect the effective radiation value, which was the same for all the three devices.

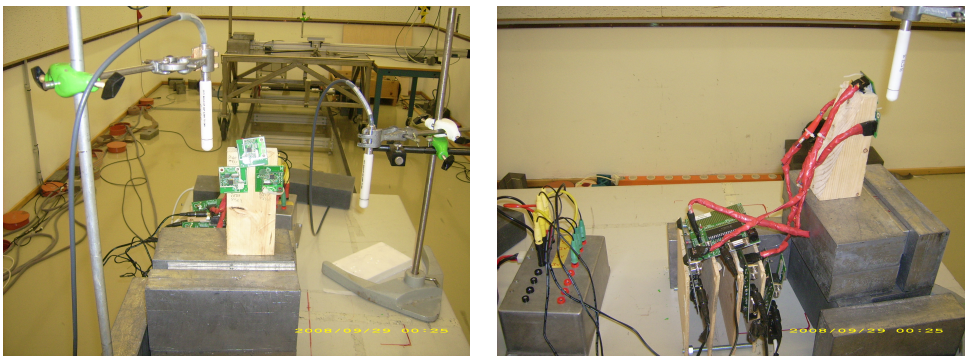

(a) Front view (b) Side view

Figure 4.10: Radiation test setup

4.6.3 Test

The first part of the test was the exposure to radiation. I defined a very high radiation level, slightly over the R level defined in [33]. The best way to perform this test would be to stop the exposure to radiation when the input current exceeds the maximum level allowed by the device. Unluckily no data about the maximum allowed current were provided for the device under test, so a very high radiation level has been selected to be sure to lead devices to failure. The radiation level to reach was 150 kRads, with a dose ratio of 7.5 rad/min. These values are very high compared to operational ones, as the total dose level is correspondent to the radiation absorbed in more than 8 years in Geostationary orbit with a 3 mm shield tickness, or to that one absorbed in 37 years in the same orbit but with a shield thickness equal to 5 mm, whereas the dose ratio for the 3 mm shield tickness is only 0.0325 rad/min[1]. The three nodes were set to send a 22 bytes packet every 333 ms to the coordinator, without acknowledgement. I selected the time interval between two consecutive sent packets, to allow a medium sharing between three device without collisions, moreover the maximum number of sent packets in two weeks was 3628800, which was compatible with the maximum number of the Unsigned Long (32 bits) integer variables user as counters of packets by the coordinator. The nodes were programmed through the software scheduling to periodically send to the coordinator a packet with a 9 bytes payload made of 3 indexes, repeated 3 times, which are updated at every sent packet. The coordinator updated these indexes, three different ones for each transmitter device, every time it received a packet, too. In this way the coordinator knew in advance which payload it had to expect from each of the three nodes. This was the way I found to obtain an estimation of the Packet Error Rate. The best way would be using a pseudo random payload, but it would be necessary to have both the transmitter than the receiver connected through the serial interface, to compare the sent packet with the received one. As it was possible to connect only one serial cable from a device inside the radiation chamber to a PC outside of it, I implemented this process using a sequential payload inside the C software of the coordinator μC, which performed the comparison between the got payload and the expected one directly at the reception, informing if it was right or wrong through outputs like those ones shown in fig. 5.3 and fig. 5.4, including the time stamp and the tick count, to

[1]Values referred to Aluminium sphere obtained by simulation done with *Spenvis* software, using *Shieldose* as radiation dose model and *Silicon* as target material .

have an indication of the reception time and of the time between the packets received from the same device and from different devices. In this way it was possible to evaluate payload bit flip (if one of the bytes making the sequence in the payload was wrong) and jumped packets (if the packet received had indexes different in comparison to the expected ones). To evaluate errors in the frame header, if the packet was received and it was detected as error, it was entirely printed, whereas if it was right, only the main information (RSSI, LQI, frame length and type, source address and the 3 index bytes) were printed. The values of i and V are referred to a block made of board + μC + GP500C device. It is known the current flowing in the GP500C is around 1.5 times higher than the measured one[2], but it was not possible to feed separately the GP500C devices, because of an unexpected reset when in communication mode as explained in par. 4.3.1. For each device input i and V was measured each minute for all the two weeks radiation exposure.

After the two weeks period inside the radiation chamber I measured the input current through the Agilent E Series power supply of the lab to have a first indication of the current consumption trend. Then the devices have been submitted to 168 hours room temperature annealing. In this phase the devices were powered at room temperature and current and Voltages measurements have been performed periodically. The current consumption value has been monitored for 72 hours immediately after the end of the first phase to verify the possibility to put the devices inside the oven at 100 °C or not.

The last phase of the test was the 100°C annealing, performed putting the device inside the oven for 168 hours. Current and voltages measurements have been performed for the last time after this phase to verify if recovering happened.

[2]The exact ratio between the 5.0 feed voltage and the maximum voltage after the linear voltage regulator is $\frac{5}{3.3} = 1.515$.

Chapter 5

Results

5.1 Functional Test

The functionality and the reliability of the software (C code + LabView) and of the interface with the device have been proved, I tested and verified all the operations and the functionalities required by the tests tasks. As a result I show several examples of the different obtained output in fig. 5.1, fig. 5.2, fig. 5.3 and fig. 5.4[1]. In case of remote control packet usage, the payload includes all the setting parameters of the node controlled, moreover it reports also the LQI and the RSSI of the packet received by the controlled node, as shown in fig. 5.1.

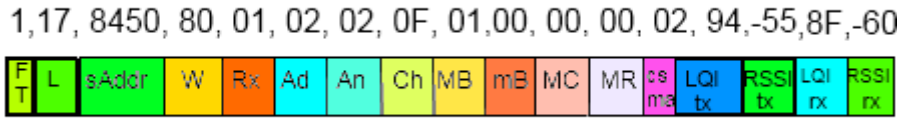

Figure 5.1: Remote control answer packet

Data required by the tests planned to be done inside the Avionics Laboratory are the only communication indexes, RSSI and LQI. The `proto_RSSI` index is a value used to backup the RSSI effective value. The payload shows simply a sequence of bytes which are updated at every packet sent by the device and can be used as counters to check the actual total number of packets

[1]The time and the tick count have been created by the LabView script.

exchanged, whereas time and tick count are not relevant for this test and can be disabled. An example is provided in fig. 5.2

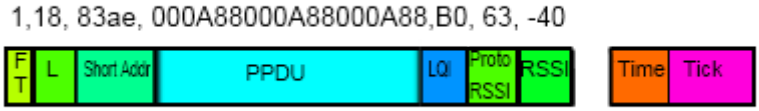

Figure 5.2: Avionics Lab packet logging

For the Packet Error Rate evaluation during the radiation test I formatted the output to have the same number of columns, both if the packet received is right, than if it is wrong. However in case it is right, as shown in fig. 5.3, common information are displayed and the error index (in the seventh column) is null, moreover the payload field shows only the 3 bytes making the MSDU, not the full 9 bytes packet payload, whereas in case it is wrong the full MPDU is displayed and the error field is not null, as evident in fig. 5.4.

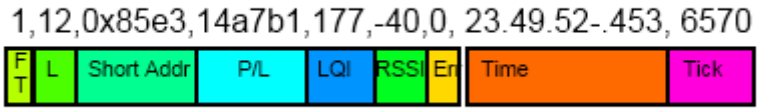

Figure 5.3: Radiation test, right received packet

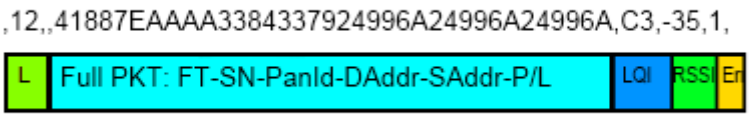

Figure 5.4: Radiation test, wrong received packet

5.2 Physical Parameters Test

The current consumption values referred to different operative modes are shown in tab. 5.1. All the measurements are referred to the block made up of picdemz board with micro-controller and GP500C device.

Table 5.1: Physical parameter test results

Mode	Current consumption [A]
Idle	0.011 ÷ 0.014
Communication	0.036
Event Sleep Mode	0.008
16 MHz Sleep Mode	0.009

The measured Voltage on the V_{ddDIG} pin of the GP chip is 1.78 ÷ 1.80 V. A little imprecision is due to the difficulty of the measure on the small pin, whereas on the V_{PP} pin is 3.3 V. Details about the GreenPeak device pins are in [28]. The output of the 16 MHz crystal on the oscilloscope screen is reported in fig.5.5 and shows correctly the expected frequency.

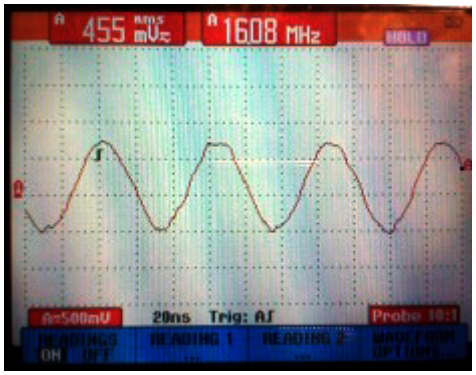

Figure 5.5: 16 MHz crystal output

5.3 Communication parameters test

The $RSSI = f(d)$ relationship I obtained using one of the the two available antennas (An 0 and An 1) horizontally oriented and using the antenna diversity mechanism (Ad) is shown in fig. 5.6, together with the theoretical curve obtained by the model defined in [12] and reported in par. 2.1. This model takes care only about the free space loss and doesn't consider reflections, present inside the Avionics Lab and affecting the result for distances bigger than 1.5 m. The trend of the $LQI = f(d)$ curve has been thought as the same of RSSI, due to the linearity between them, as reported in par. 4.4.1, and because no information about SNR dependence on distance are provided, the interpolated curve is shown in fig. 5.7. In fig. 5.8 and fig. 5.9 are shown the RSSI and LQI trends to distance for vertical orientation of the antennas and using the antenna 0 on the emitter side. In fig. 5.10 and fig. 5.11 are shown the results obtained still with vertical orientation, but using a different emitter antenna (1 instead of 0 as before), which is parallel to the floor, whereas antenna 0 is perpendicular in respect to the floor, as shown in fig. 3.2. Every point in the graph is the average obtained on 50 packets sent every 100 ms, using channel 14 and direct transmission.

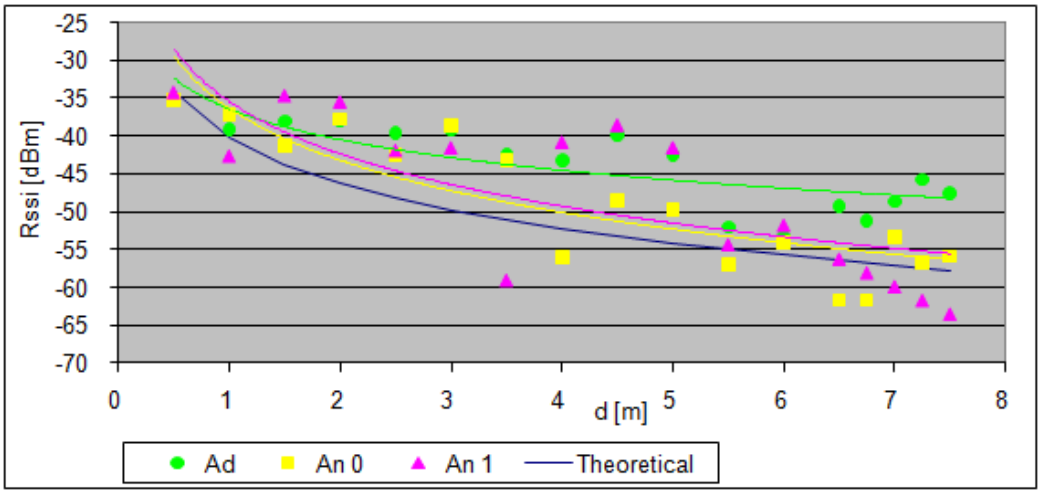

Figure 5.6: RSSI vs distance, horizontal polarization

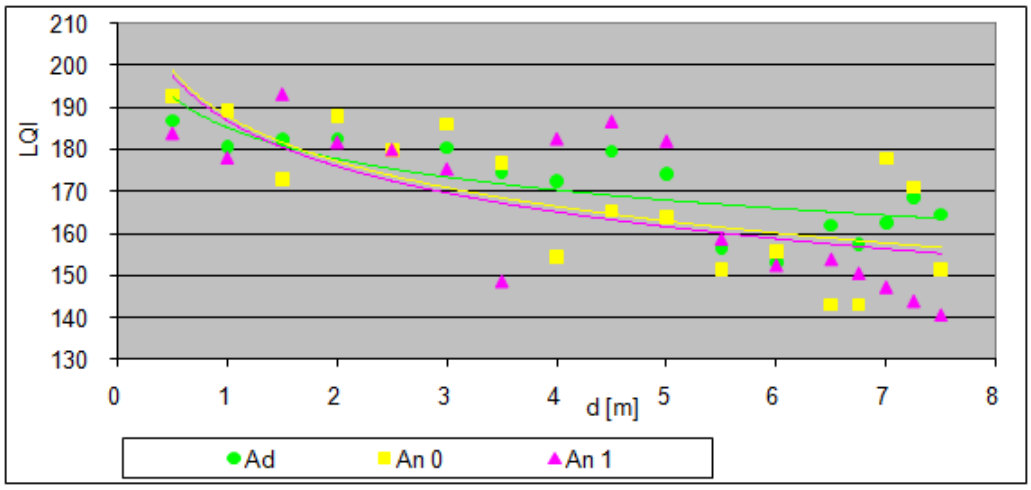

Figure 5.7: LQI vs distance, horizontal polarization

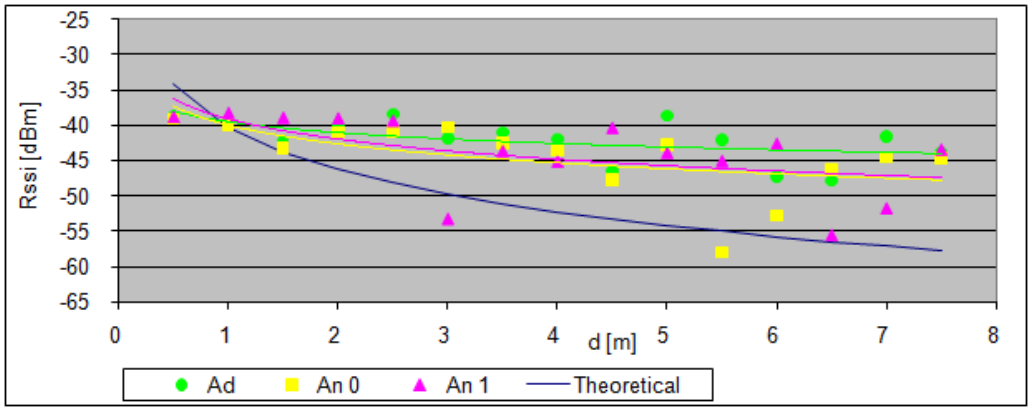

Figure 5.8: RSSI vs distance, vertical polarization, emitter antenna 0

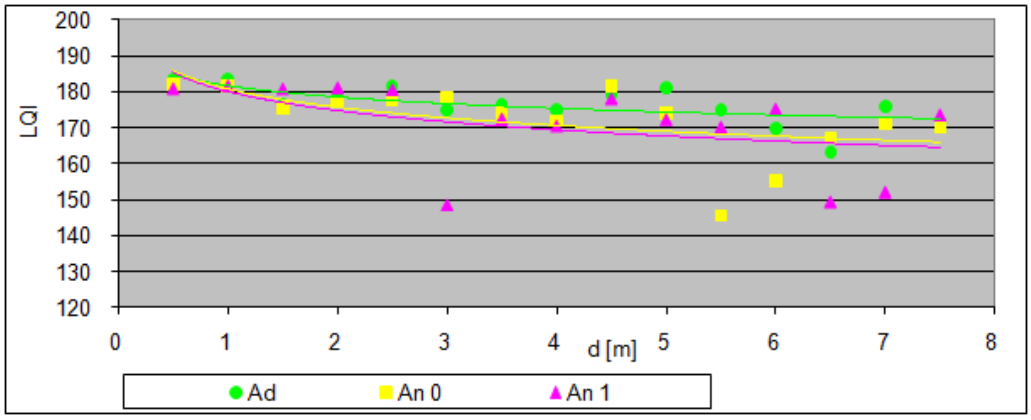

Figure 5.9: LQI vs distance, vertical polarization, emitter antenna 0

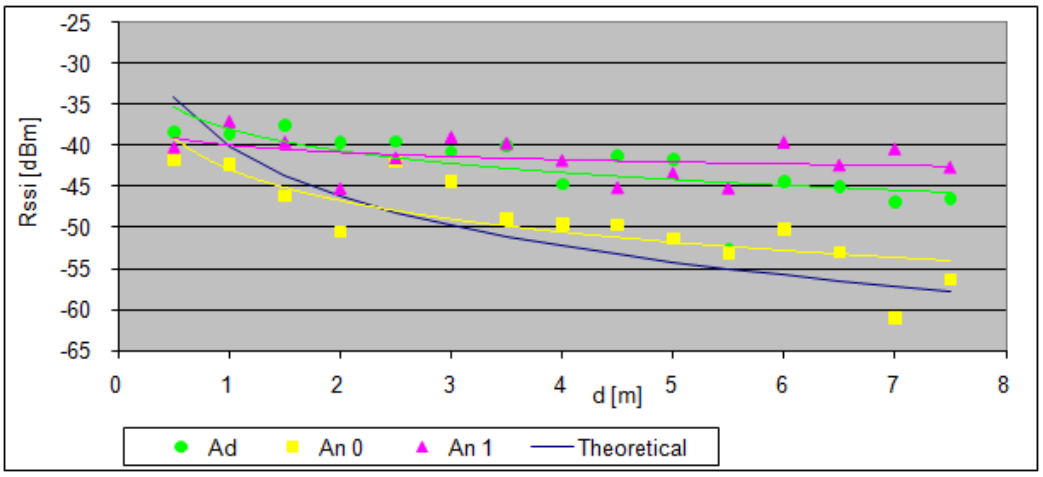

Figure 5.10: RSSI vs distance, vertical polarization, emitter antenna 1

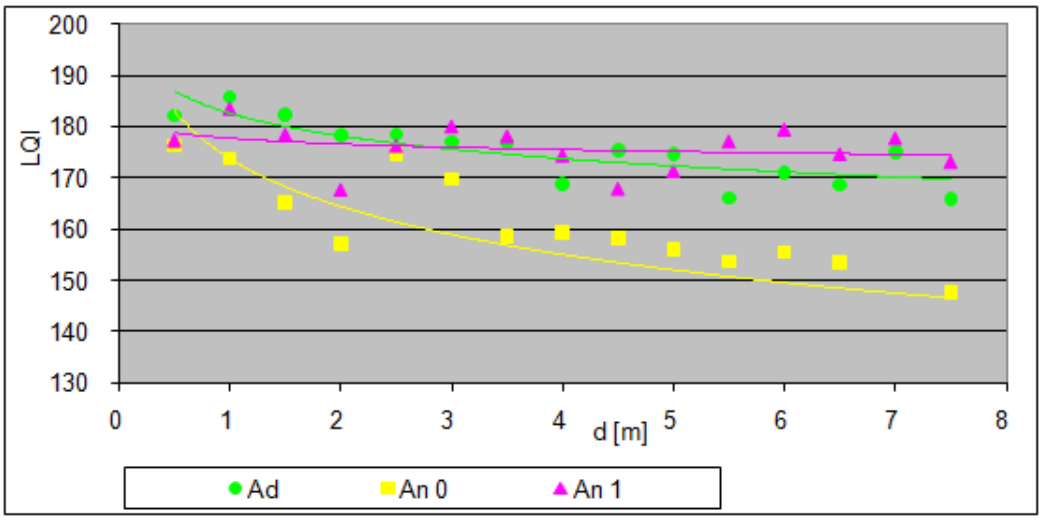

Figure 5.11: LQI vs distance, vertical polarization, emitter antenna 1

When horizontally oriented, the obtained result is almost the same and there is a good agreement with the theoretical model up to 1.5 m. Then the effect of reflections and multipath leads to sensible differences, even more evident when the devices are vertically oriented. In this case the obtained result is also different between the two used antennas. In most of the cases it seems that the result achieved using Antenna Diversity in terms of gain on RSSI and LQI, is more evident at bigger distances, when the strength and especially the quality of the signal is lower, due to reflections and multipath effect. This is confirmed from upcoming tests, too.

Then, in fig. 5.12 and fig. 5.13 are shown the $RSSI = f(d)$ and $LQI = f(d)$ graphs I obtained using horizontal orientation of the antennas inside the anechoic chamber. In fig. 5.14 and fig. 5.14, the same plots, but with a vertical orientation and using the antenna 0 of the emitter. In the end the antenna 1 of the emitter has been used to obtain fig. 5.16 and fig. 5.16. Inside the anechoic chamber vertical orientation results in good agreement with theory. Horizontal orientation results in a small difference, maybe because of reflections due to the desk where I put the devices, in this case parallel to the plane of the antennas.

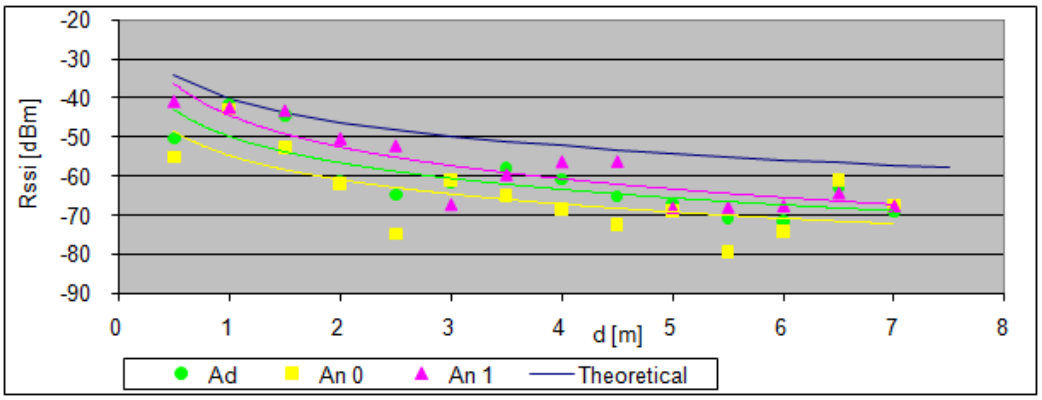

Figure 5.12: RSSI vs distance, horizontal polarization

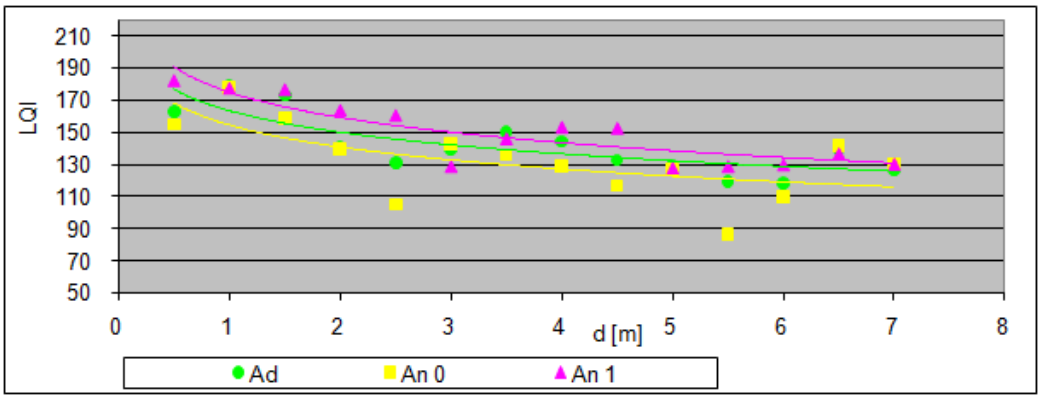

Figure 5.13: LQI vs distance, horizontal polarization

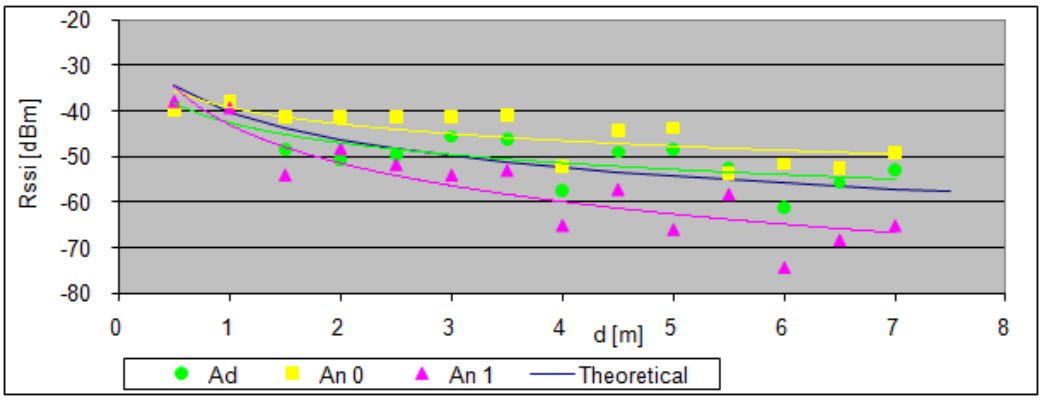

Figure 5.14: RSSI vs distance, vertical polarization, emitter antenna 0

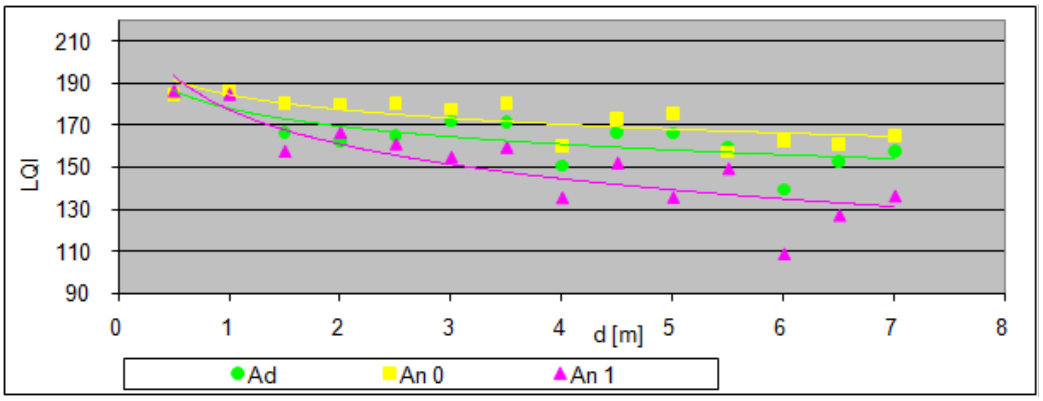

Figure 5.15: LQI vs distance, vertical polarization, emitter antenna 0

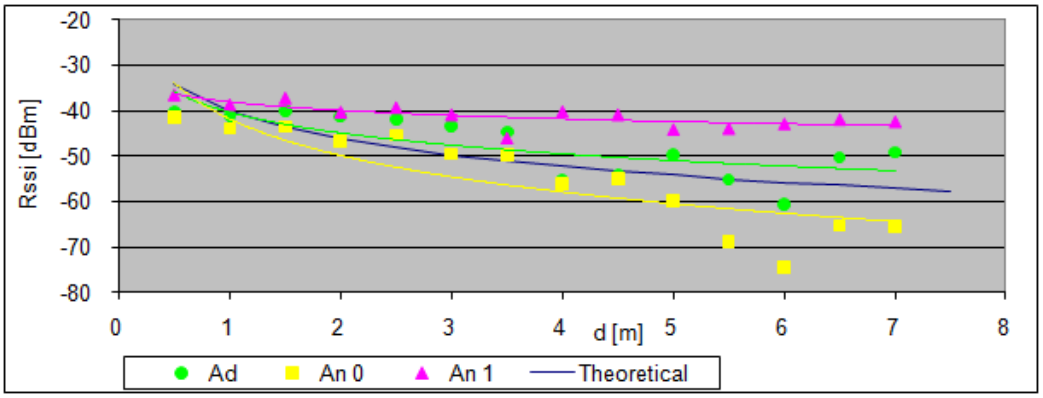

Figure 5.16: RSSI vs distance, vertical polarization, emitter antenna 1

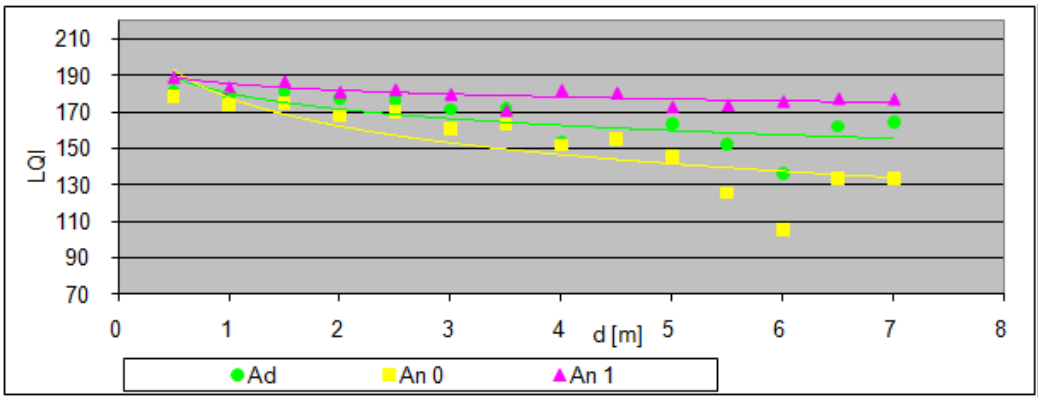

Figure 5.17: LQI vs distance, vertical polarization, emitter antenna 1

The result of the Energy Detection scan done in the Avionics Lab is shown in fig.5.18.

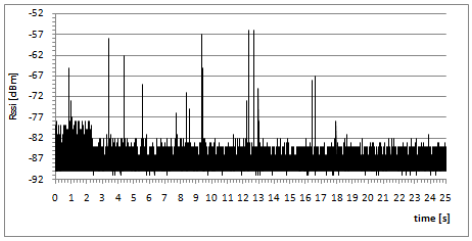

(a) Channel 11

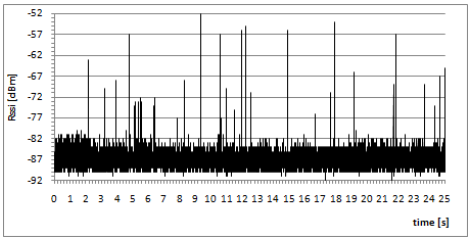

(b) Channel 12

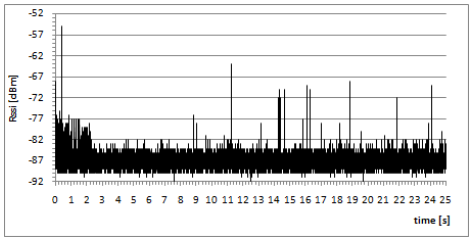

(c) Channel 13

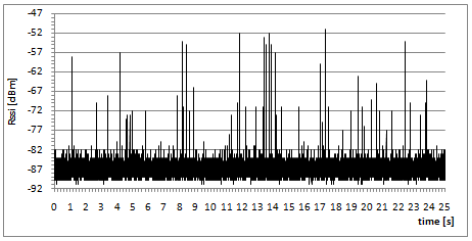

(d) Channel 14

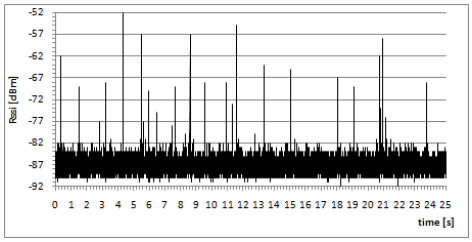

(e) Channel 15

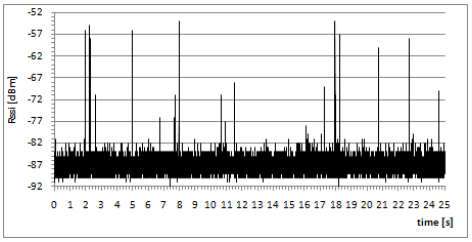

(f) Channel 16

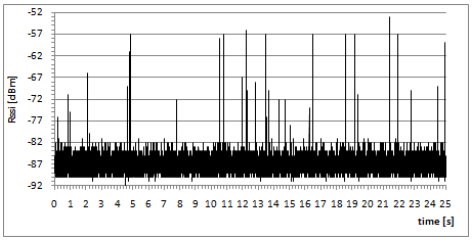

(g) Channel 17

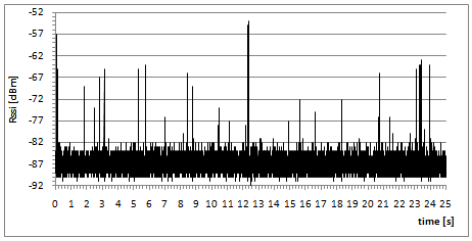

(h) Channel 18

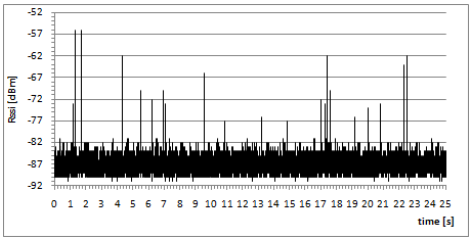

(i) Channel 19

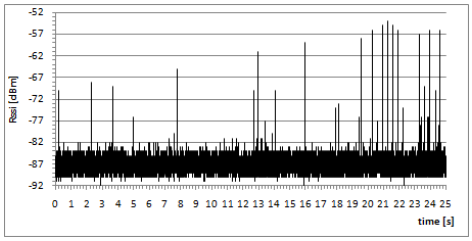

(j) Channel 20

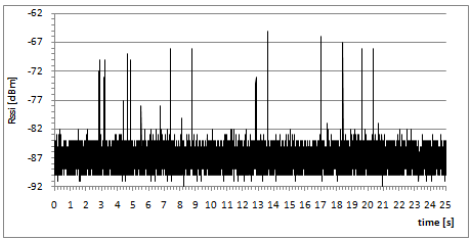

(k) Channel 21

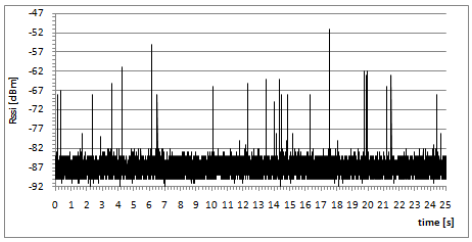

(l) Channel 22

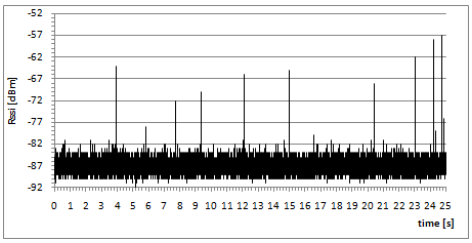

(m) Channel 23

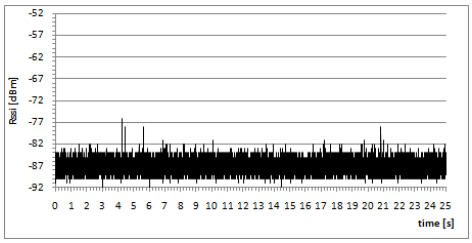

(n) Channel 24

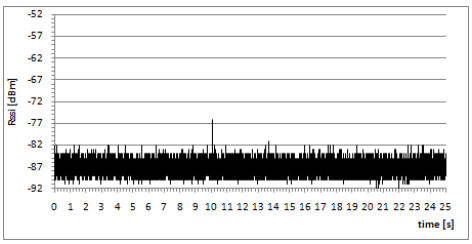

(o) Channel 25

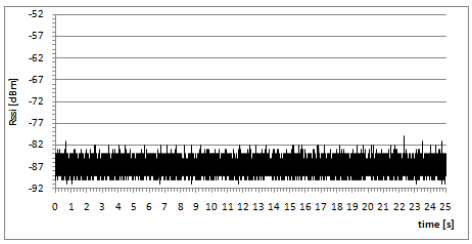

(p) Channel 26

Figure 5.18: ED scan results for all the channels

It demonstrates the existence of a signal on almost all the channels used by the IEEE 802.15.4 compliant radio transceiver. There is a lower activity only on the last three channels, but it is impossible to exclude that these are used in a different time by the Wi-Fi network present inside the laboratory. Two 802.11 access points are known to be close enough to the laboratory to interfere with the device emitted signal. The effect of this interference is shown in fig. 5.19 and fig. 5.20 referred to a set of 50 packets exchanged every 100 ms using channel 11 inside the Avionics Laboratory. There is a drop due to interference signal, both in terms of only received signal strength, related to RSSI index, than in terms of SNR and signal quality, related to LQI index. The drop which repeats regularly in time leads may be caused by interference of 802.11 beacons.

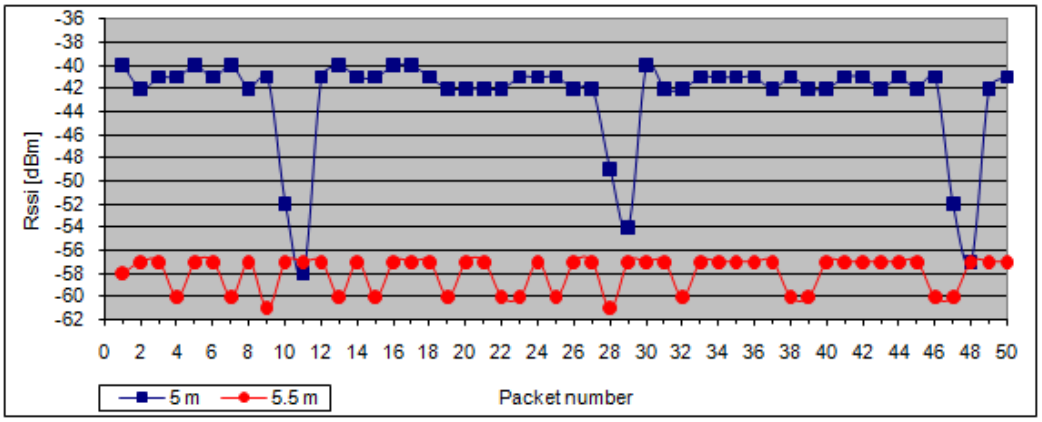

Figure 5.19: Effect of the noise on the exchanged packets RSSI

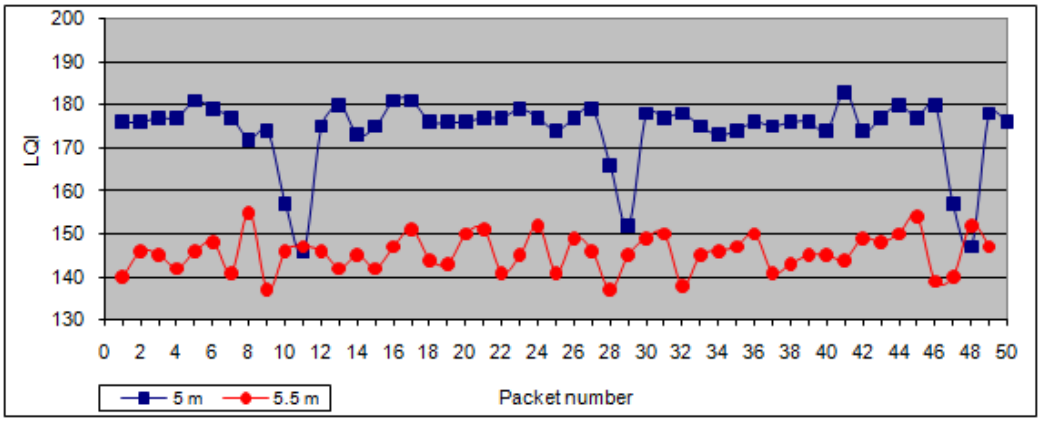

Figure 5.20: Effect of the noise on the exchanged packets LQI

In fig. 5.21 and fig. 5.22 it is shown a set of 50 packets exchanged every 100 ms inside the anechoic chamber, it shows a total absence of interference: RSSI and LQI values have very low variations and no drops.

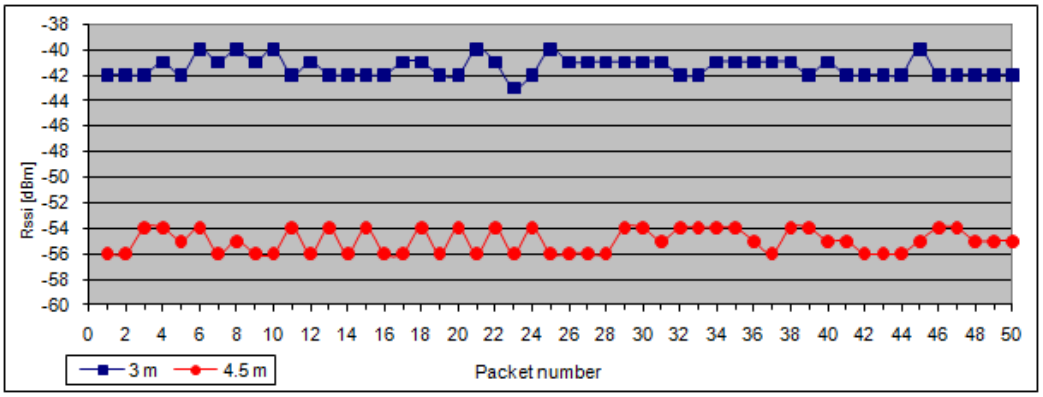

Figure 5.21: Effect of the noise on RSSI, anechoic chamber

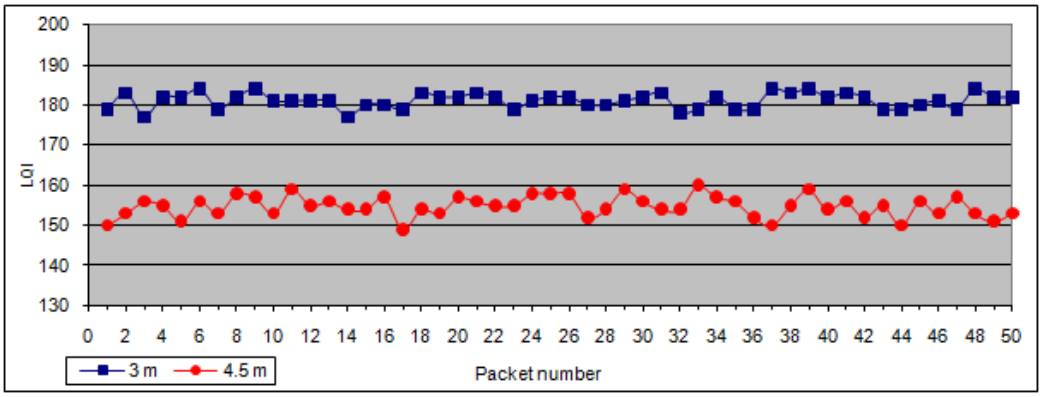

Figure 5.22: Effect of the noise on LQI, anechoic chamber

In fig. 5.23 and fig. 5.24 there are the variation of received RSSI in respect to the transmission power, whereas the LQI variation in respect to transmitted power is shown in fig. 5.25 and fig. 5.26. In both of cases the node is the receiver and the coordinator is the transmitter in the first graph and vice-versa in the second one. The full available range (from -12 dBm to +3 dBm) has been tested and every point is the average value on 50 packets exchanged. The trend follows quite well the theoretical one, as the difference is below the precision of the RSSI measurement (3 dB). These graph are referred to the test I did inside the anechoic chamber, with direct LOS between the devices.

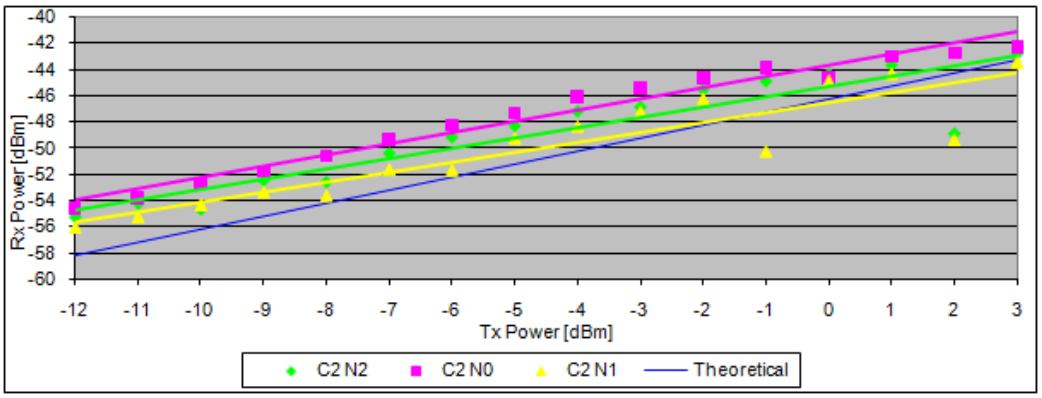

Figure 5.23: P_{RX} vs P_{TX}, 2 m distance, anechoic chamber, node

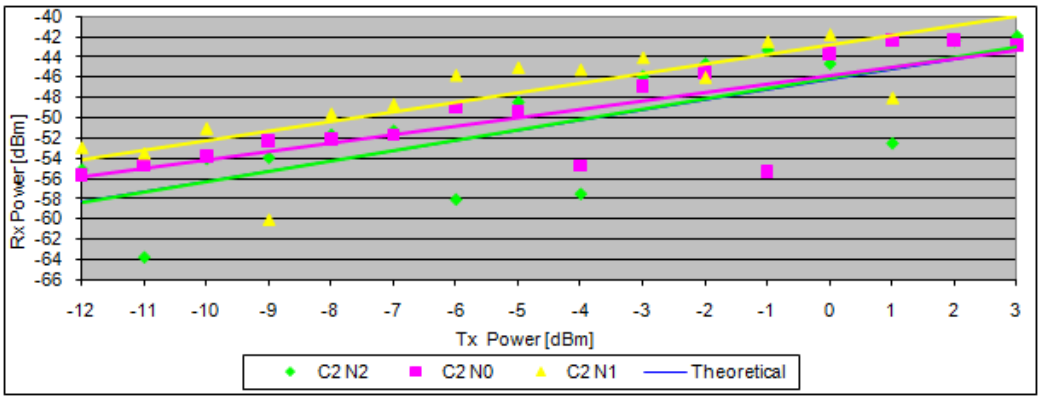

Figure 5.24: P_{RX} vs P_{TX}, 2 m distance, anechoic chamber, coordinator

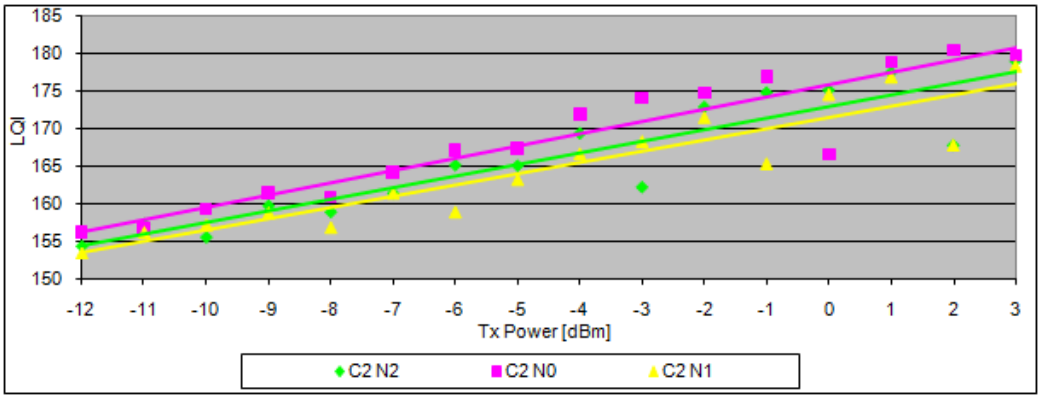

Figure 5.25: LQI vs P_{TX}, 2 m distance, anechoic chamber, node

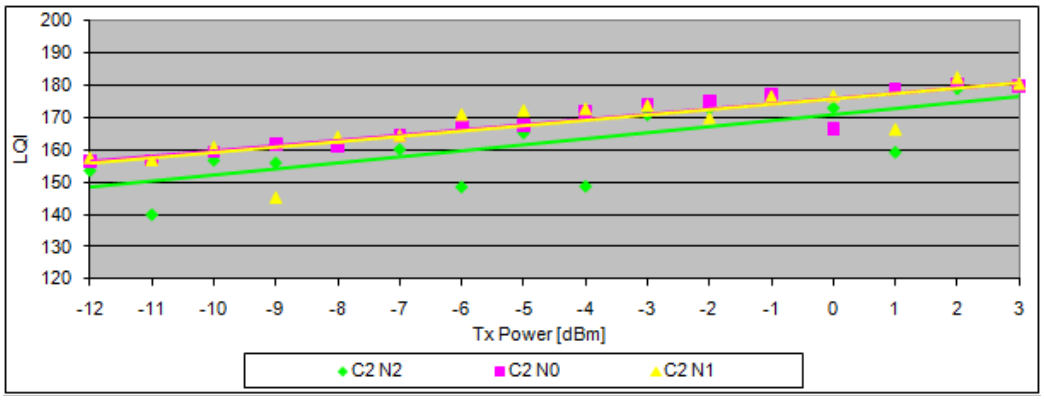

Figure 5.26: LQI vs P_{TX}, 2 m distance, anechoic chamber, coordinator

RSSI trend in respect to transmitted power, with two devices placed at a distance of 2 meters and with no direct LOS between them is shown in fig. 5.27 and fig. 5.28. The first graph refers to the node used as receiver, the other one to the node used as transmitter. In this way the test has been repeated two times, every point of the graph is averaged on 50 packets exchanged. The same considerations, but referred to LQI, are finally shown in fig. 5.29 and fig. 5.30. As for the test done to obtain the variation of RSSI and LQI in respect to distance, it seems that the antenna diversity mechanism gives benefit when the strength and especially the quality of the signal is lower, as the obstacle introduced between the two devices introduce a loss of around 20 dBm on RSSI value.

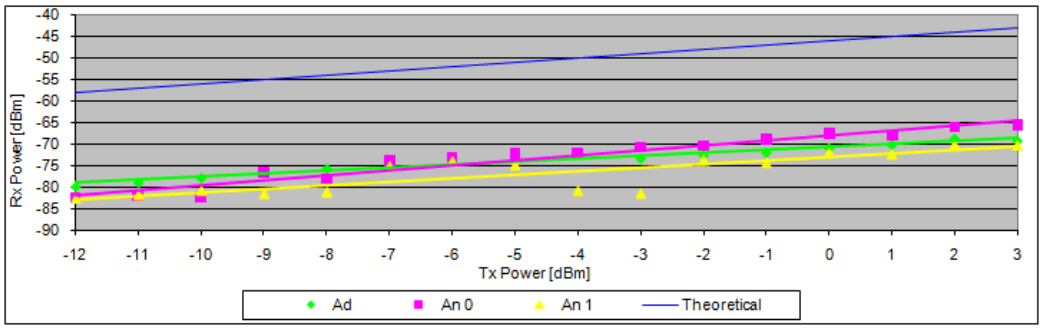

Figure 5.27: P_{RX} vs P_{TX}, 2 m distance, Avionics Laboratory, node

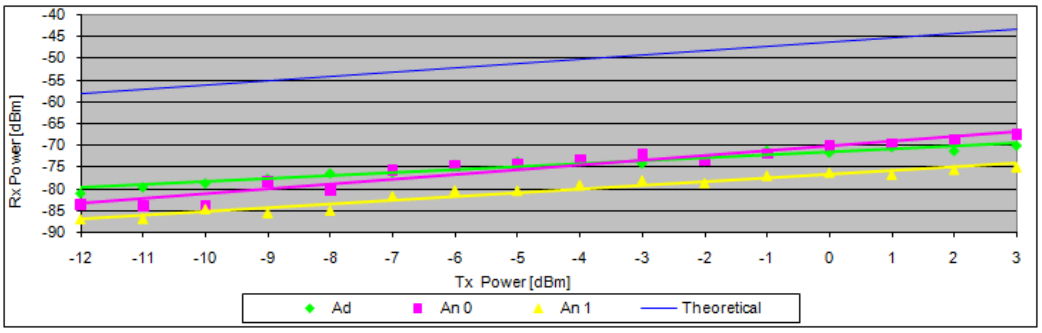

Figure 5.28: P_{RX} vs P_{TX}, 2 m distance, Avionics Laboratory, coordinator

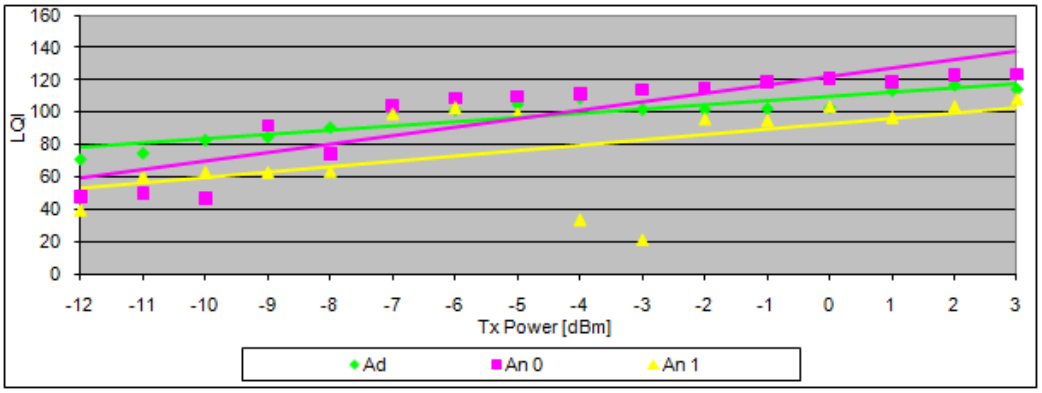

Figure 5.29: LQI vs P_{TX}, 2 m distance, Avionics Laboratory, node

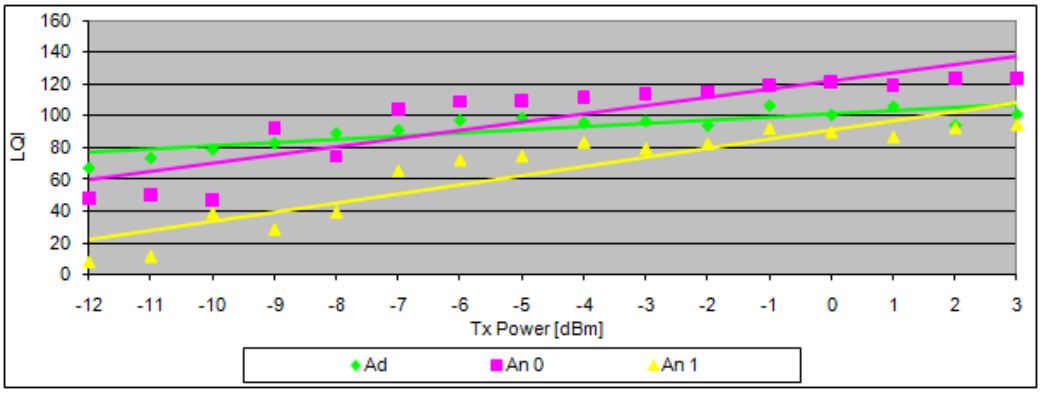

Figure 5.30: LQI vs P_{TX}, 2 m distance, Avionics Laboratory, coordinator

5.4 V-Ex Mockup Test

The results of the measurements I did to test the homogeneity of the electric field are shown in tab. 5.2, tab. 5.3, tab. 5.4 and tab. 5.5 and are referred to a transmission Power equal to 0 dBm.

Table 5.2: Closed walls, coordinator in cavity 1

Cavity	3	5	6	4	2
RSSI [dBm]	-43	-57	-62	-52	-57
σ	2	2	3	2	2

Table 5.3: Open walls, coordinator in cavity 1

Cavity	3	5	6	4	2
RSSI [dBm]	-56	-57	-59	-56	-57
σ	3	2	3	5	2

Table 5.4: Closed walls, coordinator in same cavity of the node

Cavity	3	5	6	4	2	1
RSSI [dBm]	-36	-57	-37	-37	-57	-37
σ	1.21	1.64	2.54	1.20	1.64	0.46

Table 5.5: Open walls, coordinator in same cavity of the node

Cavity	3	5	6	4	2	1
RSSI [dBm]	-41	-57	-38	-40	-57	-38
σ	2.89	1.64	2.58	1.71	1.64	1.00

I averaged for every receiving device the value obtained from nine set of measures. Each set was made up of 40 packets and is correspondent to a combination of transmitter/receiver antenna, as explained in par. 4.5.3, for a total of 360 values for each of the 26 measuring points shown in fig. 4.8.

Main and standard deviation are in this way representative values of the measured quantity, namely the received signal power. Then I averaged the RSSI values of the nodes in the same cavity, to obtain the average received signal power value and its standard deviation for each cavity. High standard deviation value suggests that the intensity of the electric field is dependent on the position and on the orientation of the receiving device inside a cavity, whereas a small value validates the multi-mode cavity theory. In tab. 5.2 there are the values obtained using the transmitter coordinator in cavity 1 and in closed walls configuration, whereas open walls configuration results are in tab. 5.3. Then the results obtained putting the transmitter device in the same cavity of the receiving nodes are reported in tab. 5.4 for the closed walls configuration and in tab. 5.5 for the open walls situation. Values obtained putting the coordinator in cavity 1 are reported only in tab. 5.4 and tab. 5.5, as they would be the same in the other tables. The standard deviation is almost always less than 3.6, the value found by the Astrium numerical simulation [31], [32] so the Electric Field can be considered homogeneous inside the cavities. As expected bigger standard deviation values are obtained in open walls configuration because of the large apertures, in this case the multi-mode cavity principle is not always applicable.

In reference to par. 4.5.1, in tab. 5.6 are summarized the crossing apertures values S_{ij}[2] given by [31].

Table 5.6: Mock-up crossing apertures

S_{ij}	**value** $[m^2]$
S_{12}	0.024
S_{24}	0.05
S_{46}	0.028
S_{65}	0.01
S_{53}	0.034
S_{31}	0.038
S_{25}	0.024

According to eq. 2.8, in tab.5.7 are shown the insertion loss values I calculated from the given data adding the 3 dB factor, indicated in [32], to take

[2]Each S_{ij} value is equal to S_{ji}, not all the values are shown in tab.5.6.

into account about material data uncertainty. These values are obtained using $f = 2.42\ GHz$, $\sigma = 3.82 \cdot 10^7 \frac{S}{m}$, $\mu = 1.26 \cdot 10^{-6} \frac{H}{m}$, referred to Aluminium. According to eq. 4.3, the E_{ij} values I obtained are reported in tab. 5.8.

Table 5.7: Mock-up insertion losses

Cavity	X_r	X_σ	X_c [dB]
1	174.44	0.44	-25.43
2	180.99	0.39	-25.59
3	233.32	0.89	-26.70
4	239.86	0.73	-26.81
5	139.56	0.81	-24.47
6	106.85	0.50	-23.31

Table 5.8: E_{ij} values

$E_{i\to j}$	**value**	$E_{j\to i}$	**value**
E_{12}	0.23	E_{21}	0.24
E_{24}	0.29	E_{42}	0.34
E_{46}	0.33	E_{64}	0.22
E_{65}	0.17	E_{56}	0.20
E_{53}	0.24	E_{35}	0.32
E_{31}	0.30	E_{13}	0.26
E_{34}	0.20	E_{43}	0.20

I identified the main paths for the six receiving cavities with the emitter placed in cavity 1.

- For receiving cavity 1:
  1. cavity 1 → cavity 1.
- For receiving cavity 2:
  1. cavity 1 → cavity 2
  2. cavity 1 → cavity 3 → cavity 4 → cavity 2
  3. cavity 1 → cavity 3 → cavity 5 → cavity 6 → cavity 4 → cavity 2

- For receiving cavity 3:
  1. cavity 1 → cavity 3
  2. cavity 1 → cavity 2 → cavity 4 → cavity 3
  3. cavity 1 → cavity 2 → cavity 4 → cavity 6 → cavity 5 → cavity 3
- For receiving cavity 4:
  1. cavity 1 → cavity 2 → cavity 4
  2. cavity 1 → cavity 3 → cavity 4
  3. cavity 1 → cavity 3 → cavity 5 → cavity 6 → cavity 4
- For receiving cavity 5:
  1. cavity 1 → cavity 3 → cavity 5
  2. cavity 1 → cavity 3 → cavity 4 → cavity 6 → cavity 5
  3. cavity 1 → cavity 2 → cavity 4 → cavity 6 → cavity 5
  4. cavity 1 → cavity 2 → cavity 4 → cavity 3 → cavity 5
- For receiving cavity 6:
  1. cavity 1 → cavity 3 → cavity 5 → cavity 6
  2. cavity 1 → cavity 3 → cavity 4 → cavity 6
  3. cavity 1 → cavity 2 → cavity 4 → cavity 6
  4. cavity 1 → cavity 2 → cavity 4 → cavity 3 → cavity 5 → cavity 6

I evaluated all the E_{RX} corresponding to these paths according to eq. 4.4 and the total received electric field in each cavity according to eq. 4.5. From these I evaluated the received power values P_{TX}, according to eq. 4.6, for each P_{TX} value.

In fig. 5.31, 5.32, 5.33, 5.34, 5.35, 5.36 are shown the variation of the received power to the transmission power inside the cavities for the closed walls configuration. Except for the cavity 1, which is the same cavity of the emitter, where saturation has been reached, there is a good agreement in comparison to the Astrium model of cavity losses.

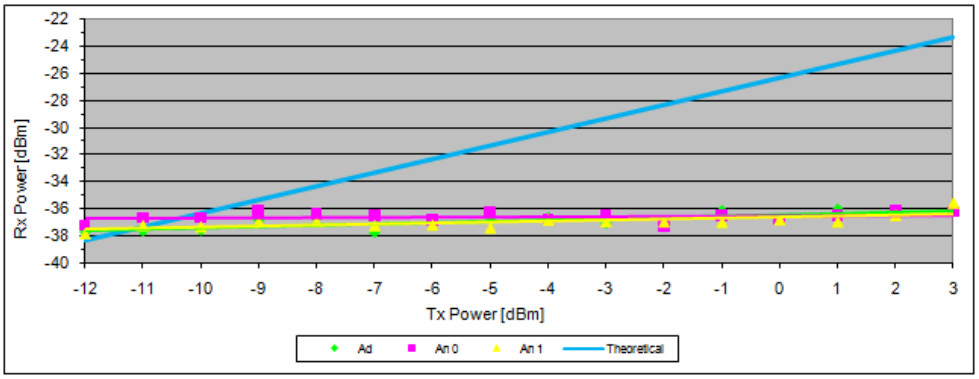

Figure 5.31: P_{RX} vs P_{TX} curves inside cavity 1

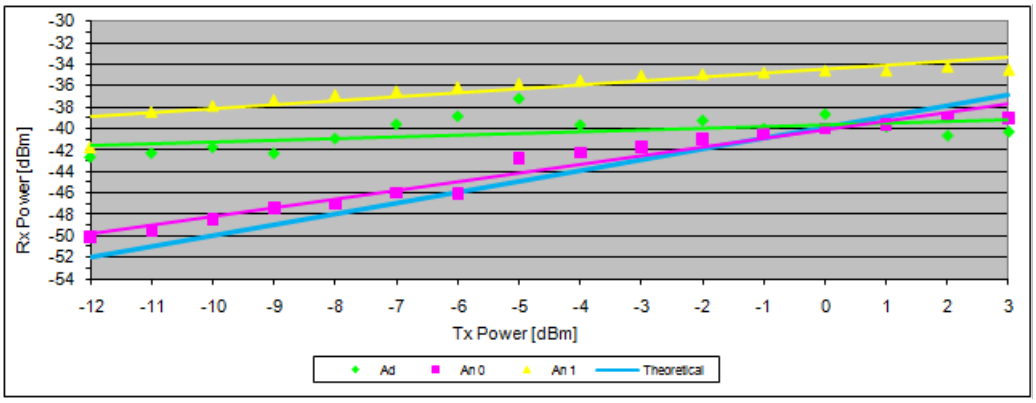

Figure 5.32: P_{RX} vs P_{TX} curves inside cavity 2

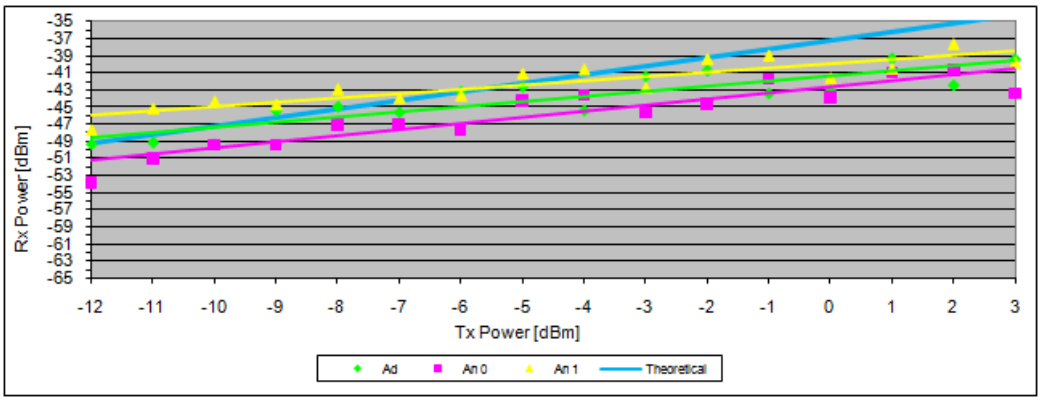

Figure 5.33: P_{RX} vs P_{TX} curves inside cavity 3

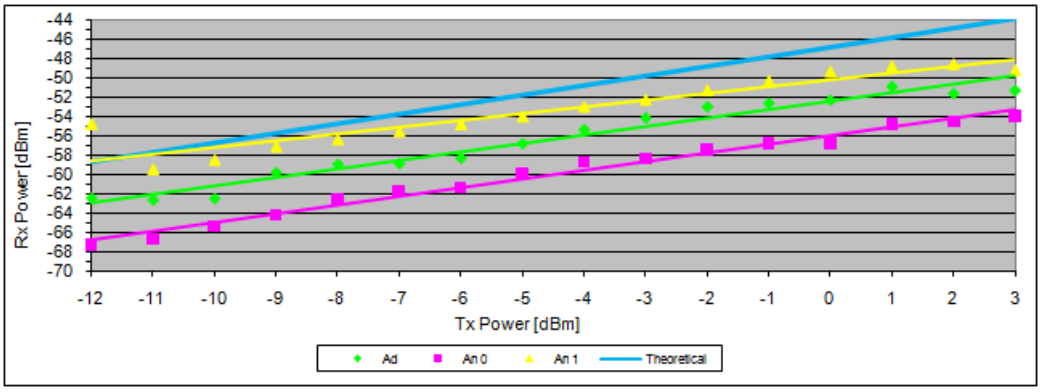

Figure 5.34: P_{RX} vs P_{TX} curves inside cavity 4

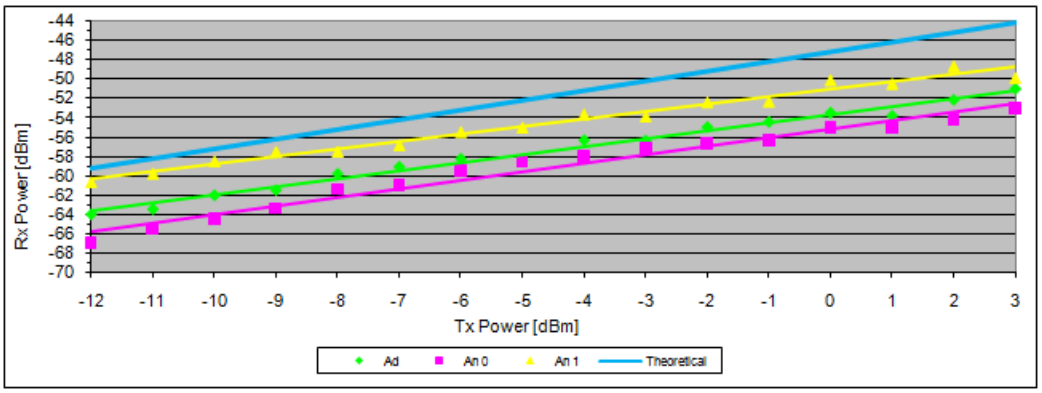

Figure 5.35: P_{RX} vs P_{TX} curves inside cavity 5

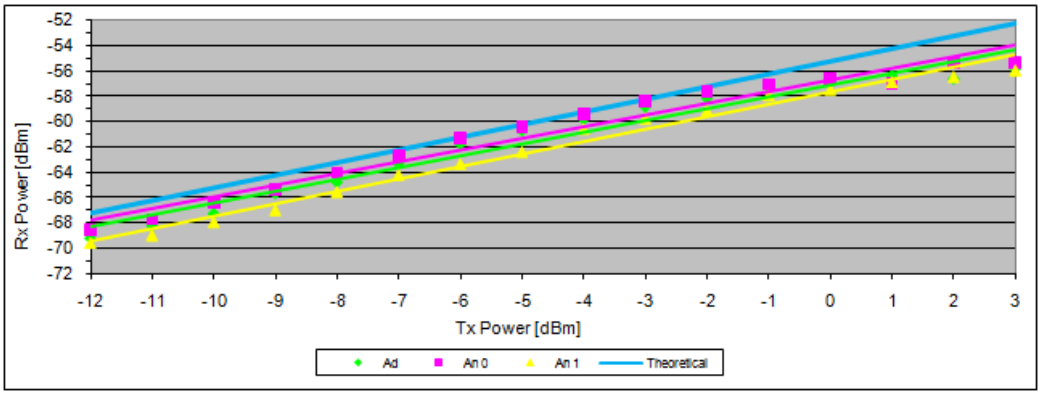

Figure 5.36: P_{RX} vs P_{TX} curves inside cavity 6

I compared the measured RSSI and LQI indexes using either the nodes placed in the 26 measuring points in fig. 4.8 than the coordinator placed in cavity 1 and in the same cavity of the nodes, used as transmitter and as receiver, to obtain overall RSSI and LQI gains and penalties inside the mock-up. The first case refers to the configuration with open walls and the coordinator in cavity 1. The six columns refer to the transmitter/receiver antennas combination: C means that the emitter is the coordinator, therefore the node is used as receiver. The number indicates the used transmitter antenna, it can be one of the two available PIFAs (0 or 1) or can be decided by the device (2) with the Antenna Diversity mechanism activated. N stands for node used as emitter, in this case the coordinator is the receiver. Each column is the average on 26 measuring set, each one made by 40 packets. Their meaning is an overall performance indication inside the mock-up, since I used the data obtained from all the cavities. In most of cases the Gain is bigger than the Penalty, with an occurrence of 60% to 70% as shown in fig. 5.37, with evident gain peaks, either about RSSI than about LQI, as shown in fig. 5.38, 5.39, 5.40 and 5.41.

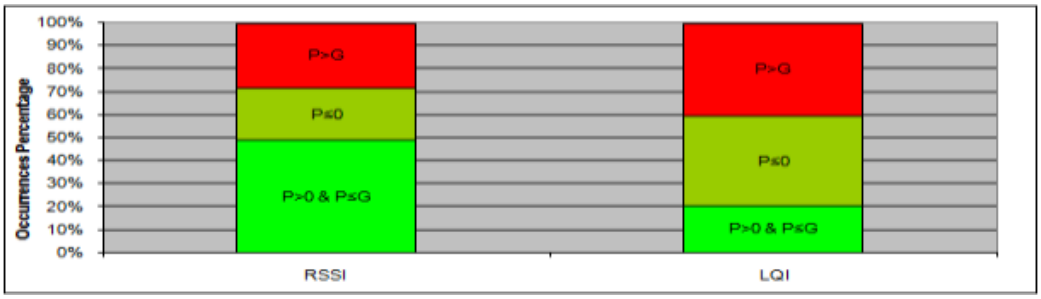

Figure 5.37: Penalty, case 1

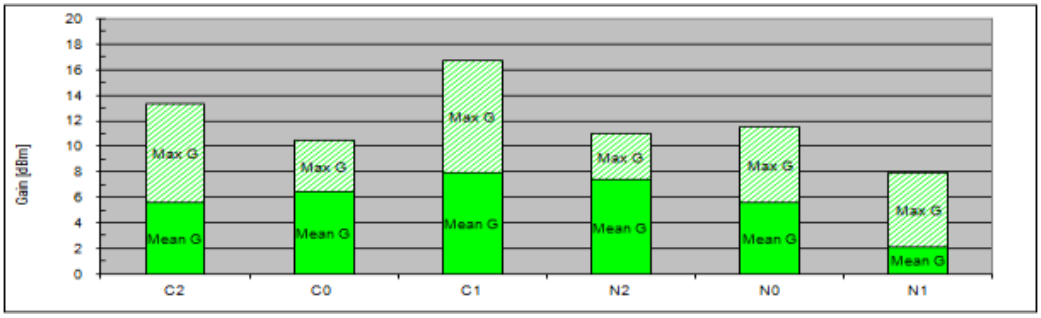

Figure 5.38: RSSI gain, case 1

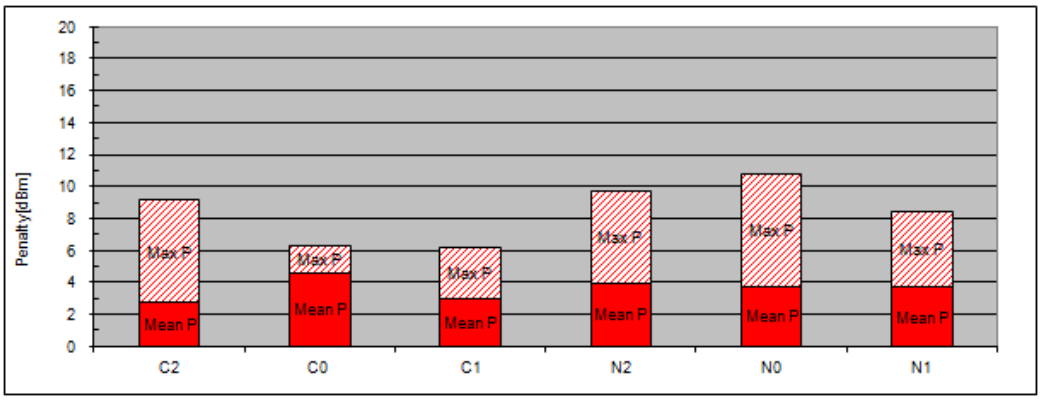

Figure 5.39: RSSI penalty, case 1

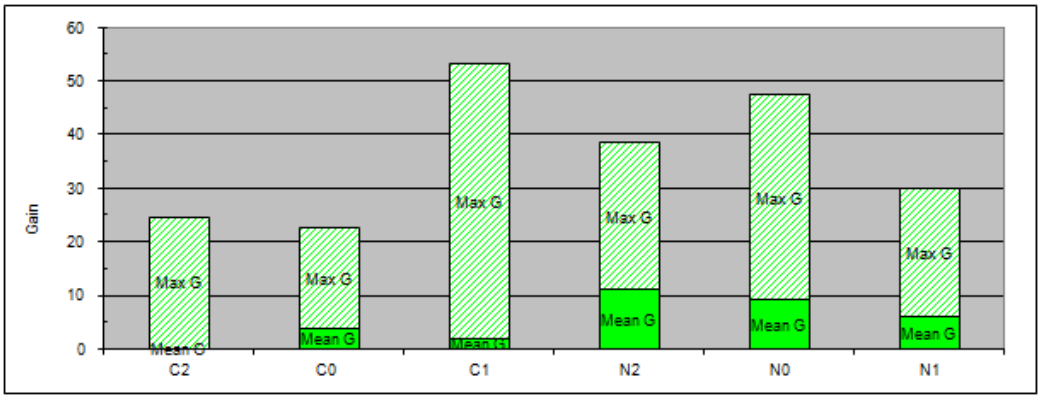

Figure 5.40: LQI gain, case 1

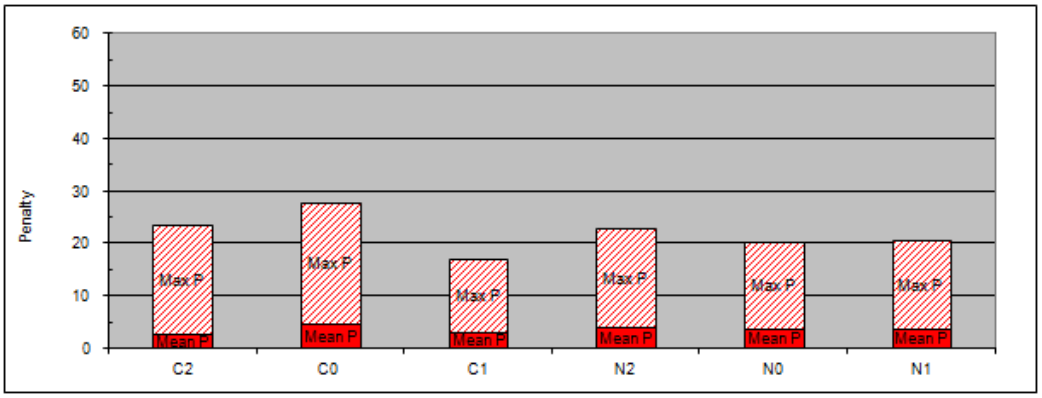

Figure 5.41: LQI penalty, case 1

The second case refers to the configuration with closed walls and the coordinator in cavity 1. The overall occurrence of cases which in Penalty is bigger than Gain, about either RSSI than LQI, is shown in fig. 5.42, together with the percentage of negative Penalty and Penalty lower than Gain cases. In fig. 5.43 and 5.43 are respectively the RSSI gain and penalty for the six transmitter/receiver combinations explained previously. In fig. 5.45 and 5.45 the same indexes referred to LQI.

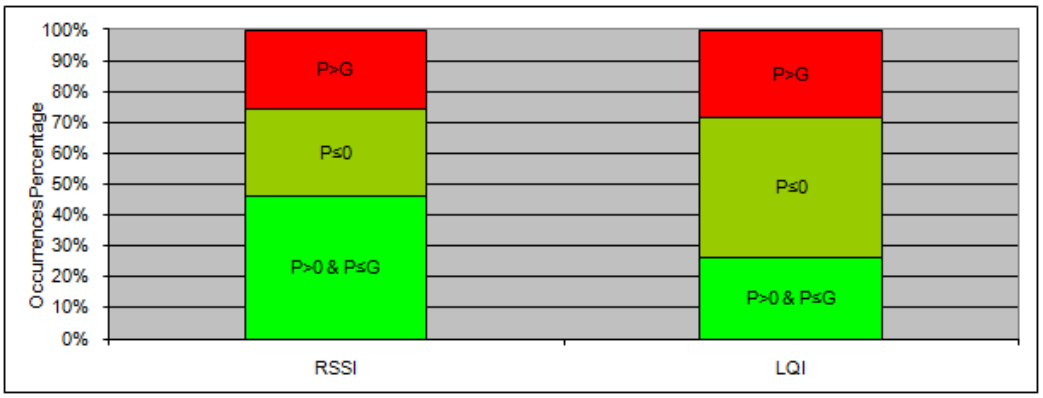

Figure 5.42: Penalty, case 2

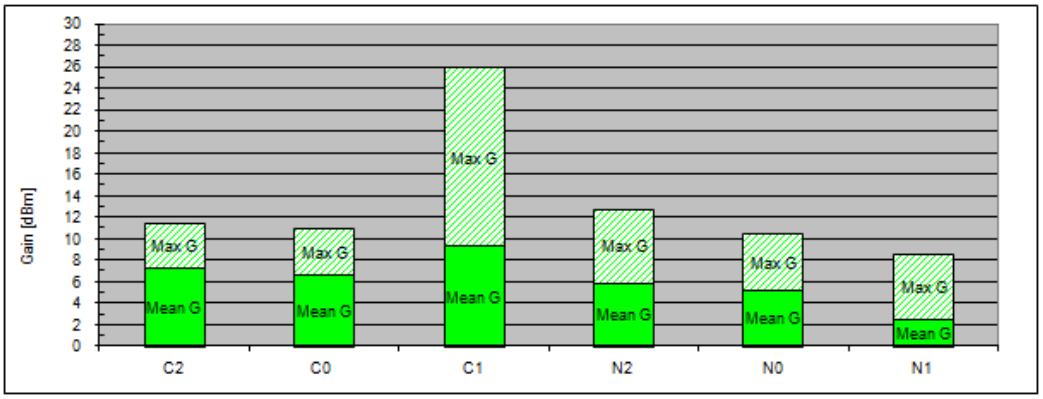

Figure 5.43: RSSI gain, case 2

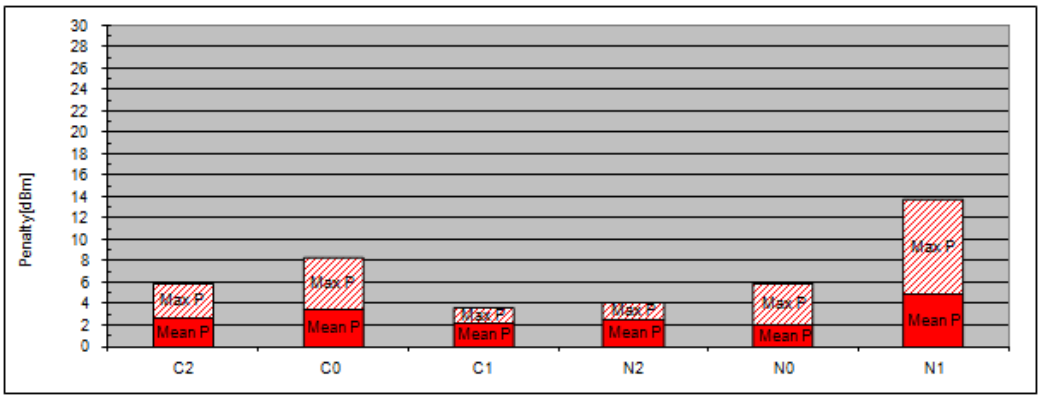

Figure 5.44: RSSI penalty, case 2

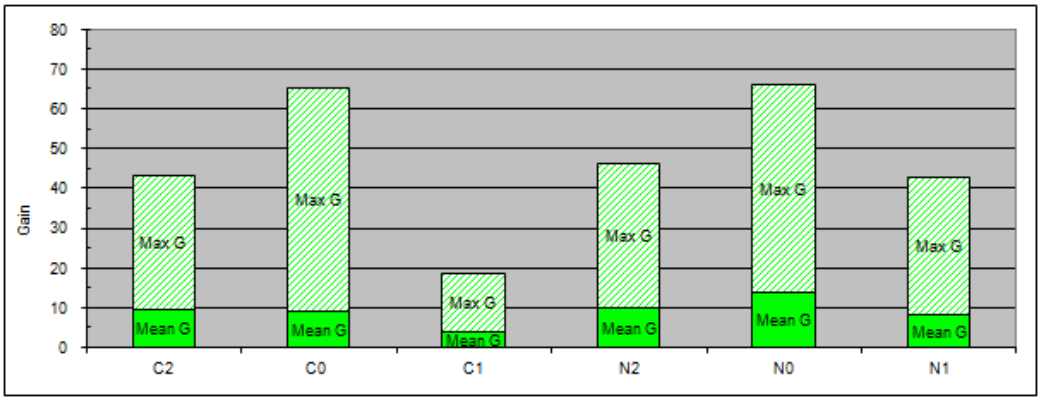

Figure 5.45: LQI gain, case 2

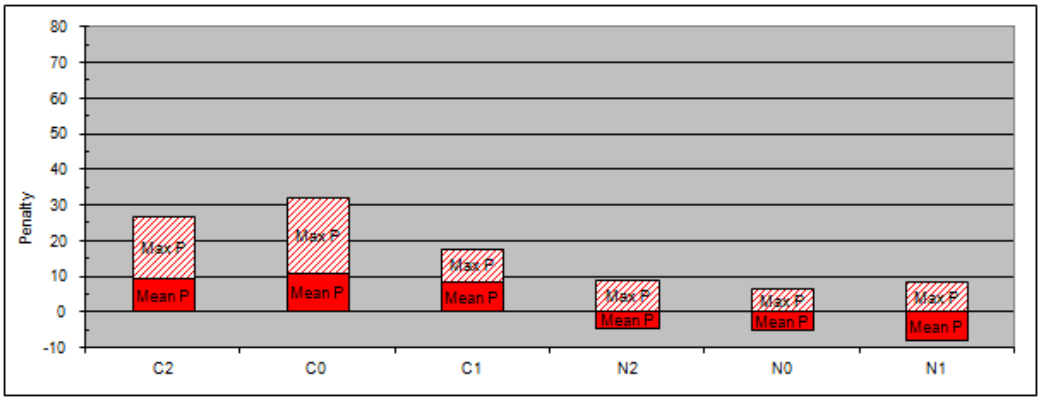

Figure 5.46: LQI penalty, case 2

The third case refers to the configuration with open walls and the coordinator in the same cavity of the nodes. In fig. 5.47 the overall cases occurrence about all the possible relationships between RSSI and LQI Gain and Penalty is resumed. In fig. 5.48 and 5.48 the RSSI gain and penalty values for the six transmitter/receiver combinations are shown, whereas the same indexes referred to LQI are in fig. 5.50 and 5.50.

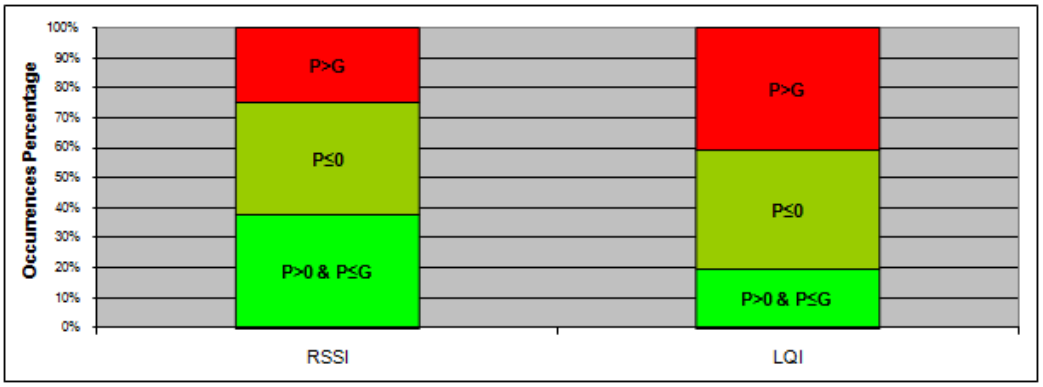

Figure 5.47: Penalty, case 3

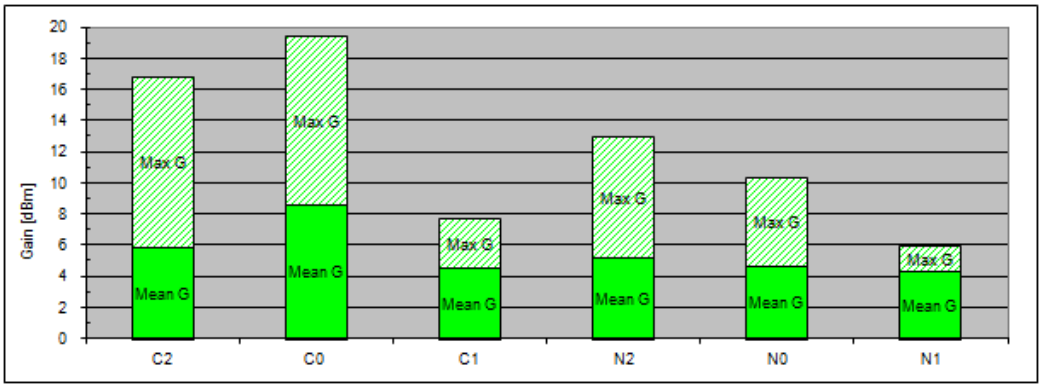

Figure 5.48: RSSI gain, case 3

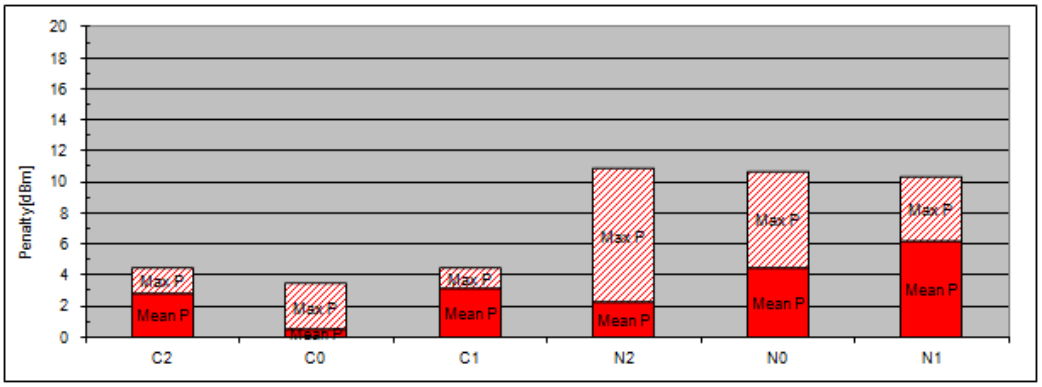

Figure 5.49: RSSI penalty, case 3

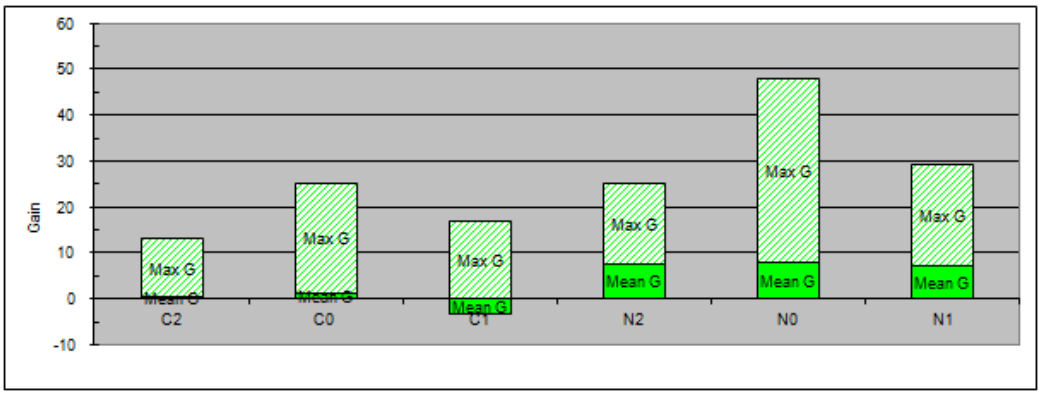

Figure 5.50: LQI gain, case 3

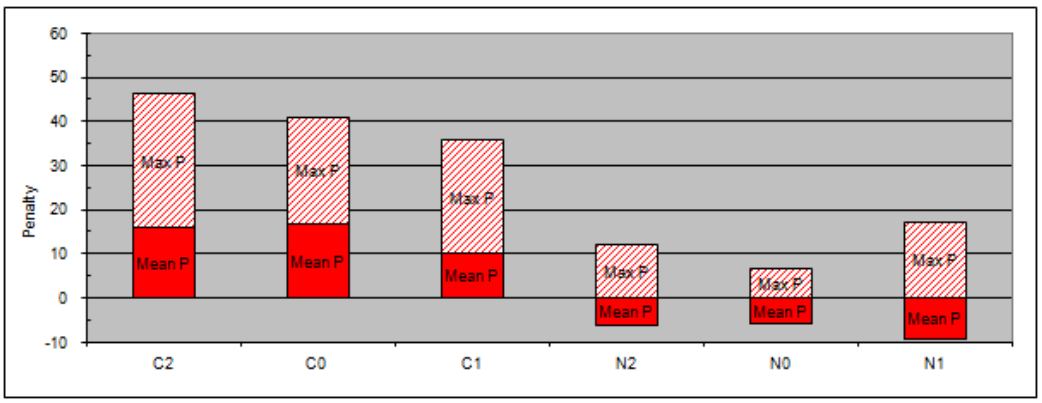

Figure 5.51: LQI penalty, case 3

The last case refers to closed walls and coordinator in the same cavity of the nodes configuration. Events occurrence about the relationships between RSSI and LQI Gain and Penalty is in fig. 5.52. In fig. 5.53 and fig. 5.55 are resumed respectively the RSSI and the LQI gain I obtained for the six transmitter/receiver combinations, whereas fig. 5.53 and 5.55 are referred to Penalty.

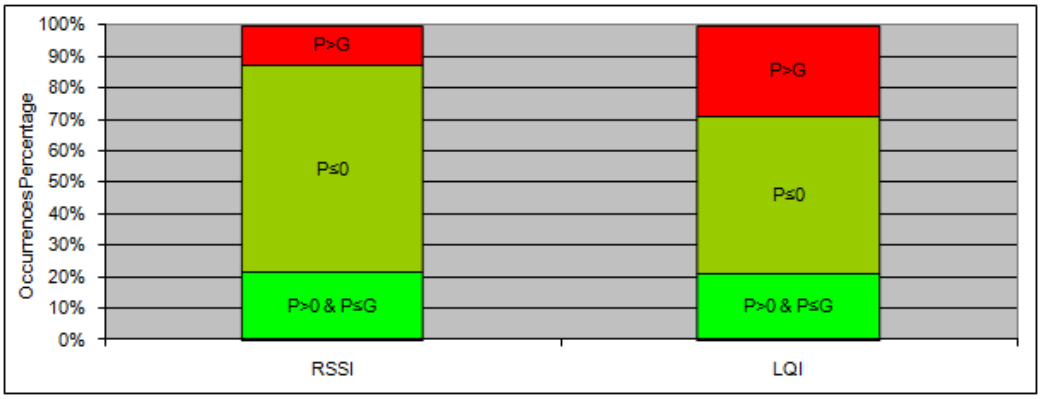

Figure 5.52: Penalty, case 4

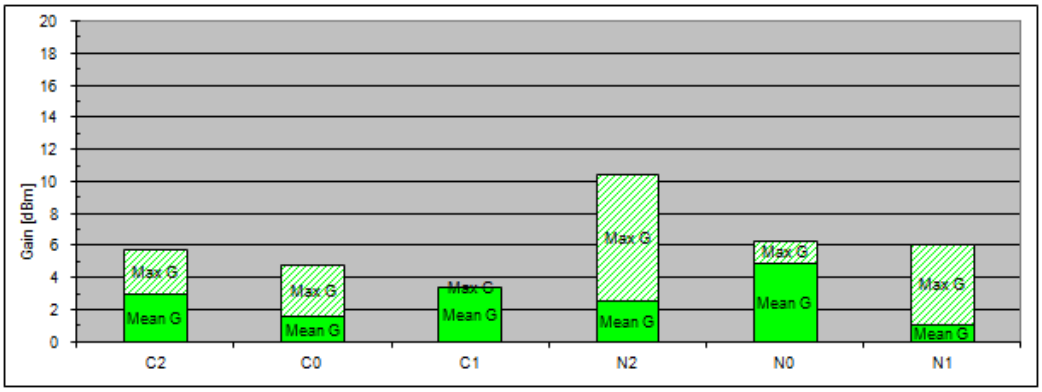

Figure 5.53: RSSI gain, case 4

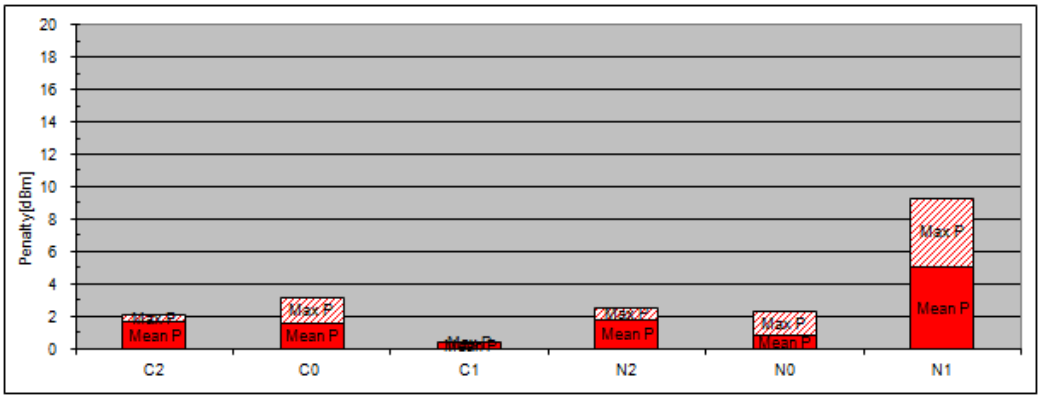

Figure 5.54: RSSI penalty, case 4

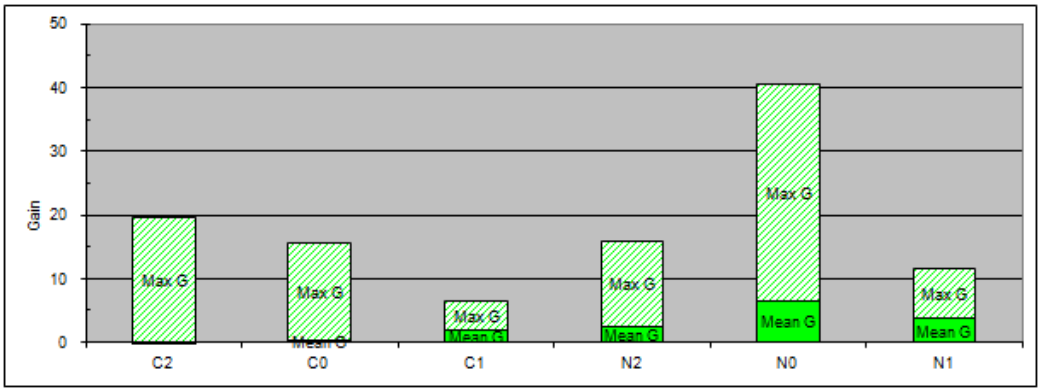

Figure 5.55: LQI gain, case 4

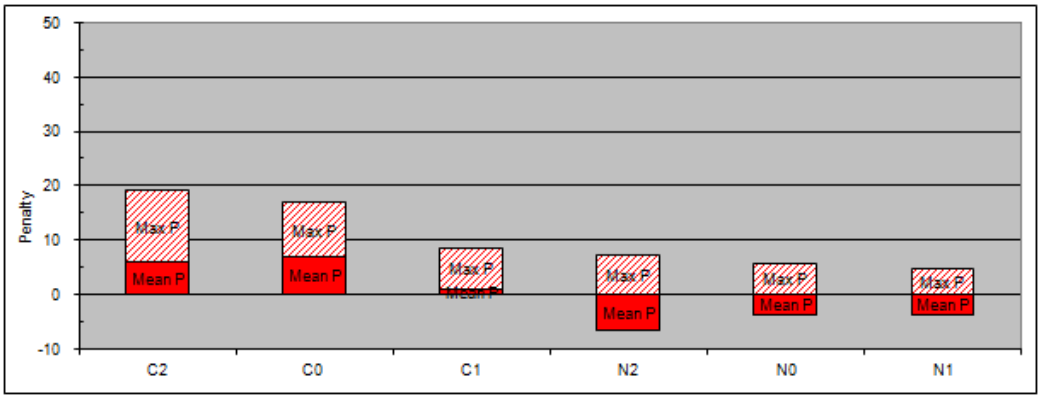

Figure 5.56: LQI penalty, case 4

The high occurrence of cases where both Penalty than Gain are positive means that using Antenna diversity it results in the middle of the performances achieved using the two antennas. This agrees with the antenna selection process of the Antenna Diversity mechanism, based on a SNR estimation. For this reason meaningful information can be obtained more from the LQI index, which takes into account both the strength than the quality of the signal, than from RSSI. The situation is in fact resumed in fig. 5.57, fig. 5.58, fig. 5.59 and fig. 5.60, referred to closed and open walls, using the coordinator or the nodes as receiving device.

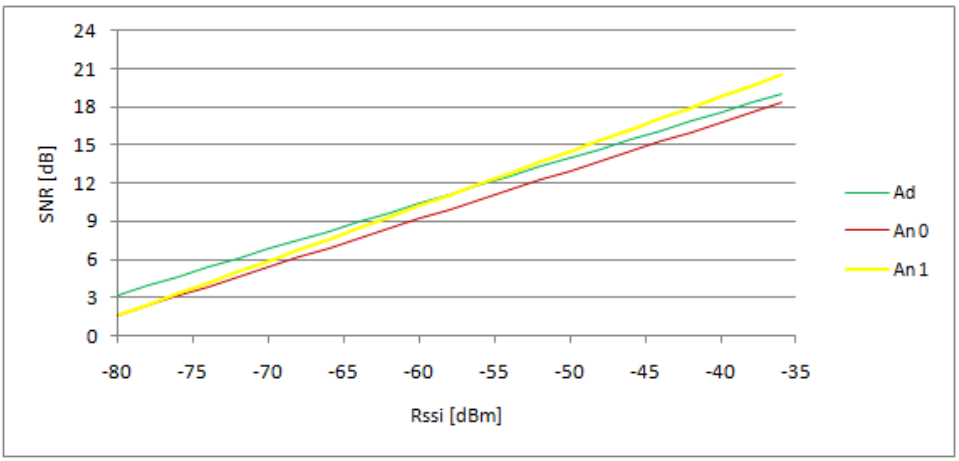

Figure 5.57: SNR vs RSSI, open walls, coordinator receiving

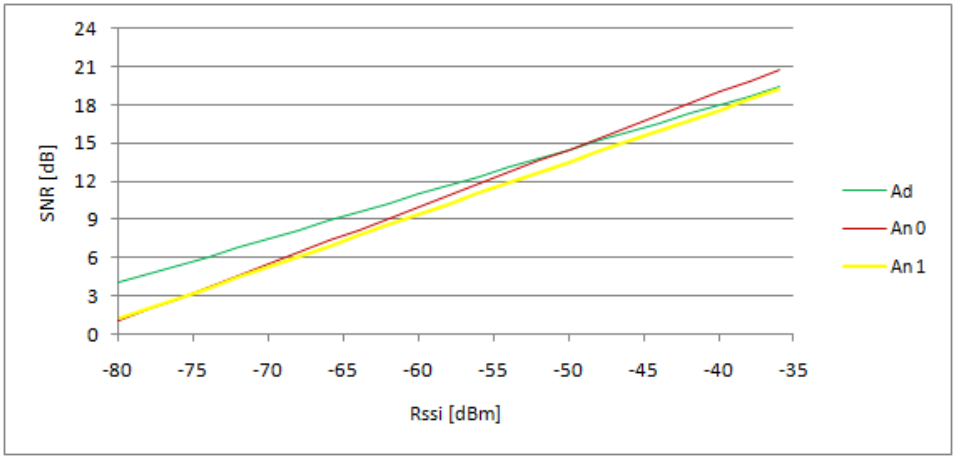

Figure 5.58: SNR vs RSSI, open walls, node receiving

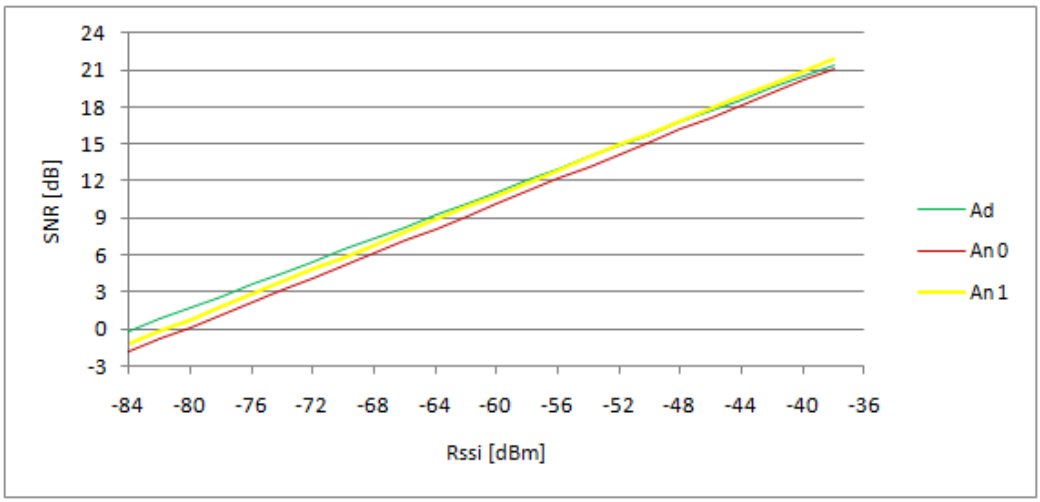

Figure 5.59: SNR vs RSSI, closed walls, coordinator receiving

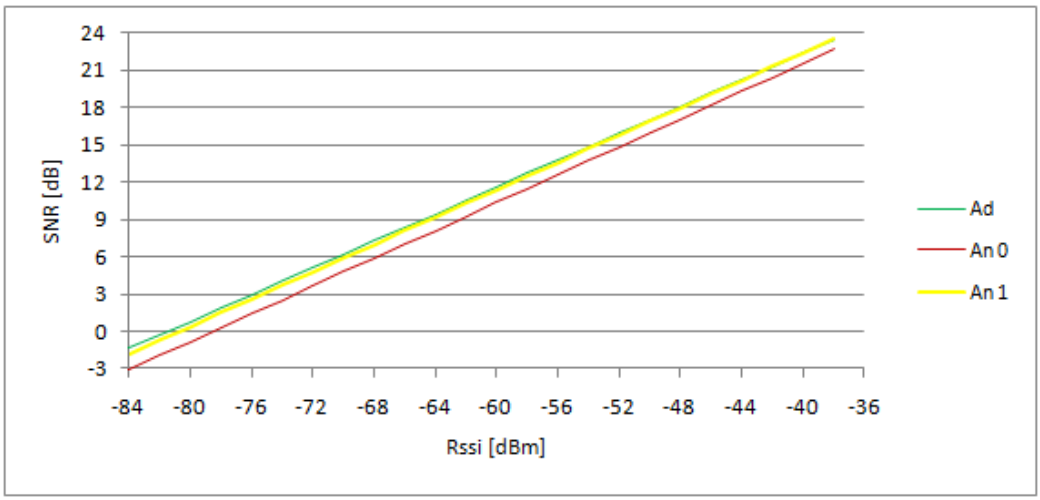

Figure 5.60: SNR vs RSSI, closed walls, node receiving

I processed the measurements obtained from the second phase of the test, obtained using two nodes per cavity and evaluating for each couple of measured LQI and RSSI, the correspondent SNR using eq. 4.1 and the graphs in par. 4.4.1. The trend I obtained suggests that for low SNR situations (which corresponds to low RSSI situation but the same can't be said of the opposite) the Antenna Diversity mechanism results in a gain in respect to the quality obtained using one of the two antennas, whereas when the SNR is fairly good, one of the two antennas is arbitrarily chosen, so giving a medium level result, between those ones obtained using one of the two PIFAs.

I evaluated overall Gain and Penalty indexes, referred to RSSI and LQI, for the four tested situation: open walls and coordinator in cavity 1, closed walls and coordinator in cavity 1, open walls and coordinator in same cavity of the node, closed walls and coordinator in the same cavity of the node, respectively indicated in tab. 5.9 and tab. 5.10 as case 1, case 2, case 3 and case 4. Averages and maximum values of Gain and Penalty, with their standard deviation (σ_m referred to mean values, σ_M to maximum values), are referred to the graphs shown in this paragraph.

Table 5.9: RSSI average and maximum Gains and Penalties

Case	G_{RSSI}	σ_m	G_{MAX}	σ_M	P_{RSSI}	σ_m	P_{MAX}	σ_M
1	6	2	12	3	4	1	8	2
2	6	2	13	6	3	1	7	4
3	5	2	12	5	3	2	7	4
4	3	1	6	2	2	2	3	3

Table 5.10: LQI average and maximum Gains and Penalties

Case	G_{LQI}	σ_m	G_{MAX}	σ_M	P_{LQI}	σ_m	P_{MAX}	σ_M
1	5	4	36	12	3	9	22	11
2	9	3	47	18	2	9	14	14
3	3	5	28	12	3	12	18	19
4	2	2	18	12	0	6	8	8

From these values I evaluated average SNR Gains and Penalties with their estimated errors, obtained through uncertainty propagation, according to [37]. E_m is referred to the mean value, E_M to the maximum one, obtained using eq. 5.1, where E_R is the random uncertainty and E_S the systematic uncertainty, due to measurement resolution. The former is the standard deviation on the SNR indirectly evaluated from RSSI and LQI direct measurement using eq. 5.2, x_i are RSSI and LQI, N is equal to 2, as SNR is dependent on these two values, according with eq. 4.1, which includes also definitions of constant values a,b and d. The variable indicated as LQI is the LQI Gain in tab. 5.10 if the random uncertainty is referred to Gain, whereas is LQI Penalty if the random uncertainty is about Penalty. The latter is evaluated using eq. 5.3,

which comes from LQI and RSSI measurement resolution, respectively equal to 1.5 and 3 dB.

$$E = \sqrt{E_R^2 + E_S^2} \tag{5.1}$$

$$E_R = \sqrt{\sum_{i=1}^{N} \left(E_i \frac{\partial SNR}{\partial x_i} \right)^2} = \sqrt{(a \cdot LQI + b)^2 \sigma_{LQI}^2 + d^2 \cdot \sigma_{RSSI}^2} \tag{5.2}$$

$$E_S = \sqrt{E_{LQI}^2 + E_{RSSI}^2} = \sqrt{1.5^2 + 3^2} \tag{5.3}$$

SNR Gain and Penalty mean and maximum values are reported in tab. 5.11 together with their estimated measurement error. Maximum Gain and maximum Penalty values are not averages of values obtained by six different samples sets, corresponding to six different emitters, as previously done for RSSI and LQI, but are referred to the case with the maximum value on the total set of measurements. I did this so I didn't introduce any further contribution due to the averaging process to the estimated error value, so that also for this case it can be considered equal to the obtained uncertainty.

Table 5.11: LQI average and maximum Gains and Penalties

Case	G_{SNR}	G_{MAX}	E_G	P_{SNR}	P_{MAX}	E_P
1	5	21	4	3	13	5
2	10	13	4	3	8	5
3	8	13	4	4	7	6
4	4	5	4	-2	1	5

5.5 Radiation test

The three devices under test and the coordinator are identified from their short address: 0x7933, 0x85E3 and 0x78BC are the nodes, whereas 0x8433 identifies the coordinator. In fig. 5.62 and fig. 5.61 current and voltage supply of all the devices during the two weeks exposure to radiation are shown. The voltage is quite stable for all the devices, except for one that have a drop, caused by a limitation of the input current (device 0x7933). This can be a failure of the power manager of the GP500C device or a current limitation on the main feed power line. All the DUT show no current increase until 65 ÷ 68 kRads, whereas the communication is still present up to 105 *kRads* for device 0x7933 and up to 145 *kRads* for device 0x85E3. Lost communication (no packets received from that time forward) is indicated with dashed lines.

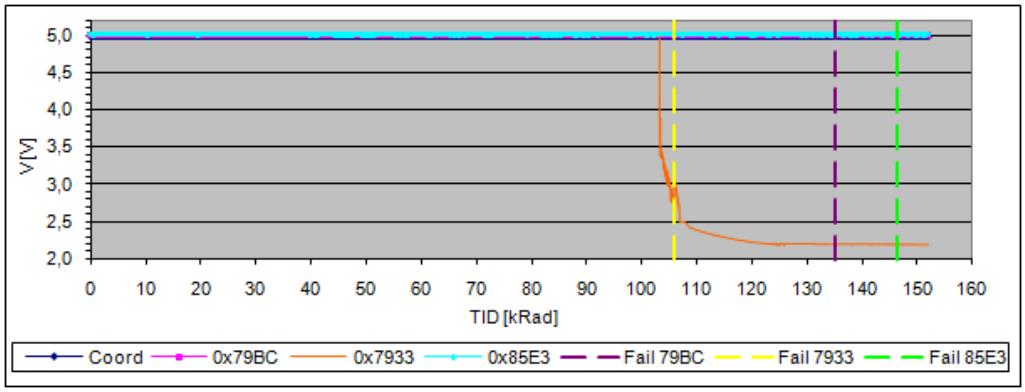

Figure 5.61: V and i values during radiation test

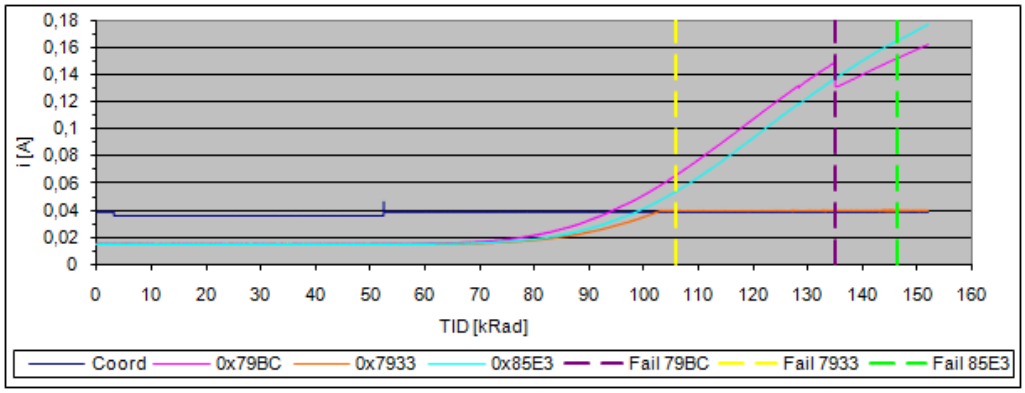

Figure 5.62: Current value during radiation test

In fig. 5.63 the feed power during the exposure to radiation is shown. At a level of around 128 kRads two devices have a little drop of around 3 mA, which could be a failure of the same component. Moreover the power trend derivative is decreasing, as shown in fig. 5.64 with a comparison between the interpolation of the last values and the actual trend. This indicates that a plateau may be reached.

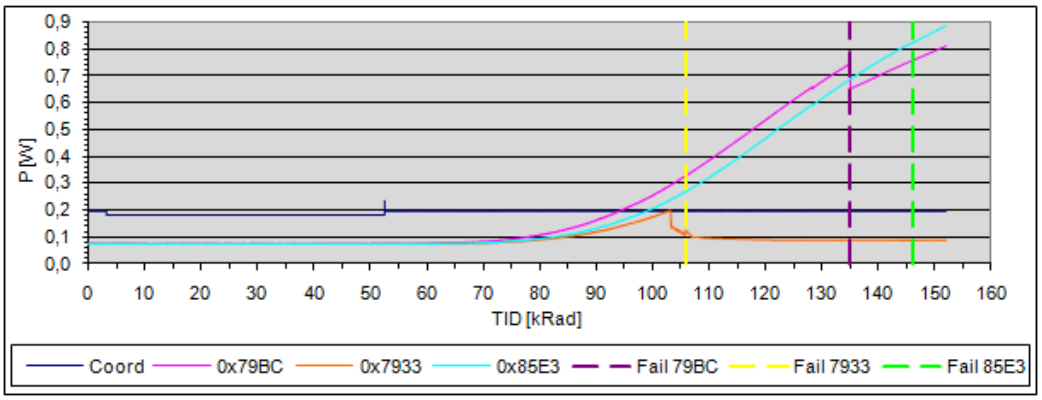

Figure 5.63: Feed power during radiation test

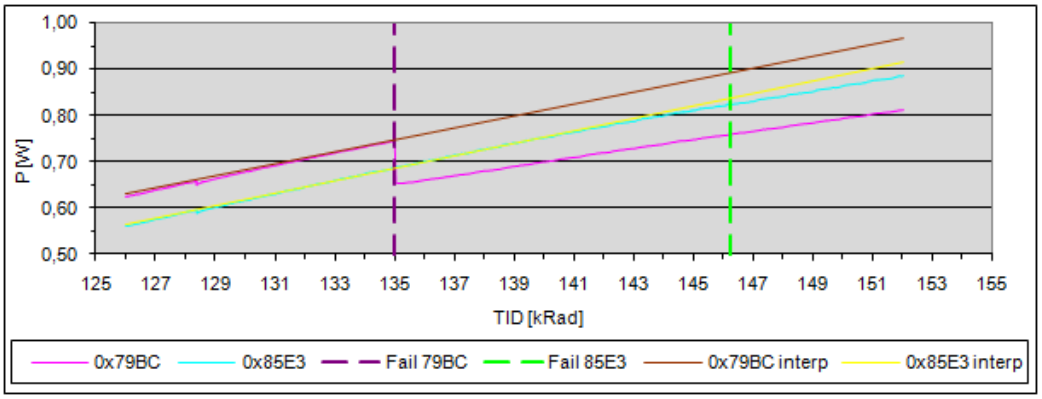

Figure 5.64: Feed power during radiation test: particular

In fig. 5.65 and fig. 5.66 is shown the current consumption for all the devices before the accelerated annealing phase. It is evident that the current consumption is one order of magnitude higher than the nominal one (represented by device 0x8433), even if, after a fast increase in the first 30 minutes, it decreases. I monitored the devices for 72 hours after the exposure to radiation, doing a measure every minute. Then I completed the 168 hours annealing phase at room temperature and I did a last measurement just before putting

them in the oven at 100℃ for the accelerated annealing phase. Every device shows recovery, as the current consumption is reduced of almost one order of magnitude in comparison to that one immediately after the exposure to radiation. The result of this measurement is reported in tab. 5.12.

Table 5.12: Current consumption after room temperature annealing

Device	0x8433	0x79BC	0x7933	0x85E3
i [A]	0.011	0.069	0.036	0.067

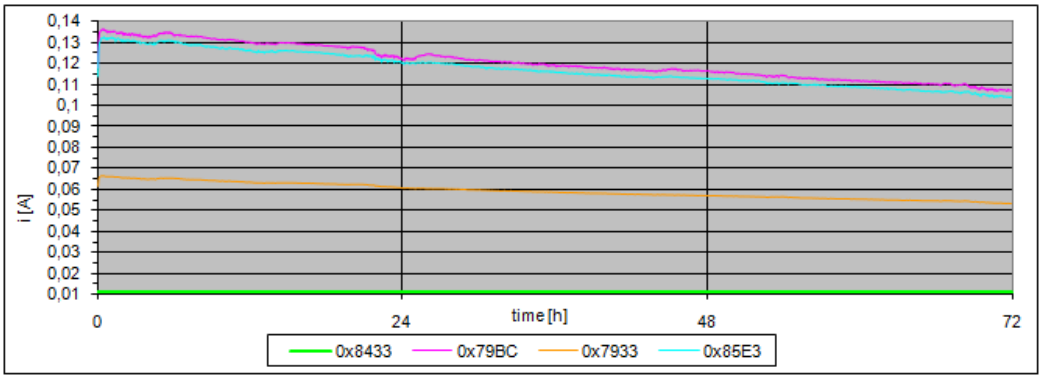

Figure 5.65: Current consumption before accelerated annealing

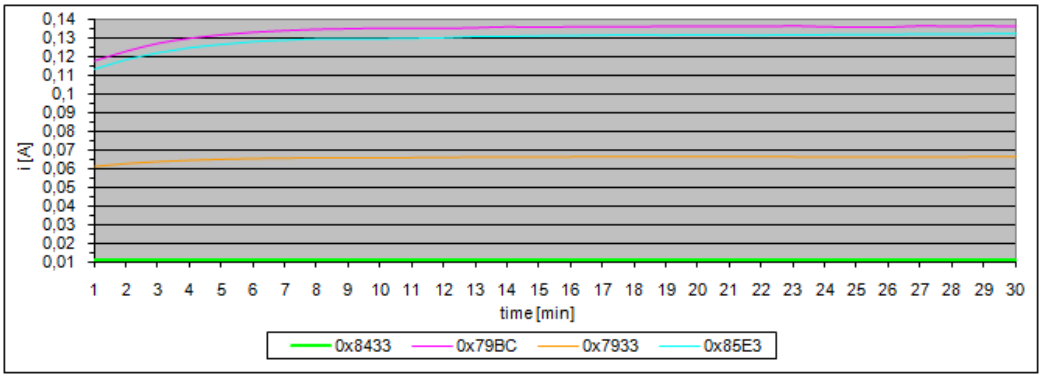

Figure 5.66: Current consumption before accelerated annealing: particular

After the accelerated annealing all the current values are quite similar to the nominal ones, so it is possible that recovery happened for some devices, as shown in fig. 5.67. Unluckily after radiation exposure devices registers

seem to be reset, so there's no way to test them in communication mode, as they have no more a stored MAC address and when starting the association sequence, it results in a reset for all the nodes.

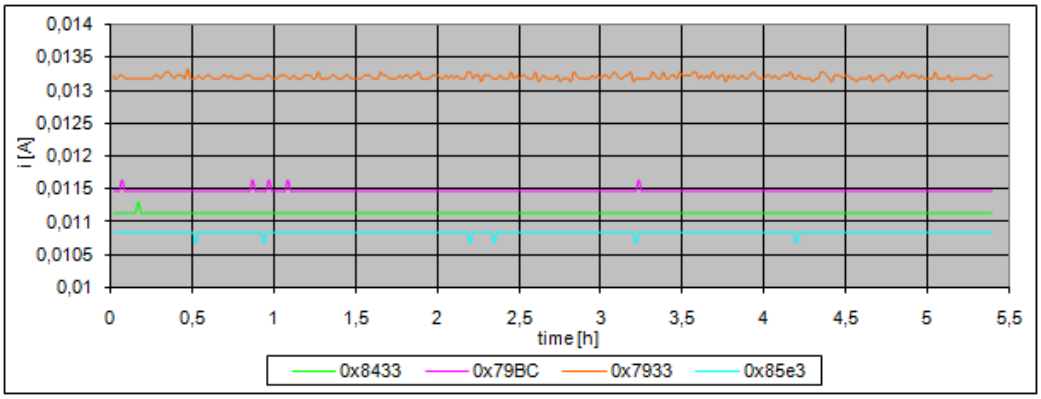

Figure 5.67: Current consumption after accelerated annealing

Further tests, done with GreenPeak staff after the annealing phase, identified a corruption of the One Time Programmable (OTP) memory for the device 0x78BC, which has power consumption and voltage on the V_{ddDIG} pin equal to nominal ones and is still working, even if the memory seems to be reset, so the default MAC address is zero and when starting the communication mode it resets. Moreover the oscillator works properly. On the other hand, the device 0x85E3 has the oscillator not working anymore and the voltage on the V_{ddDIG} pin, which is the supply of the device digital core, is null. Moreover it has a higher current consumption (3 times the nominal one), this indicated that there are still high leakage currents flowing, probably in the PSM circuits, moreover. To investigate if the leakage current is in a particular spot and to find this spot, it is possible to do a hot-spot analysis with an infra-red camera or other techniques for integrated circuits. In the end, also the device 0x7933 has a not working oscillator and fails to start up, the voltage on the V_{ddDIG} pin is null, even if the current consumption is similar to the nominal one. These two last devices shows a failure in the Analog part, likely of the PSM, identified by GP staff as a quite radiation sensitive component.

In fig. 5.68 and fig. 5.68 the number of errors respectively to time and to radiation level is shown. In the picture above it is indicated the loss of the link with the coordinator in the first two days due to the RS-232 cable unplugging. Then, in the red circles, the errors identified without collisions with packets sent by other devices. It seems that there is a drift in the timing between the sent packets, for at least one device, which causes collisions every 37 hours (in the picture below, the black arrows span the same time interval), in fact it is known that Ionizing radiation causes permanent shifts in the oscillator frequency and can change the Q factor of the crystal over 1 kRad [38], [39].

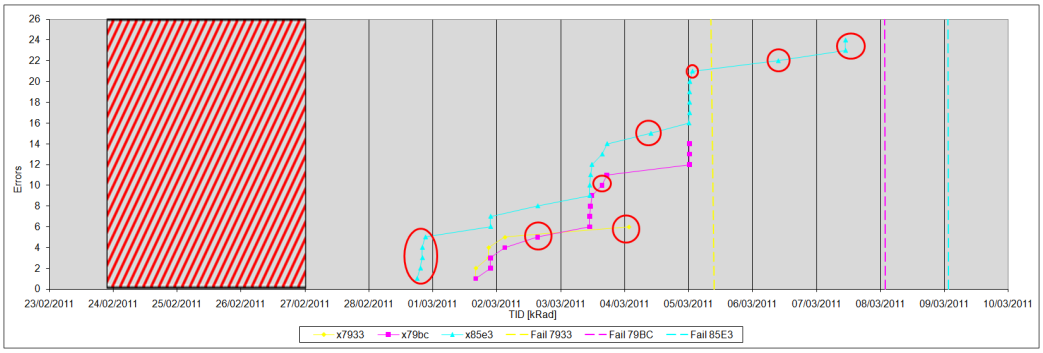

Figure 5.68: Packet errors on radiation level

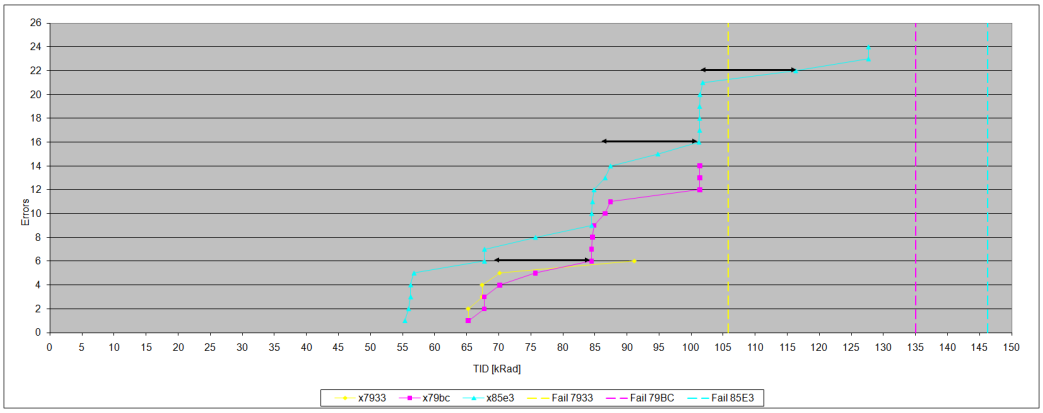

Figure 5.69: Packet errors on time during radiation test

Device 0x85E3 has a lower strength of the signal (-40 dBm, whereas the other two are around -36, -37 dBm) and it exhibits a bigger number of errors. This happens because in cause of collisions, the PiP functionality (par. 3.5) resynchronises the receiver on the packet with a stronger signal. The dashed

lines indicate the last packet received by that device, the exact number is shown in tab. 5.13.

Table 5.13: Radiation test results summary

Device	79BC	7933	85E3
Failure TID [Rad]	134995	105836	146236
Last Packet	2463953	3138930	3387180

Because of unplugging of the serial cable in the first phase of the test, there are no data about packet errors in this period, correspondent to a low radiation level (below 40 kRads). It is possible that the oscillator on the PCB with the GP500C chip was damaged by this radiation level, even if relatively not so high (compared to the final radiation level reached with this test), introducing a drift which made packets to collide at some regular interval. To supply to this loss of data I observed the behavior of other three devices doing a test simulation for slightly more than 60 hours in an office environment, which is not the same of the radiation chamber, even if the setup was the same used for the radiation test. Results are shown in fig. 5.70 and fig. 5.71.

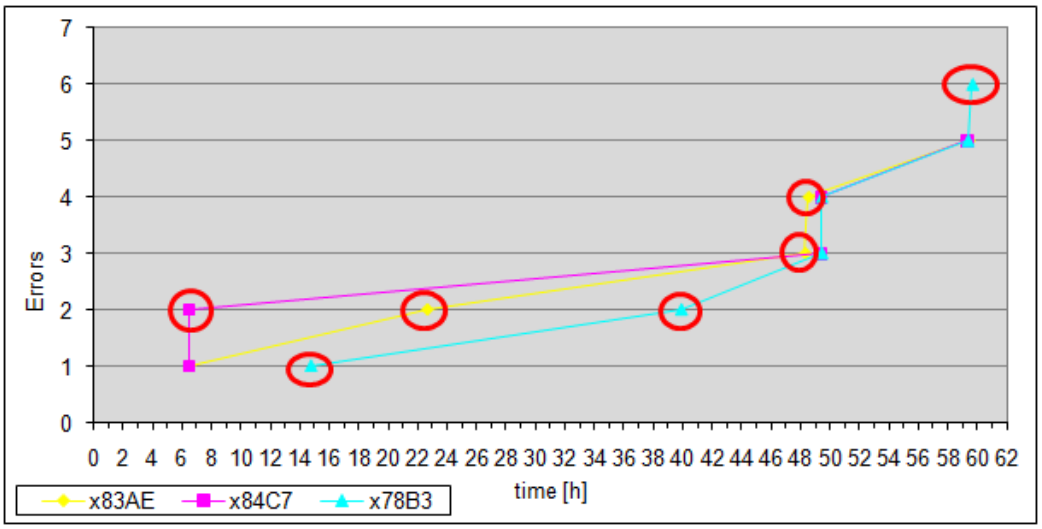

Figure 5.70: Packet errors on time

I found that collisions still occur, even if it is impossible to identify the 37 time interval due to drift, because of the short duration of this simulation. This

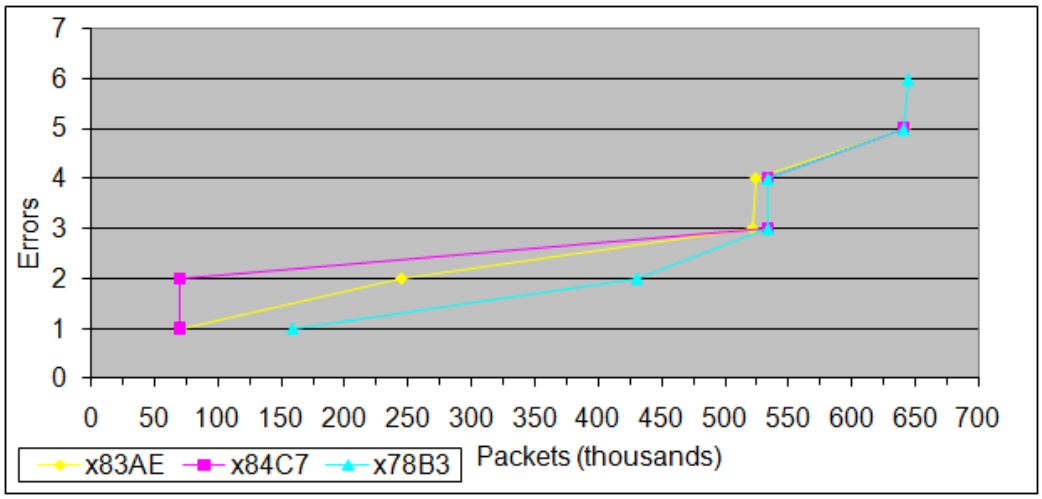

Figure 5.71: Packet errors on total exchanged

indicates that a drift is anyway present and that errors due to collisions have not to be considered for the PER evaluation. the effective errors, excluding collisions, are highlighted by red circles. Number of effective errors found during simulation are reported in tab. 5.14, whereas during the radiation test are in tab. 5.15. A rough estimation of the PER order of magnitude is around 10^{-6} both for the simulation than during the test. As expected, no increase of the PER has been identified during exposure to radiation.

Table 5.14: PER evaluation before radiation exposure

Device	**83AE**	**84C7**	**78B3**
Errors	3	1	3
Sent packets	664841	664545	664981

Table 5.15: PER evaluation during radiation exposure

Device	**79BC**	**7933**	**85E3**
Errors	2	1	10
Sent packets	3138930	2463953	3387180

Moreover, PER is certainly better (lower) than 10^{-5}, compatible with the datasheet value (10^{-5} at -82 dBm), as shown in the PER curves referred to

this value, in fig. 5.72, fig. 5.72, fig. 5.72. Horizontal lines identify the number of exchanged packets correspondent to a certain number of found errors, if dashed, or to the total number of exchanged packets, if continuous. The intersection between the horizontal line and the error confidence level curves give the CL value correspondent to that number of exchanged packets and that number of found errors. In these graphs I was conservative, as I considered all errors, also those ones inducted by collisions because of the PiP mechanism. Also considering errors caused by collisions the evaluated PER is well below the expected threshold with a confidence level equal to more than 90%. The lowest confidence level is correspondent to device 0x85E3 and is equal to 95%. I don't report curves about the estimated PER value, 10^{-6}, as the number of total exchanged packets is not high enough to obtain a valuable indication from this curve, so no indication about the confidence level of this estimation is provided. On the other hand, as previously said, this estimation aims only to compare PER value obtained under exposure to radiation to nominal one, not to give an accurate reference value, as not enough data are available.

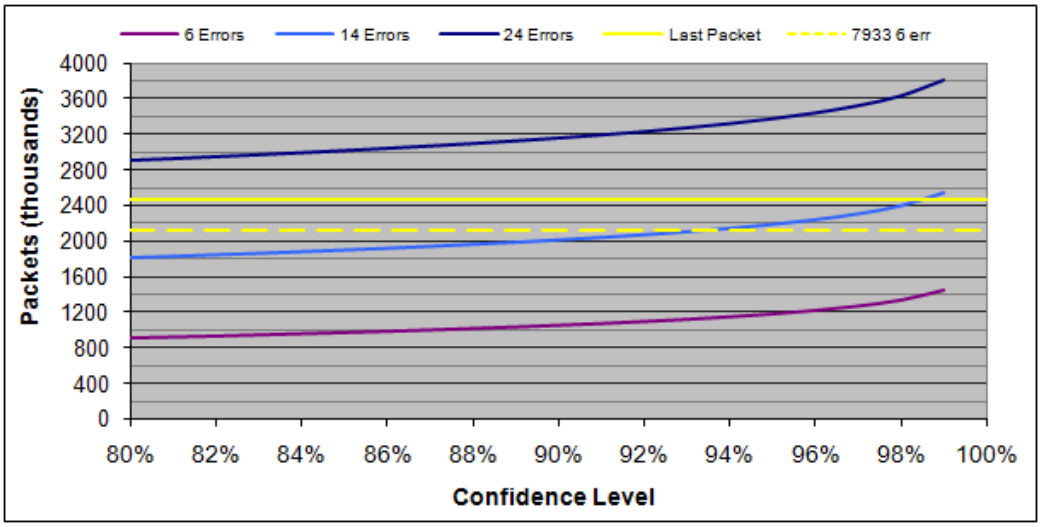

Figure 5.72: PER $10^{-}5$: device 0x7933

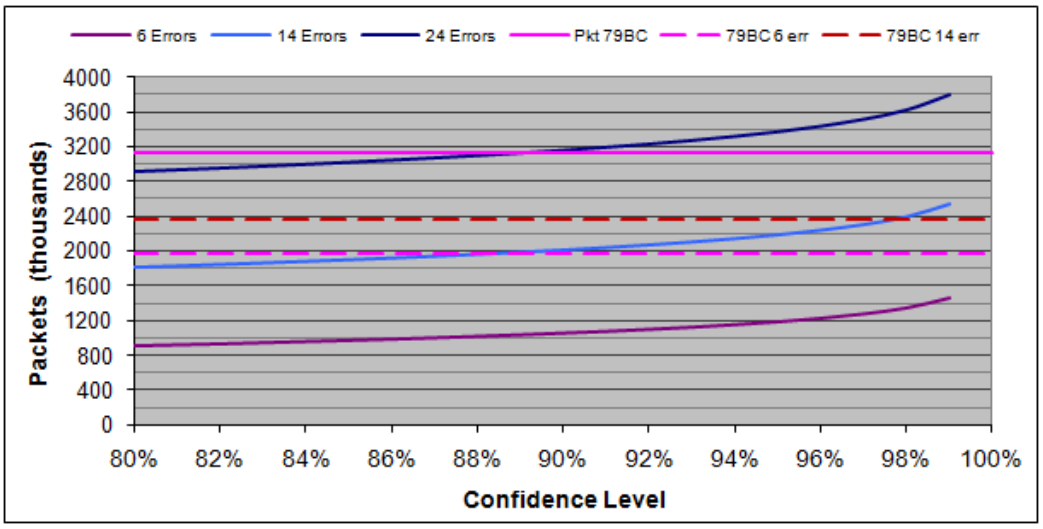

Figure 5.73: PER $10^{-}5$: device 0x79BC

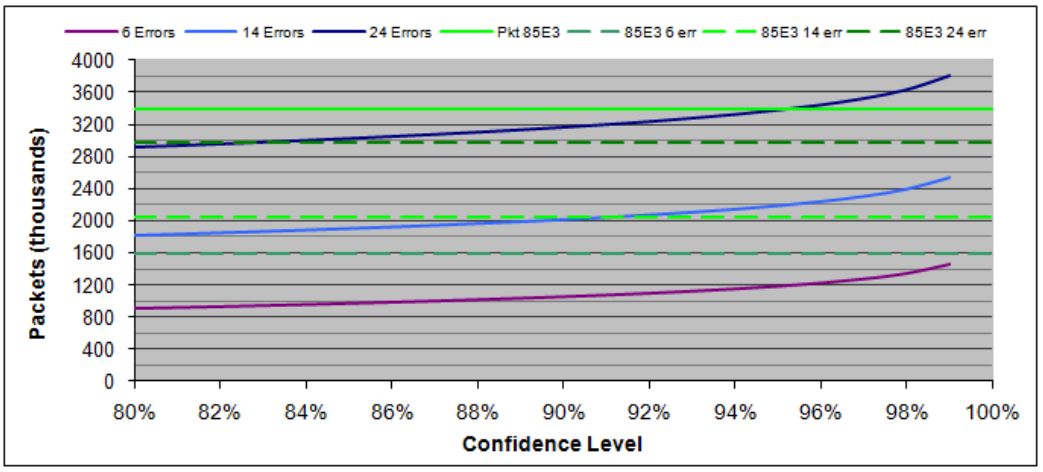

Figure 5.74: PER $10^{-}5$: device 0x85E3

Chapter 6

Temperature sensor example design

Several applications can be developed using the GP500C radio transceiver as the communication block of a smart device. In this chapter I introduce an example design of a wireless smart sensor, in particular a temperature sensor, highlighting its performances and possible employment scenario for space based activity. The purpose of this chapter is to show the practical development of a wireless smart device and its advantages in comparison to a common wired solution, using COTS components. The main blocks of a smart sensor are shown in fig. 6.1.

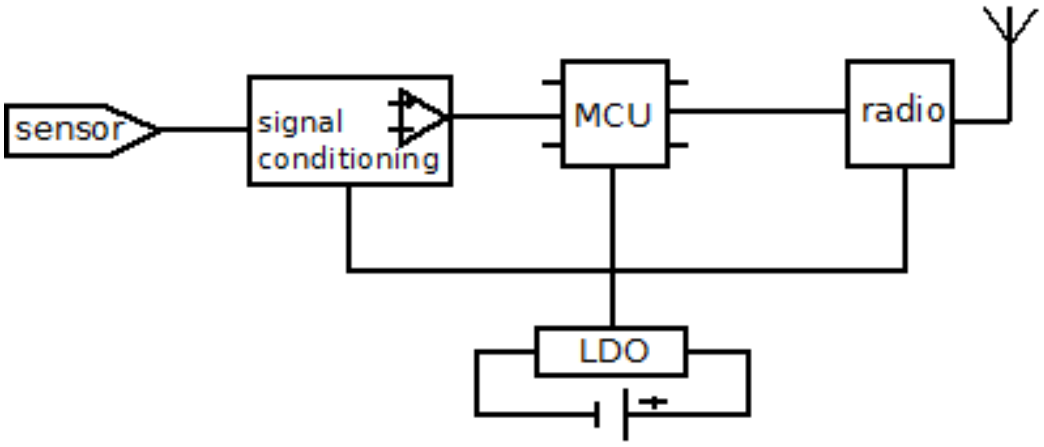

Figure 6.1: Wireless smart sensor block scheme

The sensing part can be implemented in several ways, in case of temperature sensor the main possibilities are thermocouples, resistance temperature de-

tector (RTD) circuits, thermistors and Integrated Circuit (IC) temperature sensors. The block connected to the sensing part is the signal conditioning one. It can be done of an Operational Amplifier, in case the sensing block output requires to be amplified before going to the Micro-controller Unit (MCU) and it can include an Analog-to-Digital converter (ADC) in case the sensor output is analogue and needs to be converted to a digital signal to be processed by the MCU. The smart sensor core is the MCU, it has to acquire and process the sensor output and transmit it to the radio chip. The radio chip is in this case the GP500C, which receives the MCU output through a SPI interface and sends it to an antenna for wireless transmission. To implement the Antenna Diversity mechanism I tested and explained in par. 4.5.1, more than one antenna is required.

To take advantage of the features provided by wireless technology and by the low power consumption of the GP500C radio transceiver, all the active blocks are supplied by a common button cell battery. The nominal 3 Volts supplied by the battery are used also as reference voltage by the ADC, so a voltage regulator, as a low-dropout (LDO) linear voltage regulator, is needed.

6.1 Temperature sensor

I took into consideration several technologies actually in use to define a reliable and easy to interface sensing part for the wireless temperature sensor example design. I considered thermocouple, RTD, thermistor and IC technology. The requirements the sensor block has to satisfy are wide temperature range, precision, linearity, low complexity of interface with the microcontroller, low current consumption and small size. A possible employment of this wireless sensor is within an AIT activity done inside not critical environment conditions, but requiring a big number of measuring points, for instance to check that the temperature doesn't exceed a defined threshold on a wide spacecraft area, or inside a launcher during the launch phase. Due to the temperature operational range of most of electronics components and of the battery used to supply the sensor, I selected a working measuring range equal to -20 ÷125 ℃. Thermocouple temperature range goes from less than -200 ℃ to more than 1500 ℃, it is a broadly used technology even if it requires a conditioning circuit for error compensation and its output is highly not linear. Resistance temperature detector circuit application span from -250 to +900 ℃ and even if its linear relation between resistance and

temperature simplifies implementation of signal conditioning circuitry, it requires a look up table or at least a second order polynomial (or equivalent) to linearize its output voltage result [40]. Thermistor operative range is equal to -100 to 450 ℃ and has a very high accuracy level (even ± 0.005 ℃) but it requires a look up table or at least third order polynomial to linearize its output, which is not so easy to implement in the micro-controller. IC sensors can work between -55 and +150 ℃ and they offer an accuracy of ±1 to ±2 ℃ on most of the temperature range. Even if their operative range is more limited and their accuracy less high in respect to that offered by other technologies, they are suitable for non critical measurements, for instance for monitoring purpose which in the temperature value is important relatively to a defined threshold, over a quite wide range, but not including severe temperature conditions (in this case thermocouple is the best choice). The bigger advantage is the output voltage linearity, which requires only an amplification stage (if analogue) and a conversion phase to be processed by the micro-controller. Moreover they offer ease of installation in the PCB assembly environment not provided by other technologies took in consideration. Because of these advantages, I chose to use an IC sensor for the first block of the wireless smart sensor implementation. I compared several sensors provided by different vendors, the ones with better accuracy and less power consumption compatible with the 3 V battery supply voltage are reported in tab. 6.1. Even if Digital devices give outputs ready to be processed by the micro-controller, they have a higher current consumption, so I selected an analog IC temperature sensor, the National Semiconductor LM94022, which offers the best performance/current consumption compromise, as evident in fig. 6.2.

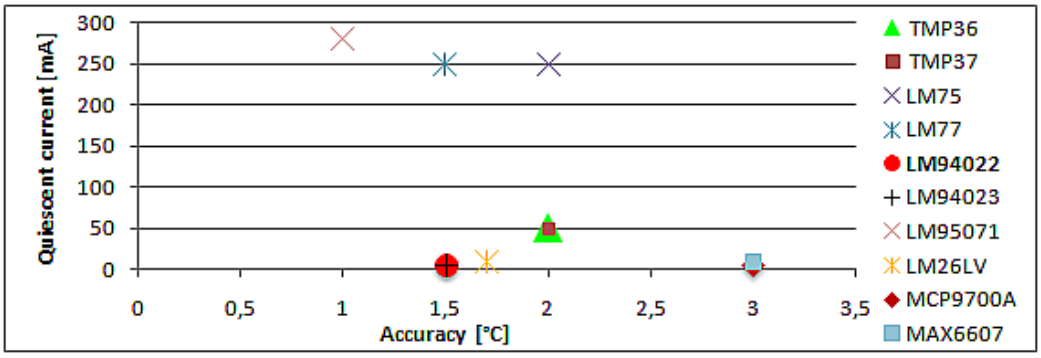

Figure 6.2: IC sensors performance comparison

It is almost equivalent to the LM94023 and has four selectable gains (whereas only two are available for the LM94023). For the operative range limits, −40℃ and +125 ℃, the output voltages are respectively 0.332 and 1.247 V. The maximum value should match the ADC reference voltage I plan to use, to obtain the best achievable resolution during the analogue to digital signal conversion process.

Table 6.1: IC temperature sensor data comparison

Sensor	**Manufacturer**[1]	**Accuracy [℃]**	**T range**		**Consumption**	**output (A/D)**
TMP35	AD	1 ÷ 2	10	125	$< 50\ \mu$A	A
TMP36	AD	1 ÷ 2	-40	125	$< 50\ \mu$A	A
TMP37	AD	1 ÷ 2	5	100	$<50\ \mu$A	A
ADT7301	AD	1	-40	150	2.2 mA	D
LM75	NS	2	-25	100	250 to 1000 μA	D
		3	-55	125		
LM77	NS	1.5	-10	65	250 to 500 μA	D
		2	-25	100		
		3	-55	125		
LM94022	NS	1.5	20	40	5.4 μA	A
		1.8	-50	70		
		2.1	-50	90		
		2.7	-50	150		
LM94023	NS	1.5	20	40	5.4 μA	A
		1.8	-50	70		
		2.1	-50	90		
		2.7	-50	150		
LM95071	NS	1	0	70	280 μA	D
		2	-40	150		
LM26LV	NS	1.7	-50	0	8 μA	A
		2.2	0	120		
		2.3	0	150		
MCP9700A	Microchip	2 ÷ 4	-40	125	6 μA	A
MAX6607	Maxim	2 ÷ 6	-20	85	8 μA	A

[1] AD: Analog Devices, NS: National Semiconductor

6.2 Amplification stage

As I plan to use the 3 V supplied by the battery as reference voltage for the ADC, an amplification stage which leads the 1.247 V signal to 3 V is required. A simple non-inverting Operational Amplifier can be used to achieve this task, the desired gain G is equal to 2.4, so input and feedback resistors (R_{in} and R_{fb} referring to fig. 6.3) can be evaluated by eq. 6.2.

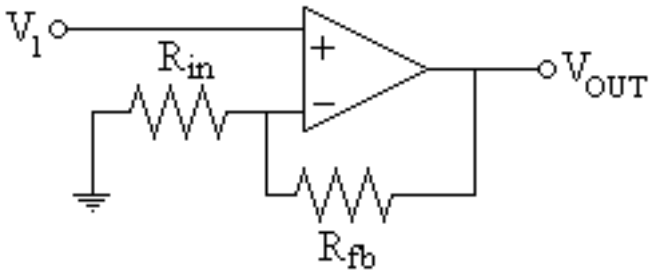

Figure 6.3: Non-inverting amplifier used configuration

$$G = \frac{V_{out}}{V_{in}} = \frac{3}{1.247} = 2.4 \tag{6.1}$$

$$G = 1 + \frac{R_{fb}}{R_{in}} \Rightarrow R_{fb} = 1.4 \cdot R_{in} \tag{6.2}$$

I chose R_{in} and R_{fb} nominal values respectively equal to 5 $k\Omega$ and 7 $k\Omega$ and the National Semiconductor LPV521 Operational Amplifier. The result of a taxonomy between low power amplifiers is this component which has a temperature range equal to -40 ℃ to 125℃, operating voltage range between 1.6 V and 5.5 V and a typical supply current of 471 nA (with maximum value between 600 and 860 nA). The main reason why I selected this for the wireless sensor example design is its unmatched low current consumption.

6.3 Micro-controller

Even if there are several micro-controller families, each one with different features, I limited the search field to the PIC micro-controller type because of the confidence I acquired with it, in terms of performance and programming software knowledge. I estimate the needed micro-controller programmable flash memory in at least 16 KB, taking into account the temperature value acquisition, its processing and communication to the radio transceiver chip

for wireless transmission. Other requirements to accomplish are low power consumption, 3 Volts supply compatibility, small package and SPI module availability. I found several micro-controllers satisfying these requirements, especially in the Extreme Low Power (XLP) product family, so I chose the one with the most basic features, the 8 bits PIC18F14K22.

This micro-controller has a nominal current consumption of 34 nA in Sleep mode and in the order of hundreds of nanoAmps in Active mode, an internal oscillator operating at 32 kHz or 16 MHz, an ADC module with a 10 bits resolution, able to convert also in Sleep mode and SPI module. Moreover the Quad Flat Package size is only 4 x 4 x 0.9 mm, suitable for a portable smart sensor application.

6.4 SPI interface

The GreenPeak GP500C radio transceiver provides a SPI module to interface with the micro-controller. The Serial Peripheral Interface is a synchronous protocol that allows a master device to initiate communication with a slave device using 4 main lines: SS, SCK, SDO and SDI, the configuration is shown in fig. 6.4.

SS (CS) - This signal is known as Slave Select or Chip Select. It is used by the Master to select the Slave it wants to communicate with.

SCK - This is the Serial Clock signal. It is generated by the master device and controls when data is sent and when it is read.

SDO - This is the Serial Data Output signal. SDO carries data out of a device.

SDI - SDI is the Serial Data Input line. It carries data into a device.

The master device, namely the μC, provides the clock signal SCK for synchronization purpose. The clock signal controls when data can change and when they can be transmitted, moreover its pulse goes along with the data, as SPI is synchronous. Data typically changes during the rising or falling edge of the clock signal, depending on two parameters: clock polarity and phase. Since SPI is a Data Exchange protocol, when data is clocked out, new data is also being clocked in. This means that each device has to read

(transmit) between two successive transmissions (receptions), even if incoming (outgoing) data are not used. When the SS signal goes low, the slave device will listen for SPI clock and data signals on the MOSI (Master Output - Slave Input) line, which is the Slave SDI, whereas the MISO (Master Input - Slave Output) is the GP500C SDO line.

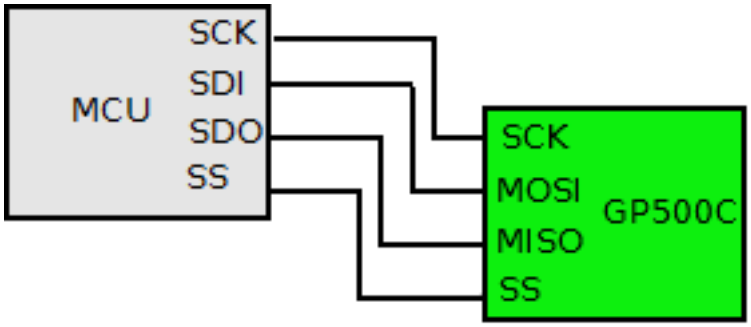

Figure 6.4: Micro-controller - GP500C device SPI configuration

6.5 Radio transceiver and Antenna

The radio transceiver I use for the wireless sensor example design is the GP500C. In particular the GreenPeak SPI module I tested provides, other than the GP chip and other needed electronics components (as the 16 MHz oscillator), two planar inverted-F antennas. These are suitable for a small and reliable wireless sensor design, due to their limited size and simple integration in a PCB, other than an almost omni-directional behavior. I plan to use two PIFAs placed at 90° to use the Antenna diversity mechanism provided by the GP500C radio transceiver, even if in the example design scheme shown in fig. 6.5 no details about them, neither about the auxiliary electronics components around the GP chip, are provided.

6.6 Power supply

I chose a standard CR-2032 button cell battery as power supply for the wireless temperature sensor. I considered several vendors, verifying that the overall performance are almost the same, in terms of 3 V output time duration and temperature range, anyway the Renata 3 V Lithium battery shows better compromise between these requirements, as shown in tab. 6.2. Anyway

the battery is the sensor component with the smaller operative temperature range and it is not able to accomplish the $-40 \div +125$ ℃ target temperature range, therefore an ad-hoc design seems to be necessary.

Table 6.2: CR2032 data comparison

Manufacturer	**Min T [℃]**	**Max T [℃]**	**Time[1][hours]**
Duracell	-20	54	600
Energizer	-10	70	300
Fujitsu	-10	60	400
Jht	-20	70	400
Maxell	-20	85	600
Mitsubishi	-20	70	400
Panasonic	-30	60	500
Renata	-40	85	500
Sony	-10	60	400
Sanyo	-20	70	400
Varta	-20	70	300

[1] 3 V output time referred to 21℃ and 15 $k\Omega$ load conditions.

Any variation in the ADC reference voltage may introduce errors into the conversion process over the operating temperature range, affecting linearity and other performance indexes of the ADC, moreover as the number of bits increases, less reference error can be tolerated[41]. The battery supplied output voltage is known to be not stable on time, moreover it is affected by environmental factors such as temperature, pressure and humidity, therefore I associate a LDO voltage regulator to the power supply. National Semiconductor offers a wide range of micro-power LDO, as the LP5951, working in a temperature range between -40℃ and + 125℃, with an input voltage of -1.8V to 5.5 V and a quiescent current lower than 100 μA.

The wireless temperature sensor example design is shown in fig. 6.5. A rough evaluation of the total power consumption can be made analyzing the values in tab. 6.3. I consider a maximum MPDU size of 127 bytes transmitted once a second at 250 kbps. To take into account also the PHY header and footer I consider only the 0.8% of the maximum allowable speed, it results in a transmission time duration t_{TX} equal to 5.08 ms, doubled considering acknowledgement reception, for a total communication time of

10.16 ms every second. I consider quite conservative conditions as this is a rough estimation.

Table 6.3: Sensor components current consumption

Component	**i** $[\mu A]$
MCU	0.6
Sensor	5.4
Op-Amp	0.4
GP500C	0.25 (18000 when Tx/Rx)
LDO	0.4
Total	7.1 (18007 when Tx/Rx)

Considering the sensor duty cycle with active and sleep modes data explained above and referring to data in tab. 6.3, the total current consumption in one hour is:

$$
\begin{aligned}
i_{TOT} &= i_{TX} \cdot \frac{t_{TX}}{3600} + i_{sleep} \cdot \frac{t_{sleep}}{3600} && (6.3)\\
&= i_{TX} \cdot \frac{t_{TX}}{3600} + i_{sleep} \cdot \frac{(3600 - t_{TX})}{3600} && (6.4)\\
&= 182.95 + 6.98 && (6.5)\\
&= 189.93 \ \ [\mu A] && (6.6)
\end{aligned}
$$

As the selected battery Capacity is equal to 235 mAh, its life time (BLT) is evaluated, using a discharge margin η of 0.7, as:

$$BLT = \eta \cdot \frac{C}{i_{TOT}} \left[\frac{mA \cdot h}{mA}\right] = 866 \ h \qquad (6.7)$$

It results in a 36 days operating sensor, which can be suitable for an AIT activity.

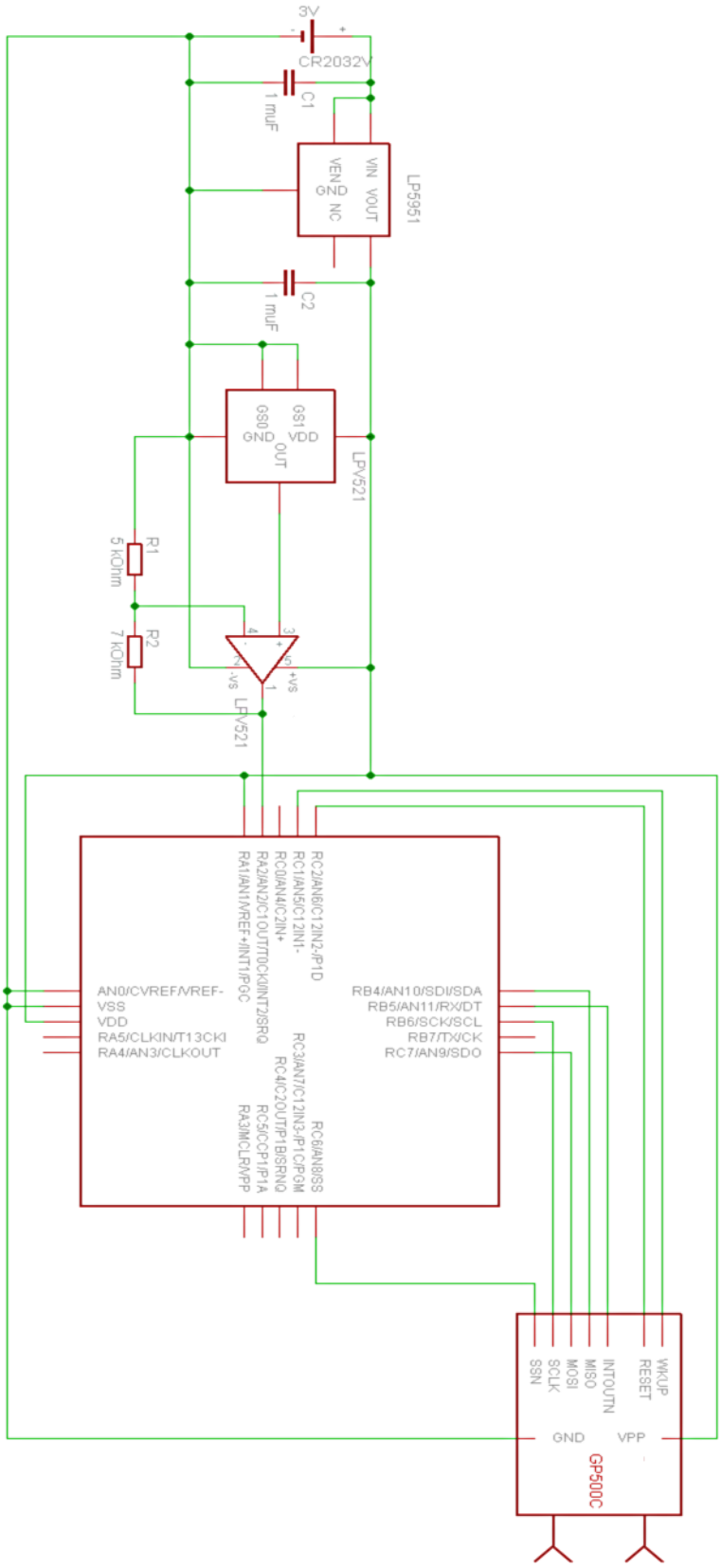

Figure 6.5: Wireless temperature sensor scheme

Chapter 7

Conclusions

The result of the test phase I did inside the Avionics Laboratory and in the Anechoic chamber is that a common laboratory environment introduces reflections and multipath fading into the communication link, therefore transmitter and receiver antennas polarization and their relative orientation heavily affects the link budget. In this situation a preliminary evaluation of the multipath effect and of the electromagnetic field propagation is necessary to define the most appropriate placement and orientation of the communicating devices. Anyway the Antenna Diversity mechanism can help to improve the link quality in situations strongly affected by noise or interference, as that introduced by Wi-Fi signal, existing inside an AIT activity representative environment like the Avionics Laboratory.

The Antenna Diversity benefit has been evaluated also inside a more specific space oriented application environment, as the Venus Express mock-up. Also in this scenario the Antenna Diversity mechanism improves quality and reliability of the communication link, especially in low SNR situations, giving a SNR average gain equal to 4 to 10 dB. In general I verified that the GP500C IEEE 802.15.4 compliant radio transceiver is suitable also in scenarios with several cavities and without LOS between communicating devices, providing a low power and low data-rate technology that can be used for AIT activities. Moreover the experimental results I obtained inside the mock-up confirm the validity of the multimode cavity theory introduced by T.H Lehman and assessed by EADS Astrium previous studies (referring to [16],[19], [31], [32]). Thereby the electric field can be assumed isotropic and homogeneous inside a cavity, so polarization and relative orientation of transmitter and receiver devices don't affect the communication quality, neither the signal strength.

This is important in case wireless sensors have to be used inside a cavity environment, as is the common spacecraft structure, because no preliminary evaluation is required about placement of devices to obtain a good communication outcome. Moreover I found a good agreement with the numerical model developed by EADS Astrium to evaluate the link budget losses inside a cavity environment introduced by apertures. As a general result it can confirmed that the minimum received power inside the mock-up is higher than the receiver sensitivity (-85 dBm), considering a standard 1 mW (0 dBm) transmission power whatever the cavity, thus a IEEE 802.15.4 compliant radio transceiver is suitable for this scenario.

I verified through TID test that the exposure to radiation does not affect the PER and that the device functionality is guaranteed up to $65 \div 68$ $kRads$. This result is compatible with a previous study done on a similar component, the Atmel AT86RF230 IEEE 802.15.4 radio transceiver (referred to [42]). The indication of the radiation level tolerated by this specific kind of component can be useful in case of future wireless application development, since this device showed to be suitable not only for AIT activities, but also for in-flight operations (concerning radiation tolerance). Moreover it helps to characterize the behavior of COTS devices under radiation, as this is one main issue for their space oriented application employment.

Finally I showed a practical application of the device I tested, using the GP500C as the communication block of a smart wireless temperature sensor, which components are exclusively COTS. The performances offered by this implementation are compatible with an AIT activity application, in terms of accuracy and time duration. One of the wireless technology main issues is the power feed, as there aren't cables, but the extremely low power consumption of this example design make it possible to use a button cell battery as power supply, resulting in a portable and easy-to-place device.

The future development of wireless application using the GP500C radio transceiver should include a further investigation of the Antenna Diversity implemented mechanism in noisy scenarios, to test the achieved performances when the SNR is extremely low. This goes beyond the purpose of this thesis, aimed to test the device in several realistic scenarios simulating possible AIT activity situations, but it is fundamental to obtain the best achievable result using the Antenna Diversity mechanism, maybe using different techniques or antennas in respect to those ones I tested, associated to the GP500C SPI module. Moreover further investigation about exposure to radiation should

be done to assess the possible employment of this component for in-flight operations. Both TID than SEE evaluations are required testing several operative modes of the device, as these can affect its behavior when exposed to radiation (for instance when in Sleep mode the probability of destructive effects induced by radiation is expected to be lower). Speaking about wireless sensors and wireless sensors network development, an evaluation of the behavior of the tested device in different network topologies and with different network parameters (number of retries, backoff exponents, number of CSMA backoffs) should be done, to find the best solution, even if this is strongly affected by the specific application which can require defined routing paths, throughputs, packets size and device duty cycles. Moreover several further test have to be done to qualify a wireless sensor to be used for in-flight operations: not only radiation test, but also mechanical, dynamic response, stress and electrical evaluations are required to obtain a reliable COTS device for aerospace oriented applications.

Appendix A

Test environments

In this Appendix some details are provided about the test environments mentioned in this thesis. These are the Avionics Laboratory, the Anechoic Chamber, the Co-60 facility of the European Space Research and Technology Centre in Noordwijk, in the Netherlands and the Venus Express mock-up. All information about Avionics Laboratory and Anechoic chamber come from [43]. Data about Co-60 facility are available in [44], whereas data about the Venus Express mock-up are found in [45].

A.1 Avionics Laboratory

The Avionics Laboratory supports avionics subsystem development process by enabling the demonstration, testing and validation of new avionics technologies and by developing control software tools. It also helps to cut mission future costs by evaluating standardised components, system architectures and building blocks for subsequent reuse. The Laboratory evaluates a broad range of avionics elements from individual microprocessors up to complete sensors and systems with application environments, through a combination of real-world testing and also complex software *test beds*. It also validates new operational concepts - such as high-speed networks or wireless communications - using the same combination of methods.
It is made up of two linked facilities, the Data Systems Laboratory and Control Systems Laboratory, often working in conjunction with the adjacent Software and Simulation Laboratory, with whom the main End-To-End Avionics Test Bench is shared.
The Data Systems Laboratory, where I did the test phase, is divided into

three sections:

On-board Computer and Data Handling Area Equipment includes bus protocol test beds, ERC32 and LEON2-FT evaluation boards and a set of interconnected Data Handling Lab units (RASTA).

Payload Data Processing Area Infrastructure required to validate on-board payload data processing architectures, high capacity and high speed storage functions and high-speed links and networks. The area hosts a full suite of test equipment for SpaceWire networks and underlying building blocks. In addition evaluation boards for digital signal processors allow demonstrating representative applications related to on-board data compression or feature extraction.

Microelectronic area Facilities here include UNIX workstations and PCs, hardware and software for designing ICs and programming FPGAs, simulation and emulation tools, prototype samples and system demonstrators.

Current areas of study includes the assessment of Micro-Electro-Mechanical Systems (MEMS) for control applications and also wireless systems on the data side to slash satellite mass and integration time.

A.2 Anechoic chamber

The EMC Laboratory aims to provide an appropriate environment to perform electrical and electromagnetic measurements to ensure EMC of units, devices or equipment. The EMC laboratory consists of two shielded rooms: a test chamber and a control room. All walls, ceiling and floors are constructed from single layer, pre-manufactored galvanized steel panels, bolted together and fixed with insulators to the support structure. Walls and ceiling are covered with absorbers and in addition a floor equipped with a layer of ferrite. The combination of the resistive absorbers and the ferrites gives an almost full anechoic test area. The rooms meet the electromagnetic wave attenuation requirements (120 dB at 10 GHz). They prevent transmission of electromagnetic waves into, or out of, the enclosure, which provides low electric and magnetic field ambient conditions. Electrical power is provided through isolation transformers an AC filters to eliminate transfer of interfering signals such as radio, TV, mobile phone base stations and RADAR.

The test room size is 8.55 m x 7.5 m x 4.75 m (Length x Width x Height), whereas the control room size is 3.45 m x 6.6 m x 2.9 m (Length x Width x Height). The environmental conditions are controlled in a temperature range of 20℃ to 24 ℃ and relative humidity ranging between 40% and 55%. The test room is equipped with a fire detection system and a fire extinguishing system with inert gas. Measurement equipment available in the EMC lab consists of:

- test tables with copper ground plane (anechoic room and control room)
- current probes, field probes, sensors, various antennas up to 18 GHz
- high end measurement receiver 30 Hz - 26 GHz
- spectrum analyser 15 kHz - 3 GHz
- spectrum/network analyzer between 10 Hz and 500 MHz
- various high performance digital signal analysers (oscilloscopes)
- various signal generators
- various RF power amplifiers
- RF power meter
- data logger
- high precision voltmeter

A.3 Co-60 facility

Radiation test facilities investigate the effects of radiation on electronic components. The Co-60 facility is used to recreate the degradation resulting from a lifetime radiation dose. The new radiation facility has been reloaded with a Co-60 gamma source. The facility consists of a larger control room and radiation cell with 14 cable feed-throughs enabling monitoring and control of experiments under test. Automated total dose and dose rate setting, monitoring and logging are available via HP-VEE control software running on a PC. This system may also be used for automated monitoring of experiments under test. While irradiating, dose rates are easily changed by use

of a rail system installed in the radiation cell. It uses a collimated Co-60 Gamma ray source, the maximum achievable rate (at a distance of 50 *cm*) is 92 Rads/min, on an uniform Area of 10 *cm* x 10 *cm*, whereas the minimum rate (at a distance of 800 *cm*) is 0.4 Rads/min, on an uniform Area of 360 *cm* x 360 *cm*. A Co-60 facility top view is shown in fig. A.1.

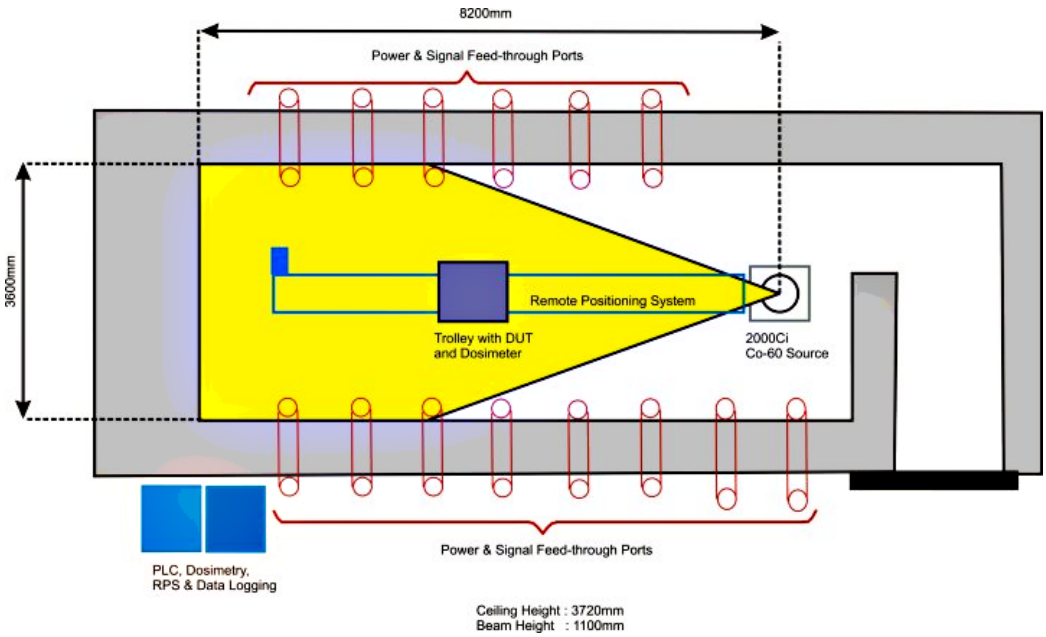

Figure A.1: Co-60 facility top view

The Computer Controlled Dosimetry System and Remote Positioning System (RPS) is based on:

- Farmer 2670 Dosimeter
- RPS (Remote Positioning System)
- HP-VEE Software

Using Hp-VEE permits remote internet monitoring of the run status.

Dosimetry System features are:

- is based on Farmer 2670 Dosimeter
- uses standard 0.6 *cc* air ionisation chamber
- can be fully controlled via RS-232 connection

- trip output interfaced to Co-60 Control system to enable lowering of source when desired dose reached.

RPS system features are:

- 6.5 m long rail
- Stepper motor controlled by a micro-controller with an RS-232 connection to the PC.
- System takes less than one minute to go from one end to the other (e.g. from minimum to maximum dose rate) with a positional accuracy of about 1 mm.

A.4 V-Ex mock-up

The mock-up I used for the tests shown in this thesis is the same used for *Optical Wireless* ESA project, based on Venus Express model. The model represents a medium size satellite, with overall size equal to about 1.70 m (L) x 1.66 m (W) x 1.39 m (H). It has been simplified with the non-representation of the external elements (antennas, solar array and so on). The main internal units are rigorously identical to the flight ones in term of dimensions and locations. The total dimension of the mock-up, including the trolley, is 1.97 m (L) x 1.97 m(W) x 2.2 m (H). The walls are made of honeycomb with aluminium skin similar to the ones used on spacecraft. The external surface of the mock-up is covered by Multi-Layer Insulator (MLI). A small part of the external surface is covered by aluminium tape in order to simulate a thermal radiator. Handles allow to open the different mock-up doors in order to have access inside the mock-up. The inner part of the mock-up is composed of:

- 35 boxes representative of the flight ones in term of dimensions and locations
- 3 tanks representative in term of dimensions and locations: 2 large cylindrical tanks in the central cavities and one spherical tank situated in another hollow
- harness added in each cavity with a routing similar of the flight one.

The units and inner walls are covered by flight PU1 black paint. The tanks and some walls are covered by Vapor Deposited Aluminum (VDA) as in flight. Two apertures (rectangular 12 *cm* x 12 *cm*) are present at the mock-up bottom level in order to enter the Electrical Ground Support Equipment (EGSE) test harness inside the cavities. The link between each independent cavity is also insured by apertures. The majority of the electric equipments representative boxes are connected together by electrical bundles. For RF link, the unit chassis need to be representative of the flight one, so it is metallic. The satellite is made up of six cavities separated by sandwich honeycomb panels. Moreover the cavities are accessible by the mean of doors present on each side of the spacecraft mock-up. In particular there are two large double doors on each side of the mock-up, as shown in fig. A.2, which in both the "open walls" than the "closed walls" configuration is displayed.

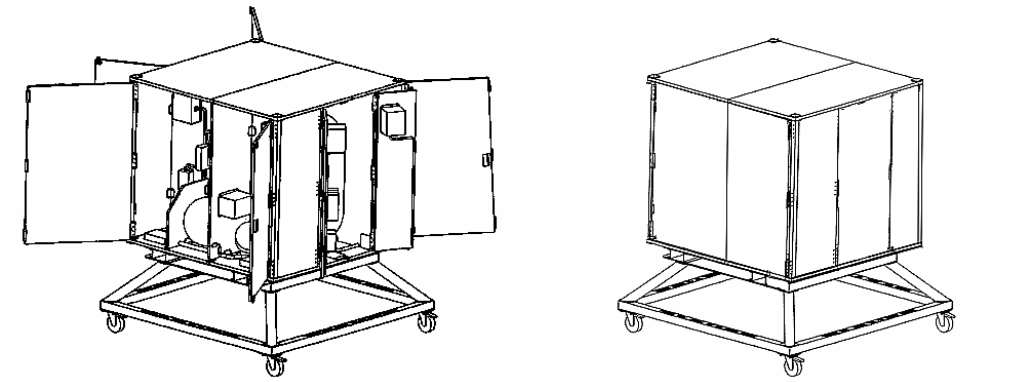

(a) Open configuration (b) Closed configuration

Figure A.2: Venus Express mock-up

Nomenclature

μC	Microcontroller
AD	Antenna Diversity
ADC	Analog-to-Digital Converter
BER	Bit Error Rate
CCA	Clear Channel Assessment
COTS	Commercial-Off-The-Shelf
CSMA-CA	Carrier Sense Multiple Access with Collision Avoidance
DUT	Device Under Test
ED	Energy Detection
EMC	Electromagnetic Compatibility
FCS	Frame Check Sequence
FFD	Full Function Device
GP	GreenPeak
HAL	Hardware Abstraction Layer
LDO	Low dropout regulator
LOS	Line-of-sight
LQI	Link Quality Indicator
LSB	Least Significant Bit

MAC	Media Access Control
MCU	Micro-controller Unit
MPDU	MAC Protocol Data Unit
MSB	Most Significant Bit
MSDU	MAC Service Data Unit
PCB	Printed Circuit Board
PDU	Protocol Data Unit
PER	Packet Error Rate
PHY	Physical Layer
PIFA	Planar Inverted-F Antenna
PiP	Packet-in-Packet resynchronisation
PL	Path Loss
PPDU	Physical Layer Protocol Data Unit
PSDU	Physical Layer Service Data Unit
PSM	Power Supply Management
RF	Radio Frequency
RFD	Reduced Function Device
RSSI	Received Signal Strength Indicator
RTD	Resistance Temperature Detector
SNR	Signal to Noise Ratio
SPI	Serial Peripheral Interface
TID	Total ionizing Dose
WLAN	Wireless Local Area Network
WPAN	Wireless Personal Area Network
WSN	Wireless Sensors Network

Bibliography

[1] Inc. Condor Engineering. *MIL-STD-1553 Tutorial*, June 2000. Document Version: 3.41.

[2] ECSS Secretariat. *ECSS-E-ST-50-13C: Interface and communication protocol for MIL-STD-1553B data bus onboard spacecraft*. ESA-ESTEC, Requirements & Standards Division, November 2008.

[3] US Department Of Defense. *Military Standard MIL-STD-1553B. Aircraft Internal Time division Command/Response Multiplex Data Bus.*, September 1978.

[4] K.A. LaBel, P.W. Marshall, C.J. Marshall, J. Barth, H. Leidecker, R. Reed, and C.M. Seidleck. Comparison of MIL-STD-1773 fiber optic data bus terminals: Single event proton test irradiation, in-flight space performance and prediction techniques. *IEEE Transactions on Nuclear Science*, 45:1633–1639, June 1998.

[5] D.A. Gwaltney and J.M. Briscoe. Comparison of communication architectures for spacecraft modular avionics systems. Technical report, Marshall Space Flight Center, Alabama, June 2006.

[6] Mike Wroble, Jack Kreska, and Larry Dungan. SAE Mil-1394 for military and aerospace vehicle applications. Lockheed Martin Aeronautics Company, National Aeronautics and Space Administration, March 2006.

[7] ECSS Secretariat. *ECSS-E-ST-50-15C: Recommendations for CAN Bus in Spacecraft Onboard Applications*. ESA-ESTEC, Requirements & Standards Division, May 2005. Draft.

[8] ECSS Secretariat. *ECSS-E-ST-50-12C: SpaceWire - Links, nodes, routers and networks*. ESA-ESTEC, Requirements & Standards Division, July 2008.

[9] Consultative Committee for Space Data Systems Secretariat. Wireless network communications overview for space mission operations. Green book, National Aeronautics and Space Administration, September 2009. Report Concerning Space Data System Standards.

[10] K.D. Champaigne, E. Krug, and D.A. Heermann. Space station truss wireless instrumentation for structural dynamics measurements. Technical report, Invocon Inc., 2005.

[11] D. Foltran and R. Zanello. Categories of COTS items for space applications and their availability on the market. Technical report, Alenia Spazio, May 2005.

[12] IEEE Computer Society. *IEEE Standard for Information technology-Telecommunications and information exchange between systems—Local and metropolitan area networks-Specific requirements. Part 15.4: Wireless Medium Access Control (MAC) and Physical Layer (PHY) Specifications for Low-Rate Wireless Personal Area Networks (WPANs)*, 2006 edition, September 2006. Revision of IEEE Std 802.15.4-2003.

[13] C. Eng. Mike Wilson. *Understanding Radio for the Practical Engineer*. MIEE, 2006.

[14] Inc. Cisco Systems. Multipath and Diversity. Document ID: 27147, January 2008.

[15] T.S. Rappaport. *Wireless Communications, principles and practice*. Prentice Hall, 2002.

[16] T.H. Lehman. A statistical theory of electromagnetic fields in complex cavities. Albuquerque, NM, May 1993.

[17] Glen Dash. Designing enclosures for EMC compliance. Ampyx LLC, 2005.

[18] C.A. Balanis. *Advances Engineering Electromagnetics*. John Wiley & Sons, 1989.

[19] Patrice Pelissou. Reducing EMC verifications for future Telecom Platforms. Technical report, ESA, EADS Astrium, 2007.

[20] Lukas Leijten. *Design of Antenna-Diversity Transceivers for Wireless Consumer Products*. PhD thesis, Proefschrift Technische Universiteit Eindhoven, 2001. Philips Electronics.

[21] W. Jakes. Microwave mobile communications. In *IEEE Press Classic Reissue*. IEEE Press, 1994. New-York, USA.

[22] Jennic Ltd. Zigbee e-learning, May 2011. `http://www.jennic.com/elearning/zigbee/index.htm`.

[23] Rodger Magness. Short-range RF wireless (proximity) networks technology assessment for space applications. Technical report, European Space Agency, April 2006.

[24] ISO/IEC 7498-1. *Information technology - Open Systems Interconnection - Basic reference model: The basic model*. ITU-T, July 1994.

[25] Cisco Certified Network Associate Tutorials. `http://www.ccnatut.info/2009/12/osi-reference-model.html`, May 2011.

[26] IEEE Computer Society. *802 IEEE Standard for Local and Metropolitan Area Networks: Overview and Architecture*, 2001 edition, February 2001. Revision of IEEE Std 802-1990.

[27] IEEE Computer Society. *IEEE Standard for Information technology-Telecommunications and information exchange between systems—Local and metropolitan area networks-Specific requirements.Part 15.2: Coexistence of Wireless Personal Area Networks with Other Wireless Devices Operating in Unlicensed Frequency Bands*, 2003 edition, August 2003. IEEE Std 802.15.2-2003.

[28] GreenPeak. GP500C datasheet rev. 1.21, March 2010.

[29] GreenPeak. Evaluation kit user manual, GP_P300_UM_00672_GP500, March 2010.

[30] GreenPeak. Emerald GP500C reference evaluation application manual, GP_P300_UM_00712_GP500C, March 2010.

[31] Patrice Pelissou. RF wireless intra-spacecraft communications: Link budget & EMC analysis. Technical report, EADS Astrium, 2009. Ref. 2125.NT.PP.08.13438.ASTR, Issue 02.

[32] SERMA s/c TE622. ESA project: Wireless intra-spacecraft communications technical report for WP 3220. Detailed designs of the application demonstrators link budget / EMC. Technical report, ESA, EADS Astrium, 2009. TE622 153306, Issue 01,.

[33] European Space Components Coordination, `https://escies.org`. *Total Dose Steady-State Irradiation Test Method. ESCC Basic Specification No. 22900*, 2007.

[34] Bernard Sklar. *Digital Communications Fundamentals And Applications*. Prentice Hall PTR, second edition edition, 2001.

[35] Maxim. Physical Layer performance: Testing the Bit Error Ratio (BER). Technical report, HFTA-010.0, 2004.

[36] J. Redd. Calculating statistical confidence levels for error-probability estimates. *Lightwave Magazine*, pages 110–114, April 2000.

[37] A.J. Wheeler and A.R. Ganji. *Introduction to Engineering Experimentation*. Prentice Hall, 2nd edition, 2004.

[38] L.D. Edmonds, C.E. Barnes, and L.Z. Scheick. An introduction to space radiation effects on microelectronics. Technical report, National Aeronautics and Space Administration, Jet Propulsion Laboratory, California Institute of Technology, Pasadena, California, May 2000.

[39] ECSS Secretariat. *ECSS-E-ST-10-12C: Methods for the calculation of radiation received and its effects*. ESA-ESTEC, Requirements & Standards Division, November 2008.

[40] Bonnie Baker. Temperature sensing technologies, Application Note 679. Technical report, Microchip Technology Inc., March 2002.

[41] P. Horowitz and W. Hill. *The Art of Electronics*. Cambridge University Press, second edition, 1989.

[42] Tamara Montes Bazán. YGT final report: Low rate TID test of AT86RF230 RF transceivers. Technical report, ESA, European Space Research and Technology Centre, May 2009.

[43] European Space Agency, Space Engineering website, June 2011. `http://www.esa.int/esaMI/Space_Engineering/`.

[44] Bob Nickson. European Space Components Information Exchange System website, June 2011. https://escies.org.

[45] Patrice Pelissou. RF wireless intra-spacecraft communications: Mock-up detailed design. Technical report, EADS Astrium, 2009. 2125.NT.PP.09.0124.ASTR, Issue 02.